

**UNDERSTANDING EFFECTS OF NANO-REINFORCEMENT-  
MATRIX INTERPHASE ON THE ELASTIC RESPONSE OF  
POLYMER NANOCOMPOSITES**

A Dissertation  
Presented to  
The Academic Faculty

By

Mehdi Karevan

In Partial Fulfillment  
of the Requirements for the Degree  
Doctor of Philosophy in the  
George W. Woodruff School of Mechanical Engineering

Georgia Institute of Technology  
December 2013

**COPYRIGHT 2013 BY MEHDI KAREVAN**

**UNDERSTANDING EFFECTS OF NANO-REINFORCEMENT-  
MATRIX INTERPHASE ON THE ELASTIC RESPONSE OF  
POLYMER NANOCOMPOSITES**

Approved by:

Dr. Kyriaki Kalaitzidou, Advisor  
School of Mechanical Engineering  
*Georgia Institute of Technology*

Dr. Suman Das  
School of Mechanical Engineering  
*Georgia Institute of Technology*

Dr. Ting Zhu  
School of Mechanical Engineering  
*Georgia Institute of Technology*

Dr. Satish Kumar  
Materials Science and Engineering  
*Georgia Institute of Technology*

Dr. Vladimir Tsukruk  
Materials Science and Engineering  
*Georgia Institute of Technology*

Date Approved: June 30, 2013

To  
my parents, my first teachers

## ACKNOWLEDGEMENTS

Today, I extremely feel accomplished and blessed upon completion of my Ph.D. dissertation. I would never be in this position without sincere and invaluable support, inspiration and direction given to me by people around me since the very first place until now. This simple expression of acknowledgment, however, does not certainly suffice.

Foremost, I would like to express my deepest gratitude to my advisor, Dr. Kyriaki Kalaitzidou, for her immeasurable amount of persistent guidance, support, and patience throughout the last four and half years, my greatest achievement era so far. I would like to thank her for furnishing me with a spirit of adventure and initiation, and with a deep confidence in conducting research and implementing what I learned in pursuit of my Ph.D. This study was not possible without her continual advice, substance of motivation and encouragement, not to mention her convincing research attitude.

I also would like to express my sincere appreciation to my committee members, Prof. Suman Das, Prof. Satish Kumar, Prof. Vladimir Tsukruk and Prof. Ting Zhu for scrutinizing my dissertation and for their valuable suggestions and perceptive comments.

I would like to thank the Materials Property Research Lab, Prof. Rosario Gerhardt, Prof. Vladimir Tsukruk and Prof. Jonathan Colton for giving me access to their characterization equipment, and specifically Prof. Suman Das, the director of the Direct Digital Manufacturing Lab, and Shaun Eshraghi for their research collaboration.

I am grateful to all of my fellow colleagues and friends: Dr. Md Bhuiyan, Brian Simpson, Chun Chu, Brian Kwong, Dr. Marwa Mohamed, and Joshua Starker. I also thank our academic staff and assistants specifically Joi Outlaw, Melissa Raine and Glenda Johnson.

I would like to acknowledge the financial support provided by the Civil, Mechanical and Manufacturing Innovation (CMMI) of the National Science Foundation (NSF) under grant No.1000323 for this study.

Above all, I should extremely thank my parents for giving me unparalleled encouragement, strength and love to confidently pursue my goals throughout my life. My specific gratefulness goes to my brother and sister, Hossein and Hajar, whose generous support and admirable patience indeed filled me with a spirit of endeavor and made all my achievements possible over past years.

# TABLE OF CONTENTS

	Page
ACKNOWLEDGEMENTS	iv
LIST OF TABLES	ix
LIST OF FIGURES	x
SUMMARY	xiv
<u>CHAPTER</u>	
1 INTRODUCTION	1
1.1 Polymer Nanocomposites: Current Status and Challenges	1
1.2 Polymer Nanocomposites: Fabrication	3
1.3 Interfacial Interactions in PNCs	6
1.3.1 Formation of interphase	7
1.3.2 Characterization of Interfacial Interaction Zone	8
1.4 Effect of Interfacial Interactions on Macro-scale Properties of PNCs	13
1.5 Motivation, Research Goal and Objectives	15
2 MATERIALS, PROCESSING AND CHARACTERIZATION	18
2.1 Materials	18
2.2 Processing of PNCs	20
2.2.1 Compounding	21
2.2.2 Injection Molding	23
2.2.3 Selective Laser Sintering	26
2.3 Characterization Techniques	27

3	EFFECT OF MANUFACTURING METHOD ON THE STRUCTURAL AND MACRO-SCALE PROPERTIES OF GNP/PA12 NANOCOMPOSITES	30
3.1	Mechanical Performance	31
3.2	Melting and crystallization behavior of GNP/PA12 composites	35
3.3	GNP-PA12 Interfacial Interactions	40
3.4	Electrical Behavior of GNP/PA12 Composites	43
3.5	Morphology of GNP/PA12 Composites	44
3.6	Conclusions	48
4	EFFECT OF INTERFACIAL INTERACTIONS ON MACRO-SCALE PROPERTIES OF GNP/PA12 NANOCOMPOSITES	50
4.1	Tensile Modulus and Glass Transition Temperature of the Nanocomposites	51
4.2	Assessment of the Interfacial Interactions	52
4.2.1	Immobilized Amorphous Phase	52
4.2.2	Transcrystalline Phase	59
4.2.3	Crystal Characteristics	61
4.2.4	Constrained Phase at the GNP Surface	65
4.2.5	Assessment of GNP-PA12 Interphase	68
4.3	Conclusions	75
5	EFFECT OF MANUFACTURING METHOD ON ELECTRICAL BEHAVIOR OF PNCs	77
5.1	Introduction	77
5.2	Factors Affecting Electrical Performance of PNCs- A Literature Review	79
5.3	Characterization of Electrical Properties of PNCs	83
5.4	Electrical Properties of GNP/PA12 PNCs: SLS v.s. IM	84
5.5	Conclusions	99

6	SUMMARY, COLCLUSIONS AND RECOMMENDATIONS	101
	6.1 Summary of the Dissertation	101
	6.2 Conclusions	103
	6.3 Research Contributions	103
	6.3.1 Scientific Contributions	104
	6.3.2 Technical Contributions	104
	6.4 Future Research and Recommendations	105
	REFERENCES	106

## LIST OF TABLES

	Page
Table 1.1 Summary of experimental characterization of interphase	11
Table 2.1 Properties of GNP used in the study	19
Table 2.2 Process parameters investigated for melt mixing injection molding processing of GNP/PA12 composites and process optimization	24
Table 3.1 Effect of manufacturing and GNP on melting temperature and crystallization characteristics of GNP/PA12 composites	38
Table 3.2 $T_g$ , $\tan\delta$ and storage modulus of GNP/PA12 composites processed by either SLS or IM (standard deviation is less than 10%)	42
Table 4.1 Thermo-mechanical and crystallization parameters used for the estimation of the immobilized amorphous phase	54
Table 4.2 $\Delta C_p$ of the GNP/PA12 nanocomposites as a function of GNP content at $T_g$	58
Table 4.3 The effect of GNP content on transcrystalline region is indicated by variations in melting peaks, crystallization induction time, and recrystallization enthalpy of PA12 crystals	66
Table 4.4 Characteristic length of the glass transition estimating the thickness of the immobilized amorphous chains	75
Table 5.1 Dependence of percolation threshold and electrical conductivity of graphite based PNCs on the fabrication method and PNC system	81

## LIST OF FIGURES

	Page
Figure 1.1 Relative Young's modulus of fully exfoliated, randomly orientated Nylon 6/MMT nanocomposites: micromechanical predictions v.s. experimental data	3
Figure 1.2 Schematic of the SLS process representing the main components of the system	5
Figure 1.3 Schematic representation of various states of dispersion and distribution combined with presence of the interphase in polymer nanocomposites compared to an ideally reinforced micro-composite	16
Figure 2.1 (a) AFM height image of pure GNP on a mica substrate and (b) the height information along the profile line across the GNP as a function of distance	19
Figure 2.2 One synthesis route for fabrication of exfoliated graphite nanoplatelets from natural graphite flake	20
Figure 2.3 Effect of compounding method and GNP content on the flexural strength of GNP/PA12 nanocomposites	22
Figure 2.4 Effect of compounding method and GNP content on the dynamic viscosity of GNP/PA12 nanocomposites measured at $\omega=0.1$ rad/s and $T=190$ °C	23
Figure 2.5 Dependence of the flexural properties (top) and impact strength (bottom) on process parameters in IM processing of 3wt% GNP composites	25
Figure 3.1 Effect of manufacturing on the tensile modulus and strength of GNP/PA12 composites	32
Figure 3.2 Effect of manufacturing on the flexural properties of GNP/PA12 composites	33
Figure 3.3 Effect of manufacturing on the impact strength of GNP/PA12 composites	34
Figure 3.4 Effect of manufacturing on the melting behavior of GNP/PA12 SLS ( $T_{m1}$ and $T_{m2}$ main and secondary melting temperatures respectively)	36
Figure 3.5 Effect of manufacturing on the XRD patterns of GNP/PA12 composites (the curves are shifted vertically for clarity)	38
Figure 3.6 Non-isothermal DSC cooling curves of SLS and IM GNP/PA12 composites v.s. temperature and GNP content	40
Figure 3.7 Effect of manufacturing method on the $\tan\delta$ (damping) of GNP/PA12 composites	41

Figure 3.8 Electrical conductivity of GNP/PA12 composites made by either SLS or IM	44
Figure 3.9 SEM images of PA12 powder at a) low and b) high magnification and 3 wt% GNP-coated PA12 powder at c) low and d) high magnification	46
Figure 3.10 SEM images of a) top surface of PA SLS b) fracture surface of 5GNP/PA12 SLS and c) fracture surface of 5 GNP/PA12 IM	47
Figure 4.1 Tensile modulus and $T_g$ of GNP/PA12 PNCs as a function of the GNP content	52
Figure 4.2 $\tan \delta$ spectra of the PNCs as a function of temperature and GNP wt%	55
Figure 4.3 Normalized storage at below and above glass transition temperatures as a function of GNP content	57
Figure 4.4 MDSC specific heat capacity of GNP/PA12 nanocomposites as a function of GNP content obtained during heating scans. The inset is a zoomed-in plot of these traces near $T_g$ demonstrating the decrease in the discontinuity of $\Delta C_p$ with GNP	58
Figure 4.5 Non-isothermal DSC cooling curves of GNP/PA12 PNCs v.s. GNP content	60
Figure 4.6 Crystallization induction time and degree of super-cooling with respect to the equilibrium melting temperature obtained from the non-isothermal DSC cooling curves of GNP/PA12 composites are a function of the GNP content	61
Figure 4.7 XRD patterns of GNP/PA12 PNCs (the curves are shifted vertically for clarity)	64
Figure 4.8 a) MDSC reversing thermograms of the melting behavior of GNP/PA12 as a function of GNP content. The arrows indicate the first ( $T_{m1}$ ) and second ( $T_{m2}$ ) melting peaks, and b) MDSC non-reversing heat flow thermograms of the PA12 and nano-composites representing the recrystallization (exothermic) peaks over the melting transition	65
Figure 4.9 Proposed model representing formation of a complex constrained phase in PA12 upon addition of GNP	67
Figure 4.10 Representative fracture surface of a) neat PA12 and GNP/PA12 composites containing b) 5wt% and c) 15wt% GNP, showing GNP agglomeration only at higher GNP contents	68
Figure 4.11 Representative AFM phase image of 0.1 wt% GNP/PA12 PNCs: a) presence of GNP on the surface of PA12 matrix, b) a magnification of (a) showing the profile lines along the interfacial interaction zone, and c) phase lag v.s. distance for the profile lines shown in (b) indicating thickness of the interfacial region	71

4.12 a) representative AFM image of sonicated GNP onto a mica substrate ( $5 \times 5 \mu\text{m}^2$ ), and b) phase lag v.s. distance for the profile lines shown in a revealing a sharp transition in phase lag data from the surface of GNP to the mica substrate	72
Figure 4.13 Representative AFM height image corresponding to the phase image illustrated in Figure 4.11a: a) topography of a $10 \times 10 \mu\text{m}^2$ scan size, b) a magnification of (a) showing the profile lines along the interfacial interaction zone between GNP and PA12, and c) height v.s. distance for the profile lines shown in (b)	73
Figure 5.1 Measurement directions used to determine electrical resistance of the SLS and IM-processed specimens through (a) longitudinal (in-plane) and transverse direction through (b) the width and (c) thickness of specimens	84
Figure 5.2 a) dependence of longitudinal electrical conductivity on the frequency of the AC voltage, process and GNP concentration of SLS and IM-made specimens and b) electrical conductivity values at AC frequency of 0.01 rad/s of the parts measured	87
Figure 5.3 a) dependence of electrical conductivity on the frequency of the AC voltage, process and GNP concentration of SLS and IM specimens and b) electrical conductivity values at AC frequency of 0.01 rad/s of the parts measured through the width (y axis)	89
Figure 5.4 a) dependence of electrical conductivity on the frequency of the AC voltage, process and GNP concentration of SLS and IM-made specimens and b) electrical conductivity values measured through the thickness (z axis) of the parts at AC frequency of 0.01 rad/s	90
Figure 5.5 SEM images of a) neat PA12 powder and b) 5wt% GNP coated PA12 powder representing the dispersion and distribution of GNP before processing	91
Figure 5.6 Fracture surface of 5wt% GNP/PA12 composites made by a) SLS and b) IM indicating presence of GNP aggregates promoting formation of conductive networks in SLS-made PNCs and absence of these paths in IM-made PNCs due to GNP agglomeration and increase of the interparticle distance	93
Figure 5.7 Schematic configurations representing dispersion/distribution and alignment of GNP in PA12 before processing steps (top), and in processed parts after IM (bottom left) and SLS (bottom right). Cross sections display planes normal to the injection flow direction and sintering plane in IM and SLS, respectively: incomplete v.s. complete conductive network of GNP	94
Figure 5.8 Electrical conductivity of the PNCs with respect to measurement direction for a) SLS and b) IM process as a function of the frequency of the AC voltage and GNP concentration	96
Figure 5.9 Comparison of electrical conductivity values in x,y and z direction of the SLS parts at AC frequency of 0.01 rad/s	97

Figure 5.10 a) inhomogeneity of SLS v.s. b) homogeneity of IM parts observed by electrical conductivity of the 5wt% GNP/PA12 PNCs measured through the length, width and thickness

99

## SUMMARY

Current technology of polymer nanocomposites (PNC) emphasizes the need for fundamental understanding of the links between manufacturing method and macro-scale properties in order to engineer processing and performance of PNCs. The manufacturing method is one key variable that dramatically defines interfacial interactions on the nano-scale and thus the properties of polymer near the interface of nanomaterial/polymer or interphase, level of dispersion and the crystallization behavior of semi-crystalline PNCs. These factors in particular govern reinforcing mechanisms at the interface and consequently impart important properties to PNCs. The current approach to manufacturing PNCs involves trial and error with elaborate, costly and time consuming experimental characterization of PNCs. Therefore, a deep insight into the links among manufacturing method, interfacial interactions and bulk properties is essential in order to design and fabricate PNCs with engineered performance.

The main goal of this study was to provide a better understanding of the effect of manufacturing methods on the macro-scale properties of PNCs, with a focus on the role of interfacial interactions, that can lead to fabrication of PNCs with multifunctional performance. The objectives of this research were to: i) determine the detail correlations among manufacturing method, nano- and microstructure and macro-scale properties of multifunctional exfoliated graphite nanoplatelets/polyamide 12 polymer nanocomposites with enhanced mechanical and electrical performance through systematic manufacturing and experimental methodologies, ii) understand correlations among nano-scale interfacial interactions, physical and structural properties of the polymer at the interface and macro-scale behavior of PNCs, and iii) evaluate effect of manufacturing method on electrical behavior of PNCs with directionally dependent performance.

This study demonstrated key correlations among manufacturing techniques, interfacial interactions and macro-scale properties of PNCs. A methodology was introduced to understand and determine the characteristics of a complex constrained region produced at the interface of nanomaterials and polymer in semi-crystalline PNCs. Finally, the study illustrated superior electrical and morphological properties of selective laser sintering (SLS) processed parts over injection molded PNCs and thus confirmed the capability of SLS in the development of electrically conductive PNCs that exhibit multifunctional performance. In conclusion, the study provided an insight into the links among process, nano-scale interfacial interactions and microstructure to better understand effects of manufacturing technique on macro-scale properties of PNCs, which enables fabrication of conductive PNCs with multifunctional performance.

# CHAPTER 1

## INTRODUCTION

### 1.1 Polymer Nanocomposites: Current Status and Challenges

Recent advances in technology of nano-structured materials have stimulated research into the design and fabrication of polymer nanocomposites (PNC) for regular or specific applications [1]. PNCs contain a polymer matrix filled with at least one reinforcement that has at least one dimension less than 100 nm [2]. The small size and unique morphological characteristics of nanomaterials, and the resulting large specific surface area (surface area per unit volume), give rise to nanomaterial-polymer interfacial interactions that dictate the load transfer quality at the interface, the distribution and dispersion of nanomaterials and the overall performance of nanocomposites [1, 3-5].

A PNC's structure can be tailored in order to enhance multiple properties at the same time, leading to multi-functional engineering materials. Applications of PNCs range from aerospace materials and defense applications, health and medicine, energy, sporting materials and automotive parts to consumer electronics, and environment [1]. However, the design and manufacturing of PNCs have posed additional challenges to the technology of composites due to the nano-scale size of the materials used and the resulting uncontrollable nanomaterial-polymer interfacial interactions [6, 7].

It has been shown that in addition to the intrinsic properties of the constituents, the properties of PNCs are highly influenced by other main variables such as nanomaterial-polymer interfacial interactions which dictate the dispersion and alignment of nanomaterials [8, 9] and are governed by the manufacturing methods used [1, 4, 10, 11]. Characterization of PNCs has, however, largely relied on extensive empirical approaches due to lack of a general understating of correlations among process-structure-

property and considerable uncertainty in theoretical modeling of PNCs [12-14]. These issues have immensely limited the ability to design and manufacture PNCs with engineered properties for specific applications. Unlike their successful application in cases of conventional composites, micromechanics models usually fail in valid property prediction of PNCs due to the presence of phenomena on the nano-scale that in turn dominate macro-scale properties. For instance, factors such as poor interfacial bonding at the interface, anisotropic properties and poor dispersion of nanomaterials are not taken into account by the theories [15]. Understanding interfacial phenomena and their correlation to fabrication method is therefore a key requirement in understanding governing process-structure-property relationship and thus revealing mechanisms responsible for the property enhancement. Figure 1.1 compares relative Young's modulus values predicated by different micromechanical theories with experimental values for nylon 6 reinforced with montmorillonite (MMT) nanoclay as function of volume fraction. It is clearly shown that the models overestimate the properties compared to the experimental results at a given concentration and that the continuum view of classical micromechanics is no longer valid in the case of PNCs.

It is concluded that is essential to precisely determine effects of a range of variables on the macro-scale properties of PNCs in order to design and manufacture PNCs with engineered properties [15-17]. Determination of correlations among all these variables is however a multi-directional task, as can be envisioned in numerous previous studies. Since the focus of this study is investigating the influence of manufacturing method on the macro-scale properties of PNCs, with an emphasis on the role of interfacial interactions, the following briefly describes common manufacturing methods of PNCs and how the interfacial interactions form and dictate the macro-scale properties of PNCs.

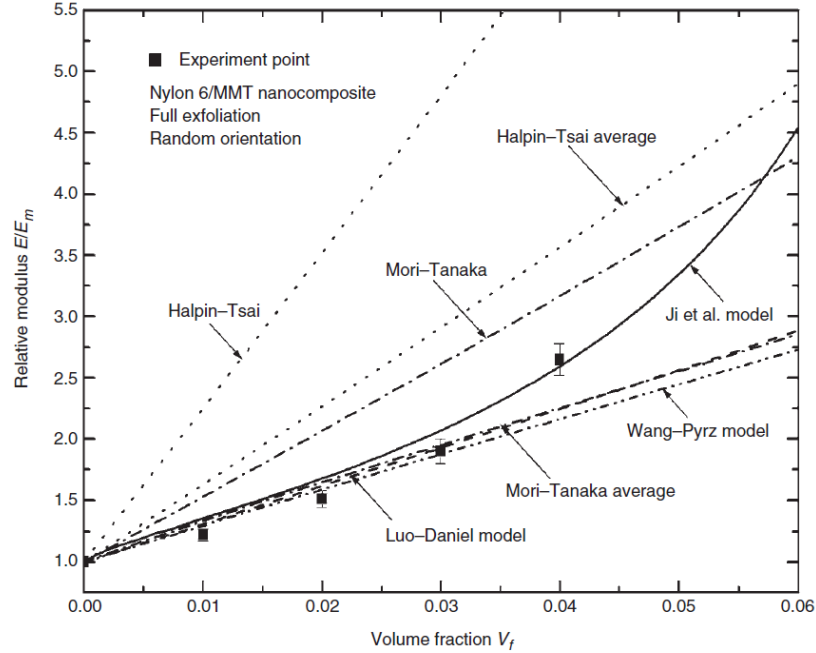


**Figure 1.1 Relative Young's modulus of fully exfoliated, randomly orientated Nylon 6/MMT nanocomposites: micromechanical predictions v.s. experimental data [18]**

## 1.2 Polymer Nanocomposites: Fabrication

Interfacial interactions are born during PNC fabrication regardless of the composite's constituents [19]. Conventional techniques have been employed to disperse nanomaterials within the polymer. The most common methods include solution blending, in-situ polymerization, and melt blending techniques. Other methods such as solid-state shear pulverization, spin casting, melt fiber and coagulation spinning have been used more commonly recently [20, 21]. Solution blending is performed using three main steps including dispersion of nanomaterials in a compatible solvent that may be enhanced in presence of surfactants, mixing the solution with a polymer, and recovering PNCs by precipitating, molding or casting process [22, 23]. The method is limited to polymers that are effectively dissolved in common solvents [24]. In-situ polymerization, used mainly in cases of low viscosity thermoset matrices and a limited number of thermoplastic monomers, involves dispersion of in a monomer followed by polymerization (initiated by

heating or radiation or by diffusion) of the reinforced monomer. The methods mentioned above have two major limitations: i) the use of hazardous chemicals and ii) low yield fabrication and thus high production cost [25]. In the melt blending processes nanomaterials are dispersed within a polymer matrix as the blend is subjected to high shear forces and temperatures; these steps are followed by injection molding (IM) [23, 26, 27]. An advantage of melt blending is its simplicity, large scale production with no or minimum use of hazardous chemicals. Melt blending may however induce polymer degradation and separation of nanomaterials from the matrix phase and unintentional alignment of nanomaterials [22, 28]. Moreover, the large shear forces often break down the network of fillers within the polymer, which in the case of conductive fillers results in an increase of the electrical percolation threshold and thus unnecessary costs in fabrication of polymer composites when products with enhanced electrical properties are desired [29-31].

The main challenge that needs to be overcome in all of the methods discussed above is the high tendency of nanomaterials to form agglomerates within polymers during processing. Functionalization has shown promise in terms of improving the initial dispersion of nanomaterials in the solvent or monomer and enhancing the interfacial adhesion [32-34]. Techniques such as sonication have been used to enhance dispersion of nanomaterials, but the method is effective only for polymers of low viscosity and small volume quantities.

Selective laser sintering (SLS), developed in the late 1980s, has been recently considered as an alternative polymer processing technique to the conventional processes. SLS is a powder-based additive manufacturing process in which three-dimensional solid parts are fabricated by successive sintering of a pre-heated raw powder according to the cross-sectional information of a CAD model [35-37].

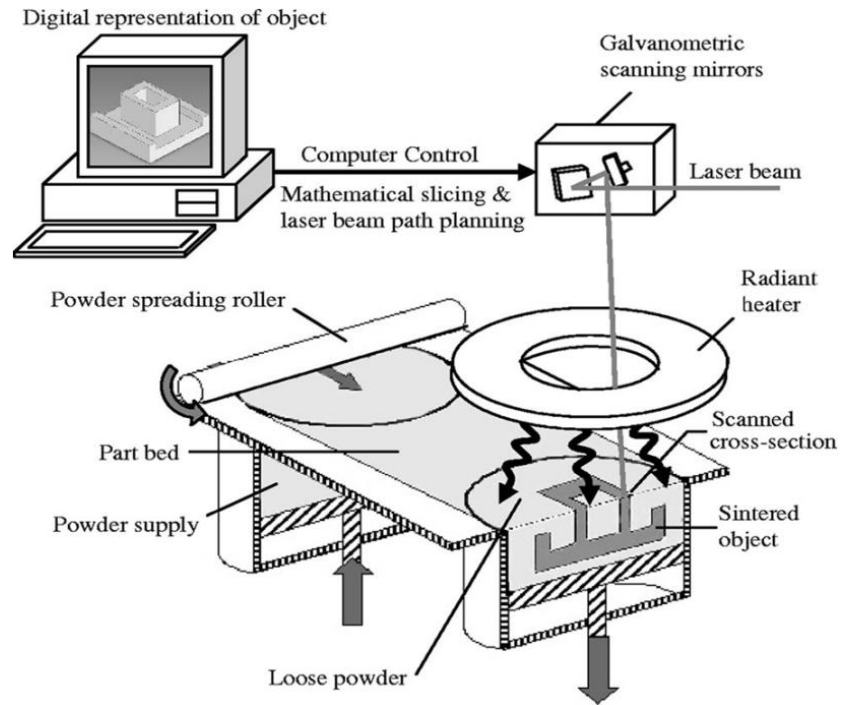


**Figure 1.2 Schematic of the SLS process representing the main components of the system [35]**

SLS enables fabrication of parts with enhanced complexity and precision while expensive specific tooling is no longer required. The method enables fabrication of functionally graded materials i.e., composition and properties of the composites vary along the part thickness [38]. These provide greater design flexibility and implementation of the SLS-processed parts than of those parts processed by conventional techniques; this make SLS a competitive technology for processing of polymers and composites [37, 39, 40]. However, SLS polymers normally do not exhibit the full performance of real products required in high-end use due to the intrinsic properties of polymers and the porous structure of the sintered parts. These issues have motivated increasing research into development of novel SLS starting polymers reinforced with nanomaterials [38, 41-43]. Moreover, similar to other processing techniques used for reinforcing polymers, a prime factor in SLS is uniformity of the starting SLS powder and dispersion quality of

nanomaterials. A schematic diagram of the SLS process and the main elements of the system are given in Figure 1.2.

Preparation of the composite powder required in SLS however is not easily realized due to density difference between fillers and polymer powder, as is seen in direct mixing processes. A number of preparation methods have been reported elsewhere [36, 44, 45]. Composites of graphite nanoplatelets (GNP) and polyamide12 (PA12) have been made using SLS, and it has been shown that the sintered functionalized GNP/PA12 parts demonstrated the greatest property improvement due to the reinforced interfacial adhesion [45]. In another work, preparation of the SLS powder using melt mixing and cryogenic milling for SLS fabrication of carbon nanofibre-PA12 composite has been reported and, it was revealed that the effective reinforcement of the polymer was highly affected by the size and morphology of the prepared powder [36]. Previous research also reports the use of solid state mixing for preparation of the SLS powder for SLS processing of carbon black (CB)/PA12 composites. It has been demonstrated that the composites prepared by SLS had an electrical conductivity several orders of magnitude greater than the conductivity of the corresponding composites made by melt-mixing and injection molding [29, 35]. However, the observations have revealed that the SLS parts had a lower modulus and strength compared to the melt-mixed parts, due to the presence of CB aggregates and to porosity in the CB/PA12 parts [46]. Studies that elaborate on the correlation between the interfacial interactions induced during the sintering process and the macro-scale properties of sintered PNCs are lacking. This brief review reveals that the potential of SLS to manufacture PNCs for commercial applications still needs to be determined.

### **1.3 Interfacial Interactions in PNCs**

The macro-scale properties and even the processability of PNCs not only depend on the properties of material constituents but they are also remarkably influenced by the

nanomaterial-polymer and nanomaterial-nanomaterial interfacial interactions [10]. The latter induce the interfacial coupling (adhesion) of polymer to nanomaterial surface and nanomaterial agglomeration and hence influence the quality of interfacial load transfer [10, 15, 47, 48].

### **1.3.1 Formation of interphase**

The high aspect ratio and small size of nanomaterials result in significant nanomaterial/polymer interface and thus significant interfacial interactions [49]. These interactions can lead to local adsorption of polymer chains at the interface, mechanical interlocking, and interdiffusion of polymer chains, and can be altered by the chemical and physical characteristics of the interface and polymers [49, 50]. The strength of the interactions can vary from strong covalent bonds to very weak interfacial interactions due to van der Waals forces that favor the interactions among nanomaterials or repulsive forces between the PNC constituents [51-53]. One main result of nanomaterial/polymer interactions is the reduction of the mobilization of polymer chains and thus the decrease of the entropy of the polymer chains [46, 54, 55] and rarely the increase of the entropy of polymer chains [56, 57]. The interfacial interactions modify the polymer properties at or near the interface and lead to creation of an interfacial zone or what is identified in the literature as an “interphase”.

The interphase is responsible for communication between fillers and bulk polymer and may have distinct chemical, physical, microstructural, and mechanical properties different from those of the composite components [58-61]. Interphase properties depend on factors such as the thermodynamic compatibility and morphological nature of the reinforcement and polymer, the dispersion of fillers, the size and number of polymer crystallites, in the case of semi-crystalline polymers, and the manufacturing method and processing conditions used to fabricate the composites [60, 62-64]. For example, formation of a soft or hard interphase, with respect to the stiffness/modulus of the host

polymer, has been observed [65-68] ranging from 10 Å to several microns [10, 69]. Since the interphase characteristics depend on the nature of interfacial forces and the characterization methods, contradictory results or non-conclusive results have been reported [70, 71].

The interfacial interactions dictate the quality of dispersion of nanomaterials within the host polymer and thus the macro-scale properties of PNCs [15, 72, 73]. Good dispersion provides more reinforcing sites and thus more effectively restricts the shearing or deformation of the polymer chains around nanomaterials [74]. However, agglomeration of nanomaterials cannot really be avoided due to reasons including their incompatibility with polymers, large surface-to-volume ratio and natural agglomeration tendency due to van der Waals forces [10, 17, 75]. Furthermore, the nanomaterial-polymer repulsive interactions are responsible for the agglomeration of nanomaterials and changes in physical properties of polymer due to the entropy decrease of polymer chains near the nanomaterial surface [76]. Surface modification has been used to enhance the adhesion between nanomaterials and polymer and thus to reduce the agglomeration level. Major challenges, however, include maintaining the original properties after surface treatment and thermomechanical stability among all components [10, 75].

### **1.3.2 Characterization of the Interphase**

Polymer behavior at or in the vicinity of interfaces has been studied for more than 30 years [49]. The interphase is usually formed as a result of processes such as interdiffusion of atoms or molecules, cross-linking, immobilization, and crystallization of thermoplastic polymers. Herein, the methods used for the interphase characterization including the mechanical and thermomechanical techniques are briefly reviewed.

#### Spectroscopic and Mechanical Approaches

Several spectroscopic techniques such as solid-state nuclear magnetic resonance, Raman spectroscopy (shifting of the G band peaks) and FTIR spectroscopy have been

successfully utilized to analyze chemical reactions at the interface [60, 77-79]. X-ray photoelectron spectroscopy (XPS) has been used to evaluate the interphase in terms of composition (atomic concentration) [80, 81]. However, the techniques mentioned above normally do not provide information about the size/geometry of the interfacial zone. The interfacial adhesion has been assessed using scanning electron microscopy (SEM) or transmission electron microscopy (TEM). However, these techniques similarly fail to provide quantitative information [82, 83].

In contrast, nanoindentation and nanoscratch techniques have been used for characterization of mechanical properties and thickness of the interfacial zone [60, 84, 85]. As reported, the nanoindentation method was first utilized to estimate the interphase in carbon fiber-epoxy composites [86]. Today, it is feasible to perform a nanoindentation experiment using atomic force microscopy (AFM) with enhanced spatial and displacement resolution [87, 88]. Nanoindentation has been, however, challenging due to issues such as “reinforcement stiffening” at the filler-matrix edge and unavoidable large indenting steps to avoid overlapping [60]. Nanoscratch tests rely on the interactions between the tip and components, which provide information about changes in the friction coefficient of the compositions under the tip in order to determine boundaries between phases. Few studies have successfully demonstrated direct application of AFM pull-out tests for the study of the interfacial strength [60, 89]. The quantification of the interphase, however, is still unresolved using such techniques [53, 89].

Scanning probe microscopy (SPM) techniques have been used to overcome the limitations associated with quantification, size of the interphase and required resolution. Furthermore, the AFM contact mode and the force modulation mode have been used to characterize interphase properties [88, 90-92]. The AFM force volume imaging can be used to extract quantitative mechanical information, but the technique is very slow for detailed modulus mapping purposes [93, 94]. AFM phase imaging has been used to identify the interphase through the stiffness contrast between two adjacent materials [63,

70, 95]. Although the technique has acceptable accuracy and reproducibility, the data can be hardly interpreted because of the interaction forces induced on the tapping tip [70, 96]. Other AFM tapping mode methods such as the HarmoniX require complicated operation and particular geometry of probes and are limited to modulus mapping of PNC surfaces with moduli <10 GPa [94, 97].

Table 1.1 shows the interphase characteristics as determined using various techniques. One can conclude that the measured interphase characteristics may remarkably vary depending on the characterization method and are specific to the material system studied [93]. In particular, composites of thermoset polymers reinforced with silane-treated glass fibers have been reported to have a relatively large interphase with thickness of 1  $\mu\text{m}$  or several times thicker upon aging in water due to interdiffusion of silane agent promoted by hydrolysis [60]. Contribution of sizing agents to increased size of interphase in carbon fiber reinforced epoxy systems has been reported elsewhere too [98]. Presence of an interphase with a thickness as small as 3 nm has been also reported for an unsized carbon fiber/epoxy system [98].

It should be noted that the 3 nm interphase is too small to be measured using AFM nanoindentation experiments. The trouble lies in limitations in physical size of the indentation probe and the lateral resolution of the AFM indenter. As reported, finite element models have shown promise in determining such narrow interphase zones on the basis of the response of material near the reinforcement and experimental interphase thicknesses obtained for the case of measurable (large) interphases [98, 99]. The small size of 3 nm appears to be close to the typical interphase thickness obtained by thermomechanical theories based on the relaxation of polymer chains around the glass transition [100]. It is noted that the typical diameter of glass fiber ranges from 3 to 25  $\mu\text{m}$ . The size may vary upon sizing and coating processes and define the interphase thickness [99, 101].

To overcome these limitations, very recently researchers have utilized quantitative nanomechanical approaches such as the AFM peak force tapping mode to better discriminate between the nanomaterial-polymer interaction forces. The method benefits the usual imaging speed in a way similar to that of the conventional tapping mode while providing a map of several mechanical properties. Moreover, the peak force method provides very low intermittent contact of the tip and polymer surface. It also controls the peak force with absence of the lateral forces on the tip that results in i) small deformation on the surface (<3 nm) that leads to an enhanced imaging resolution, and ii) decrease in the tip damage. Modeling techniques such as fracture mechanical analysis or shear lag analysis have also been developed to study the interphase. Such techniques are well conducted for study of the interfaces in brittle materials but are insufficient to describe the interphase as a volumetric region [90, 102, 103]. On the basis of the background review, just very few studies have been reported using the peak force tapping mode for nanomechanical characterization of PNCs [97].

**Table 1.1 Summary of experimental characterization of interphase**

<b>Composite system</b>	<b>Measuring method</b>	<b>Thickness</b>	<b>Modulus/hardness relative to matrix</b>
Carbon fiber-epoxy	AFM nanoindentation	3nm	Softer [70]
Glass fiber-polyester	Nano-scratch	4-5 $\mu\text{m}$	Harder [70]
Silane treated Glass fiber-epoxy	Nanoindentation/interfacial force microscopy	8 $\mu\text{m}$	Softer and harder [92]
Sized SiO <sub>2</sub> - epoxy	Phase imaging AFM and nanoindentation	2.4-2.9 $\mu\text{m}$	Softer [60]
Carbon black-rubber	Analytical/non-linear data regression	14-27 nm	30-58 MPa [60]

### Thermomechanical Methods

It has been shown that the configurational rearrangement and relaxation processes of long segments of polymer chains are significantly sensitive to the local environment restrictions surrounding the chains [104-106]. The links between the amount of the

immobilized chains at the interface and thermomechanical/thermal properties such as the glass transition ( $T_g$ ) have been widely illustrated using dynamic mechanical analysis (DMA) and differential scanning calorimetry (DSC) [107-109]. Previous research has shown strong dependence of polymer chain immobilization within the interphase upon the size of the interface area, the presence of secondary hard phases such as crystallites and the dispersion state of nanomaterials [10, 110, 111]. The existence of immobilized amorphous phase in poly(butylene terephthalate) (PBT) nanocomposites reinforced with single-wall and multi-wall nanotubes has been reported using DMA. The study relates the decreased normalized  $T_g$  peak and the corresponding narrower shape of the curve to the enhancement of the immobilized chains [112]. The changes in  $T_g$  values originating from the restriction of polymer chains is not always sufficient by itself to evaluate altered dynamics of polymer chains. Certain impediments exist regarding the error range and the lack of necessary resolution of the DMA measurements, as well as the mechanism and the details of the modification near the particle surface. For instance,  $T_g$  has been reported to increase [113-115], decrease [116] or be invariant when competing factors such as agglomeration are present [113, 115, 117].

Studies of calorimetric relaxation strength ( $\Delta C_p$ ) in bulk PNCs have been used to complete the DMA studies [115, 118, 119]. A method, first introduced by Wunderlich et al. [120, 121], has made advances to determine the polymer amorphous domain with limited mobilization via study of the transition from the solid like to liquid like behavior of the amorphous phase based on changes in the specific heat capacity,  $C_p$ , [111, 122]. Although the method was originally used to quantify the amount of amorphous phase immobilized by polymer crystals in semi-crystalline polymers, the technique can be similarly applied for semi-crystalline and amorphous PNCs where hard fillers restrict mobilization of polymer chains. The effect has been indicated by a dramatic reduction in  $\Delta C_p$  due to the immobilization of polymer chains at the interface since the immobilized chains do not contribute to the relaxation strength at  $T_g$  and remain still active before

melting [100, 123]. The review of previous published work, however, shows little or no research that comprehensively investigates the character, amount and properties of the interphase in correlation with macro-scale properties of PNCs [62, 72, 124].

#### **1.4 Effect of Interfacial Interactions on Macro-scale Properties of PNCs**

Understanding how interfacial interactions influence macro-scale properties is key in manufacturing PNCs with engineered properties [7, 9]. Many researchers have linked the altered performance as well as structural integrity of PNCs to the dominant effect of interfacial interactions on the macro-scale properties [1, 125, 126]. In particular, an increase in tensile modulus has been frequently reported due to extensive polymer chain immobilization within the interphase [74]. The tensile strength and toughness of PNCs have been shown to be also sensitive to soft-type interphases [60, 127].

The study of changes in thermomechanical properties such as the  $T_g$  has been widely utilized to assess the interphase due to the high sensitivity of these properties to mobility of polymer chains at or near the nanomaterials surface [128]. It has been demonstrated that the strength of interfacial adhesion affects bulk properties of TiO<sub>2</sub>/poly (methyl methacrylate) (PMMA) nanocomposites prepared by solution mixing and it has been shown that TiO<sub>2</sub> particles with surface modification induced greater increase in the  $T_g$  and elastic modulus of PNCs than unmodified particles [15]. In other studies, the counteracting effects of nanomaterial agglomeration and unmodified or desirably enhanced adhesion between nanomaterial and polymer have been considered as challenges in fabrication of PNCs. For example, effect of grafting polymerization onto the surface of nano-silica particles on the tensile behavior of reinforced polypropylene (PP) has been reported. It has been revealed that stronger interfacial interactions existed at low loadings, beyond which this effect was suppressed by agglomeration [129]. In a recent work, previous findings on negative effects of nanomaterial clustering on the interfacial interactions between nanomaterial and matrix have been confirmed using a

simulation method. It has been demonstrated that clustering resulted in the loss of interphase volume fraction [64]. The interplay among particle size, nanomaterial-matrix adhesion, filler content and mechanical properties has been illustrated elsewhere, with an emphasis on leading role of nanomaterial-matrix adhesion on the composite strength and the toughness of PNCs [62]. In other studies, the importance of interfacial interactions in the degradation of PNCs has been highlighted and ascribed to the retarded scission of polymer chains due to the restriction effects that nanomaterials impose against the mobility of polymer molecules [74].

It should be noted that together with the factors mentioned earlier, the picture of interfacial interactions in the case of semi-crystalline polymers is more complicated than that of fully amorphous polymers due to the effect of the nanomaterial on the degree of arrangement and packing perfection of polymer chains and hence on the nucleation and growth of crystallites [130, 131]. Since the nanomaterial surface has a restriction effect on the mobility of polymer chains, interfacial interactions dictate polymer crystallization, including nucleation and growth [10, 49, 50, 132, 133]. It has been shown how repulsive and/or attractive interactions at the interface define the type of crystalline phases, the size and perfection of crystallites and degree of crystallinity in semi-crystalline PNCs [130, 134]. For instance, the crystalline phase change in melt mixed PP/graphite PNCs has been reported and correlated to the polymer chain immobilization and conductive nature of GNPs [135].

From the above review, it can be clearly understood that there might be a few well established and uniform trends for macro-scale properties as a function of PNC components and level of mixing of them. These trends however cannot be universally applicable to predict the behavior of PNCs that exhibit unexpected performance, since phenomena at the nano-size dominate properties. Therefore, understanding correlations among the manufacturing method and the macro-scale performance with a focus on the key role of interfacial interactions is critical for the design and fabrication of PNCs that

take advantage of “nano” effects and that exhibit expected enhancement in multiple properties.

### **1.5 Motivation, Research Goal and Objectives**

The design and fabrication of light weight, high performance PNCs with multifunctional behavior for targeted applications has attracted huge interest in recent years. However, PNCs generally do not exhibit expected trends and properties upon addition of nanomaterials, which results in contradictory or inconclusive results. The manufacturing method is a prime factor that strongly defines the quality of interfacial interactions and thus the macro-scale properties of PNCs. However, fundamental knowledge that demonstrates possible links between the manufacturing method and macro-scale behavior of PNCs has not been sufficiently established in PNC research. Therefore, the current approaches for manufacturing PNCs mainly rely on time-consuming, elaborate and costly trial-and-error based attempts due to lack of sufficient understanding of process-structure-property relationships of PNCs. Particularly, these limitations are of critical importance as manufacturing trends shift from basic research activity at lab-scale to large-scale manufacturing of PNCs.

Moreover, in processing PNCs, a central question in regards to the governing links between manufacturing method and macro-scale properties of PNCs is how the manufacturing technique used defines nano-scale interfacial interactions in PNCs. The answer to the question requires considering detailed knowledge of these interactions. Interfacial interactions, which are expected to be significant due to large specific area of nanomaterials, dominate the properties of PNCs and should be taken into consideration. However, the effect of the unique length scale of nanomaterials on interfacial interactions, and thus the macro-scale performance of PNCs, cannot be easily performed by scaling arguments that are valid at micro-size down to nano-size. The interphase is also affected by the dispersion and distribution quality of the nanomaterials when scaling

down from micro to nano-size reinforcements. A schematic that demonstrates possible situations, which are mainly reported in cases of polymers reinforced with nanomaterials, is shown in Figure 1.3. Therefore, a scientific knowledge that describes details among process-structure-property relations with emphasis on the role of interfacial interactions is a key tool to effectively fabricate PNCs and motivated the study.

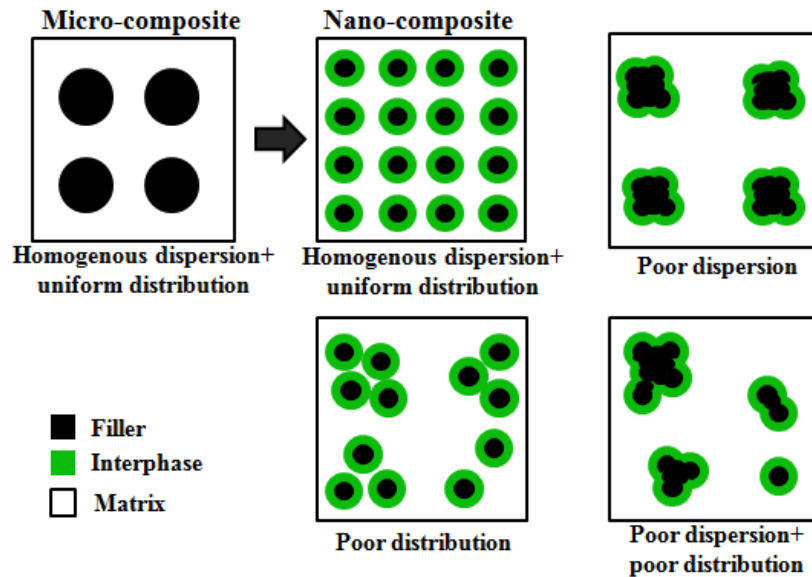


**Figure 1.3 Schematic representation of various states of dispersion and distribution combined with presence of the interphase in polymer nanocomposites compared to an ideally reinforced micro-composite**

The main goal of this study is to provide a comprehensive methodology to understand effects of manufacturing method on macro-scale properties of PNCs with a focus on the role of interfacial interactions in the fabrication of electrically conductive PNCs with engineered multifunctional performance. The specific objectives of this research were to:

- determine the detailed correlations among manufacturing method, nano- and microstructure and macro-scale properties of multifunctional exfoliated

graphite nanoplatelets/polyamide 12 polymer nanocomposites with enhanced mechanical and electrical performance through systematic processing and experimental methodologies.

- understand the correlations among nano-scale interfacial interactions between nanomaterials and polymer, the physical and structural properties of the polymer at the interface and the macro-scale behavior of PNCs.
- evaluate the effect of manufacturing method on the electrical behavior of PNCs with directionally dependent functionalities.

## CHAPTER 2

### MATERIALS, PROCESSING AND CHARACTERIZATION

#### 2.1 Materials

PA12 powder (VESTOSINT<sup>®</sup> X 1553 white, Evonik Industries, Essen, Germany), with an average granule diameter of 50-100  $\mu\text{m}$  and melting temperature ( $T_m$ ) in the range of 176-184  $^{\circ}\text{C}$ , was used as the matrix in this study [136]. The powder is a white, odorless, semi-crystalline thermoplastic polymer. PA12 has a lower concentration of amide groups (nitrogen-containing organic compounds) than other commercially available types of polyamide and this gives PA12 several main characteristics. PA12 absorbs very little moisture which leads to its high dimensional stability; it has excellent fatigue and impact resistance, great resistance to chemicals, high damping ability and features high processability. Thus PA12 has found many commercial applications such as in electronics industries, transportation, food technology and many others. Moreover, in spite of advances in powder choice for additive manufacturing techniques in recent years, PA12 has remained a major polymer material due to extensive established research concerning advanced and conventional processing of PA12, and its better processability and low cost compared to other sintering polymers [44].

Exfoliated graphite nanoplatelets (GNP) from XG Sciences were used as the reinforcement phase. In general, GNP can be dispersed in water, solvent, thermoset and thermoplastic polymers and can enhance the properties of polymers due to its excellent in-plane mechanical, structural, thermal, and electrical properties [137-139]. GNP is commercially available and its superior properties have made it an ideal alternative choice of reinforcement that can lead to low cost PNCs with enhanced multifunctional performance. A range of properties of GNP used in this study is represented in Table 2.1.

Figure 2.1 illustrates a representative AFM phase image of a single GNP on a mica substrate giving information about typical dimensions and shape of GNP agglomerate.

**Table 2.1 Properties of GNP used in the study [140-142]**

Physical structure	Platelet
Chemical structure	Graphene
Diameter ( $\mu\text{m}$ )	$\sim 1$
Thickness (nm)	10-20
Tensile modulus (in-plane) (GPa)	$\sim 1000$
Tensile Strength (GPa)	10-20
Electrical resistivity ( $\Omega\cdot\text{cm}$ )	$\sim 50 \times 10^{-6}$ (in-plane) $\sim 1$ (normal)
Thermal conductivity (W/m.K)	3000 (in-plane) 6 (normal)
specific surface area	300-750 $\text{m}^2/\text{g}$
Density ( $\text{g}/\text{cm}^3$ )	2

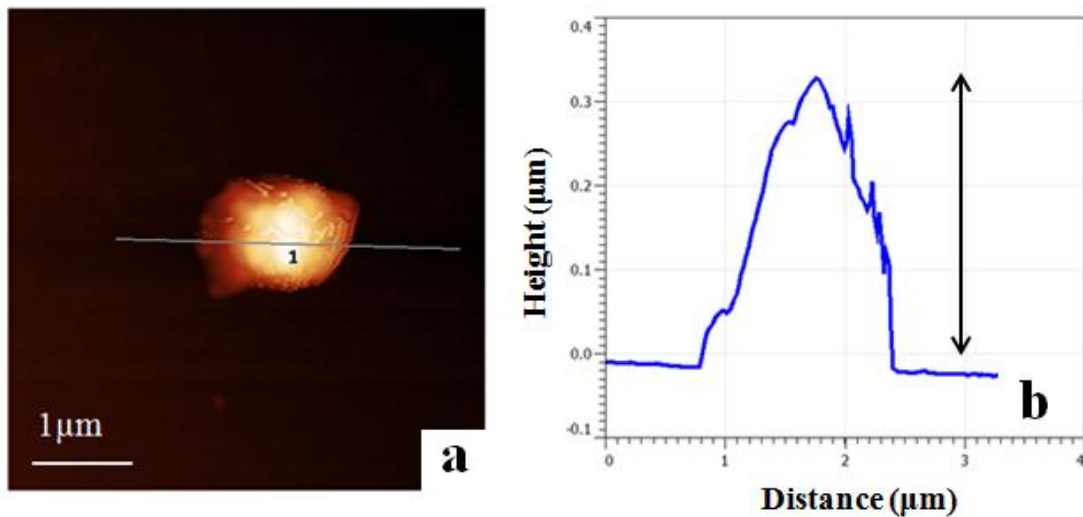


**Figure 2.1 (a) AFM height image of pure GNP on a mica substrate and (b) the height information along the profile line across the GNP as a function of distance**

The exfoliated graphite consists of stacks of graphene sheets held together by van der Waals forces and is the product of an exfoliation process of acid intercalated graphite

layers (e.g. graphite treated by an oxidizing acid) followed by rapid heating in a microwave, shear pulverization using a vibratory mill and sonication to increase the characteristic properties of graphite such as the aspect ratio and surface area [25, 140, 143]. Figure 2.2 schematically shows typical steps used to produce high aspect ratio exfoliated graphite nanoplatelets with small diameters (right) from intercalation of natural graphite (left). It is noted that GNP consists of multilayer graphene sheets with an interplanar spacing of 0.335 nm [144]. Based on the overall thickness of GNP used in this study (Table 2.1), it is estimated that around sixty graphene sheets stack to form a GNP layer of 20 nm thick.

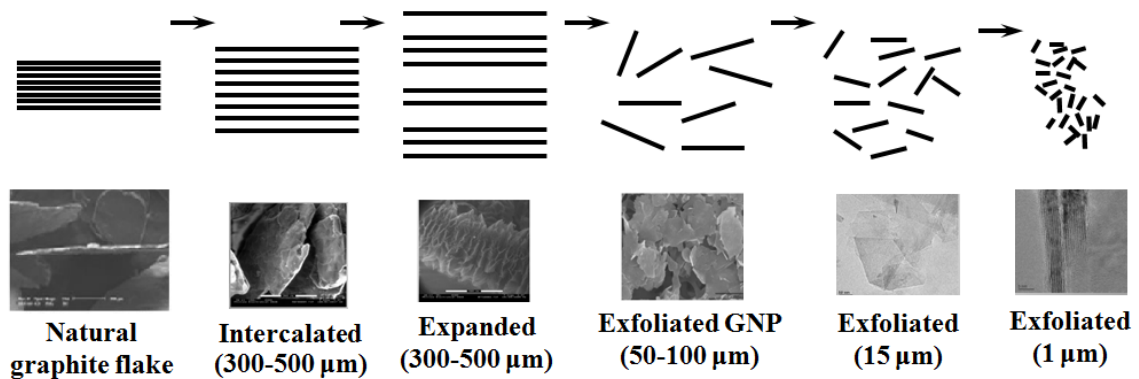


**Figure 2.2 One synthesis route for fabrication of exfoliated graphite nanoplatelets from natural graphite flake [25, 140]**

## 2.2 Processing of PNCs

In this study, the composites were made in a two-step process: i) compounding and ii) forming/shaping using either injection molding (IM) or selective laser sintering (SLS). For a given material system, compounding is the key factor that defines the orientation, alignment and agglomeration of the nanomaterials within the polymer, which, in turn, dictate the performance of the resulting nanocomposites.

### 2.2.1 Compounding

The compounding method used is the coating method reported in [27] for compounding GNP with PP powder. In more detail, the PA12 powder was coated with GNP up to 15 (wt%). As-received GNP was mixed in isopropyl alcohol (IPA) using ultrasonic energy (UIP500hd, Hielscher USA) for 45 min with amplitudes of 80% and manual mixing of the neat PA12 powder in the solution [27]. The solution of the nanocomposite powder was filtered, and the residual coated powder was then thoroughly dried in a vacuum oven at 100 °C for 10 hrs to minimize the hydrolytic degradation. The GNP/PA12 compound was kept in sealed containers to avoid degradation of the material upon contact with the air moisture.

The coating method used for compounding was found to be more effective compared to the direct melt mixing, based on the mechanical and rheological properties of the PNCs as is shown in Figures 2.3 and 2.4, respectively. The hypothesis is that the coating method results in more homogeneous dispersion of GNP within the PA12 matrix. The strength of composites is dictated by the load transfer ability at the GNP-PA12 interface so it is more sensitive, compared to the modulus to the presence of agglomerates. Thus as a first attempt to assess the effect of the compounding method on the dispersion of GNP within the PA12 matrix, the flexural strength of composites made by the coating method followed by injection molding was compared to that of those made by direct melt mixing followed by injection molding. It is noted that the optimized processing parameters (presented below) of the extruder and injection molding unit were used in the assessment of the compounding method. According to Figure 2.3, the coating method significantly enhances the flexural strength of GNP/PA12 composites, especially at low GNP contents, indicating more homogeneous dispersion and distribution of GNP within the polymer.

The GNP-PA12 interfacial interactions were assessed using the rheological behavior of the polymer nanocomposites at melt state. A detailed comparison of the

dynamic viscosity of the nanocomposites at low frequency as a function of the compounding method employed and the GNP content is presented in Figure 2.4. Low-frequency dynamic viscosity is used because it is sensitive to the presence of nanomaterials and to the strength of the interfacial interactions [145, 146]. The results clearly indicate that stronger interfacial interactions are present when the coating method is used due to more available GNP surface. The findings are in good agreement with the flexural strength results reported in Figure 2.3 and with experimental results, reported elsewhere [147], that demonstrated direct correlation between degree of dispersion of nanomaterials and viscosity. Therefore, the coating method is utilized in the rest of the study.

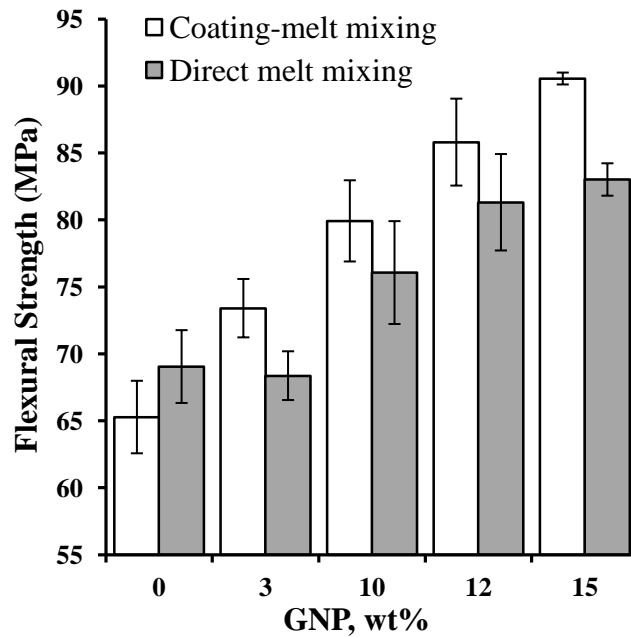


**Figure 2.3 Effect of compounding method and GNP content on the flexural strength of GNP/PA12 nanocomposites**

In order to eliminate any effect of the coating method (extensive immersion in isopropyl alcohol) on PA12 a control PA12 specimen using the coating method was made

and tested. Furthermore, to eliminate any effect of possible cross-contamination that may be interpreted wrongly as property enhancement, every time a composite was made using the injection molding unit, a control PA12 was made as well.

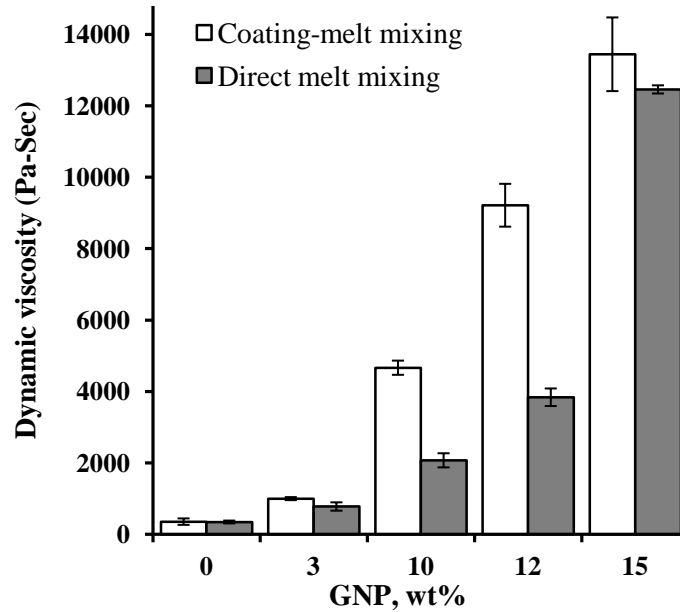


**Figure 2.4 Effect of compounding method and GNP content on the dynamic viscosity of GNP/PA12 nanocomposites measured at  $\omega=0.1$  rad/s and  $T=190$  °C**

### 2.2.2 Injection Molding

This traditional polymer processing method was chosen as a more economical and simple technique compared to other common methods; it and has shown promise in scaled up fabrication of most thermoplastic PNCs [26, 27]. In this work, GNP-coated PA12 powder prepared by the coating method described above was fed into a DSM Micro 15cc Compounder (vertical, co-rotating twin-screw micro extruder) followed by injection molding. The processing parameters, optimized with respect to the flexural and impact properties for the resulting PNCs, were  $T_{\text{barrel}} = 190$  °C, screw speed of 60 and 100 rpm for 1 and 2 min, respectively,  $T_{\text{mold}}=80$ °C and a pressure of ~750 KPa. These

processing conditions are a result of an optimization process. As reported [26], the processing conditions in melt mixing and injection molding, such as the screw RPM, extrusion temperature, shear intensity, melt residence time and mold temperature, are critical factors that determine the dispersion and distribution state of nanomaterials and thus the final properties of the parts.

In this study, several sets of parameters were examined to optimize the IM process. The GNP concentration of 3wt% was chosen as an intermediate loading considered in this work. The optimal processing parameters were chosen as those that maximized the flexural properties and the impact resistance of the 3 wt% GNP/PA 12 PNC, since the latter are remarkably sensitive to the level of agglomeration. Table 2.2 shows the processing parameters optimized and their corresponding range.

**Table 2.2 Process parameters investigated for melt mixing injection molding processing of GNP/PA12 composites and process optimization**

Run ID	RPM	T <sub>barrel</sub> (°C)	Residence time (min)	T <sub>mold</sub> (°C)
IM1	200	180	3	70
IM2	100	190	3	70
IM3	100	190	3	80
IM4	100	190	1	80
	200		2	
IM5	60	190	1	80
	100		2	
IM6	60	190	4	80

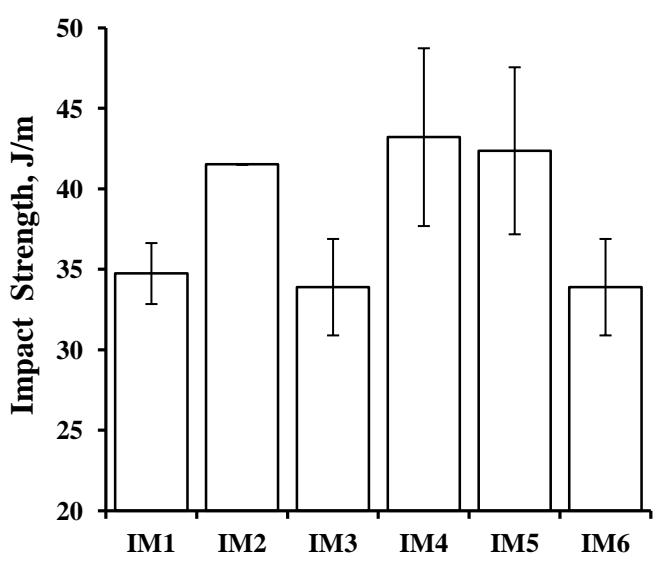
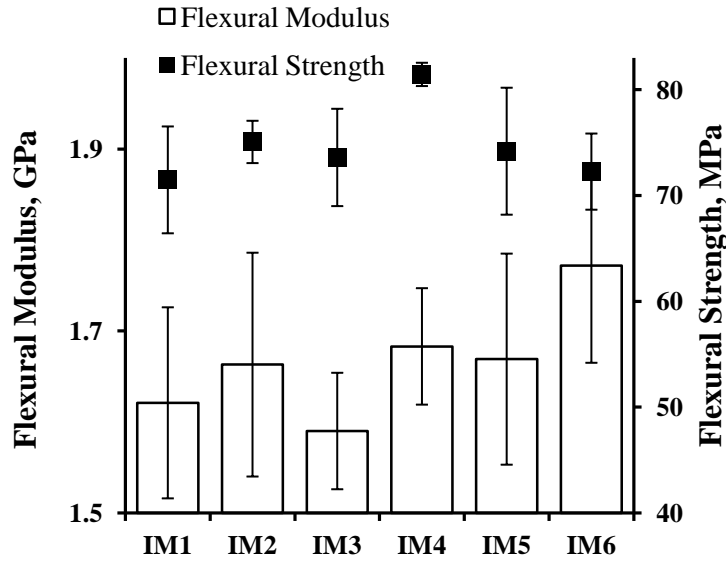


**Figure 2.5 Dependence of the flexural properties (top) and impact strength (bottom) on process parameters in IM processing of 3wt% GNP composites**

Figure 2.5 (top) illustrates variations in flexural modulus and strength of melt mixed and injection molded composites as a function of the processing parameters. It is clearly demonstrated that the composites fabricated using parameters corresponding to IM4 exhibit maximum flexural strength while maintaining a flexural modulus that was similar to that found in other runs. Figure 2.5 (bottom) depicts the impact resistance of

the PNCs as a function of the processing parameters. It is shown that the IM4 and IM5 runs result in maximum impact performance of PNCs. Thus according to Figure 2.5, the processing conditions that correspond to the IM4 run were determined as the optimum ones and employed in the rest of this study.

### **2.2.3 Selective Laser Sintering**

Selective laser sintering was also employed to make GNP/PA12 nanocomposites. SLS, an additive manufacturing technique, has the following advantages compared to traditional polymer/composite processing methods as mentioned earlier in section 2.1: i) controlled placement/orientation of nanomaterials, ii) absence of large shear forces that are present in conventional melt mixing processes, iii) no need for expensive tooling such as molds, iv) ability to fabricate functionally graded parts where composition and properties vary through the thickness, and enhanced design flexibility and detailed features on the sintered parts. Furthermore, very recent studies have shown SLS makes it feasible to fabricate PNCs of PA12 matrix reinforced with carbon based nanomaterials. The studies have demonstrated multiple-property enhancement for the sintered PNCs that also exhibited lower electrical percolation threshold than the parts made by IM process [35, 148].

Preparation of the composite powder with an appropriate particle size and morphology is of a key stage since the compounding not only affects the final characteristics, such as dimensional accuracy and of porosity level, but it also dictates the processing ability of the composite, particularly in additive processes [44]. A Sinterstation® 2000 commercial SLS machine (3D Systems Inc., Valencia, CA) was used to process the GNP/PA12 composite powder. A sieve shaker was used before the SLS process to eliminate the agglomerates and to provide the coated PA12 with more uniform grain size. The processing parameters were optimized with respect to the tensile strength. In this study, a range of laser powers from 5.5 to 10.5W and of scan speeds from 635 to

1524 mm/s were investigated for parameter optimization, because previous research showed that these were the most important of other controllable SLS variables that affect the quality and properties of the parts [35, 149]. The parameters used, which maximized the tensile strength of 5wt% GNP/PA12 composites and yielded SLS parts with good geometric accuracy and density are: laser power of 8.5 W, laser scan speed and spacing of 762 mm/s and 152.4  $\mu\text{m}$  respectively, part-side temperature set-point of 171 °C (PA12) and 170 °C (PNCs) and powder feed temperature set-point of 100 °C. The process was operated at a roller speed of 76.2 mm/s, powder layer thickness of 101.6  $\mu\text{m}$  and piston temperature of 135 °C.

### 2.3 Characterization Techniques

The tensile properties of the specimens were determined according to ASTM D638 using an Instron 33R 4466 apparatus with a 500 N load cell and an extensometer (Instron 2630-101) with a gage length of 10 mm. A displacement control with a velocity of 2.54 mm/s was applied. The flexural properties were measured based on a three-point bending test according to ASTM D790 on an MTS 810 Material Test System (MTS Systems Corp., Eden Prairie, MN) at a crosshead speed of 1.27 mm/min and a span of 50.80 mm. The impact resistance of the specimens was determined according to ASTM D256 using an Izod pendulum test. Each data point reported is an average of five repetitions.

The thermomechanical behavior was studied by dynamic mechanical analysis (DMA, Q800, TA Instruments) using the single cantilever mode at oscillation amplitude of 0.015 mm and a fixed frequency of 1 Hz. The composites were heated from ambient temperature to 150 °C at a heating rate of 5°C/min.

The X-ray diffraction (XRD) patterns, from 8° to 50° (2 $\theta$ ) at a scanning rate of ~3°/min with divergence and scatter slit of 1/4 ° and 1/2° respectively, of the neat PA12 and the composites were obtained using a X'Pert Pro Alpha 1 (PANalytical, Almelo,

Netherlands) diffractometer in the Bragg–Brentano geometry using a monochromatic, filtered Cu K $\alpha$ 1 radiation. The X-Ray equipment was operated at 45 kV and 40 mA.

Standard differential scanning calorimetry (DSC) and modulated DSC (MDSC) work were performed on a DSC Q2000 (TA Instruments, New Castle, Delaware, USA) using specimens of about 7-10 mg. Nitrogen was used for purging. Measurements were performed from the equilibrate temperature of -30 °C to 200 °C at a heating rate of 3 °C/min and a heating-cooling rate of 5 °C/min on the MDSC and standard DSC modes, respectively. The MDSC makes it possible to decompose the total heat flow signal into reversing and non-reversing heat flow signals. The reversing signal demonstrates heat capacity events including the glass transition and melting, whereas the non-reversing signal most often contains kinetic events such as crystallization and crystal perfection [150]. The reversing heat flow curves upon the heating scan were used to study the melting behavior of the specimens. No annealing or additional scans or thermal history removal was used in order to compare the effects of manufacturing process on the properties of interest.

Electrical conductivity measurements were taken with a Solartron 1260 coupled with a 1296 Dielectric Interface using 0.1 Vac for frequencies ranging from 10 MHz down to 10<sup>-2</sup> Hz. The measurements were performed through cross-sectional planes of bulk PNCs through the length, width and thickness (mutually perpendicular directions) of the composites.

To estimate the interphase characteristics such as thickness and stiffness, AFM experiments were performed. A Veeco AFM with Nanoscope V controller, operated in tapping mode using an aluminum coated cantilever (length of 225  $\mu$ m, spring constant of 45 N/m, resonance frequency of 190 KHz), with silicon tip of 2 nm nominal radius provided by Nanoscience Instruments Inc. Phoenix, AZ was used. To avoid detrimental effects of the soft polymer substrate under the tip and occurrence of artifacts due to contaminations, tapping mode (v.s. contact mode) was used for measurements.

Composites with 0.1 wt% filler content were studied in order to avoid interactions among fillers.

The morphology of the composites and the GNP coated PA12 powder were studied with a Zeiss DSM 940A scanning electron microscope (SEM) operating at 5 kV accelerating voltage. Prior to the SEM study the fracture surface was gold-coated to minimize the charging effects during the SEM observations.

# **CHAPTER 3**

## **EFFECT OF MANUFACTURING METHOD ON THE STRUCTURAL AND MACRO-SCALE PROPERTIES OF GNP/PA12 NANOCOMPOSITES**

Two primary reasons for fabrication of PNCs are their enhanced macro-scale properties and their multifunctional performance compared to polymers, which make them potential candidates for various applications. Properties exhibited by PNCs are directly correlated to their hierarchical microstructure, which is mainly affected by the properties of the constituents, the nanomaterial-polymer interfacial interactions and processing methods/conditions employed to make the composites. Although some established trends are exhibited by polymer properties modified with addition of nanomaterials, in general PNCs present unexpected macro-scale properties, as a variety of phenomena at the nano-scale dominates the macro-scale properties. Therefore, further understanding of the complex process-structure-property relationships is a critical factor in manufacturing PNCs with tailored macro-scale performance and multi-functionality. In particular, the manufacturing method/conditions dictate the structural and morphological characteristics and thus the property enhancement or deterioration of reinforced polymers [207,208]. It has been well demonstrated that proper dispersion and specific controlled orientation of nanomaterials, as well as enhanced quality of adhesion between the nanomaterials and the polymer, are dramatically dependent on the manufacturing method/conditions and are required in development of PNCs with desired properties. On the other hand, understanding the correlations that bridge the gap between the manufacturing method/conditions and the micro-scale behavior of the composites remains a major technical and scientific challenge.

The goal of this chapter is to provide a better understanding of how the manufacturing method affects the macro-scale performance of GNP/PA12 composites including tensile, flexural and impact properties, thermo-mechanical properties and electrical conductivity. This work will focus on the role of structure, morphology and interfacial interactions. To achieve this, two classes of manufacturing methods are employed: i) SLS and ii) IM. In order to eliminate the effect of compounding on the properties of composites, the same compounding method, which is coating of the PA12 powder with GNP as discussed in chapter 2, was employed in both cases. GNP/PA12 composites containing 0, 3 and 5 wt% of GNP were made. The following notation is used throughout the chapter: i) PA12-IM (injection molded neat PA12), ii) 3 and 5GNP/PA12-IM (injection molded 3 and 5wt% GNP/PA12 specimens, respectively), iii) PA12- SLS (SLS sintered neat PA12), iv) 3GNP/PA12-SLS and 5GNP/PA-SLS (SLS-processed 3 and 5wt% GNP/PA12 specimens, respectively).

### **3.1 Mechanical Performance**

The tensile modulus and strength of GNP/PA12 composites made by SLS and IM with 0, 3 and 5 wt% GNP are shown in Figure 3.1 The following observations are made: i) SLS processing of neat PA12 dramatically increases both the strength and the modulus compared to the corresponding properties of PA12 processed by IM, ii) addition of GNP to PA12 processed with IM enhances the strength and modulus of neat PA12. However, when SLS is used addition of GNP improves the modulus but not the strength. Specifically, addition of 3 wt% GNP leads to the greatest modulus enhancement both in SLS and IM-processed composites with 48% and 22% enhancement in modulus respectively compare to that of the neat PA12 processed similarly.

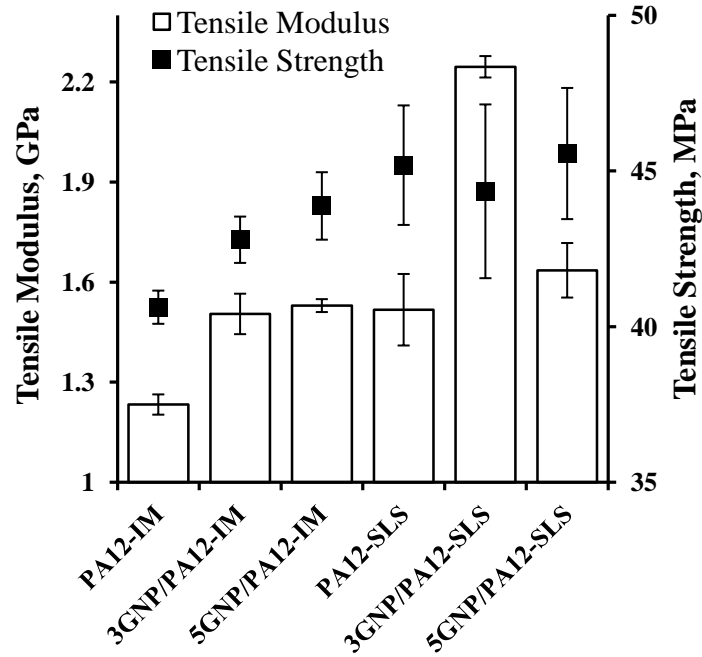


**Figure 3.1 Effect of manufacturing on the tensile modulus and strength of GNP/PA12 composites**

The reduction in tensile modulus of SLS composites at 5wt% GNP and the lack of strength enhancement are correlated to unavoidable GNP aggregation that acts against the reinforcing ability of GNP. As the GNP content increases, GNP interferes with the sintering process, masking the polymer powder, leading to variations in the melting of PA12. The tensile strength is sensitive to the dispersion state of nanomaterials [142, 151], so it is speculated that IM composites exhibit better dispersion/distribution of GNP. The different densities of the SLS and IM composites ( $1.037$  and  $1.05 \text{ gm/cm}^3$  respectively for 5wt% GNP) do not justify the observed differences in mechanical properties.

The flexural properties of SLS and IM-processed GNP/PA12 composites are presented in Figure 3.2. Once again, both the modulus and the strength of neat PA12 increase significantly when processed by SLS. Composites processed with SLS exhibit lower strength and modulus than the SLS-processed neat PA12 but similar if not better strength and modulus than the corresponding composites processed by IM. It is also

noted that regardless of the manufacturing method used, the 5wt% GNP composites have lower strength than those with 3wt% GNP, an observation that agrees with the tensile results indicating the presence of agglomerates at higher GNP content.

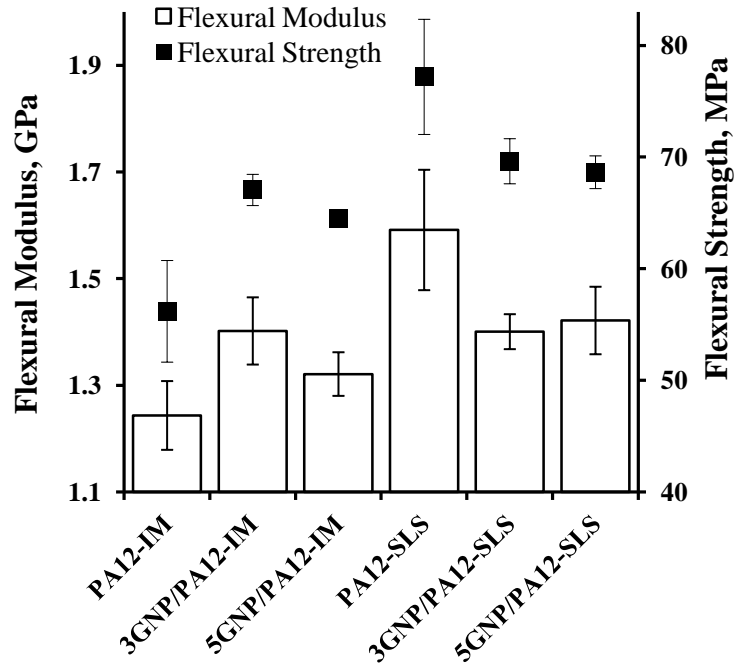


**Figure 3.2 Effect of manufacturing on the flexural properties of GNP/PA12 composites**

The impact strength of GNP/PA12 composites, presented in Figure 3.3, is significantly affected by the manufacturing method and GNP content. The impact strength of composites made by IM increases with GNP content, whereas the strength of the composites made by SLS decreases. It is noted that the manufacturing method had no significant effect on the impact strength of the neat PA12. The decrease in the impact strength of SLS composites may be due to GNP absorbing part of the laser energy; this would reduce the energy available to locally melt the PA12 particles and inter-diffuse

their boundaries resulting thus in structures that can absorb less energy before fracture is reached. The results are in agreement with those reported elsewhere [142, 148, 152].

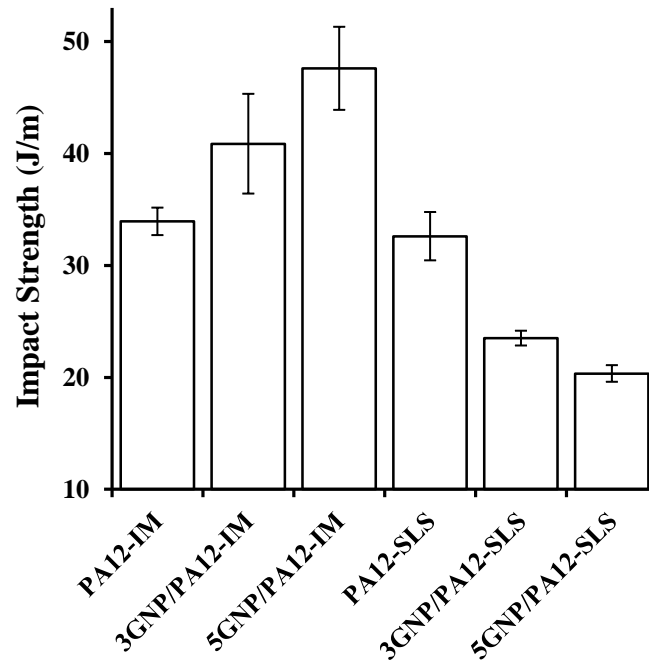


**Figure 3.3 Effect of manufacturing on the impact strength of GNP/PA12 composites**

To better understand how the manufacturing method used to make the composites affects their mechanical properties one needs to investigate the processing-structure relationship first that is understanding how the processing affects the polymer characteristics such as the glass transition temperature, thermo-mechanical properties, degree of crystallinity, and morphology including the dispersion and distribution of the GNP within the polymer. As reported the mechanical properties of polymers filled with nanomaterials are remarkably influenced by the structural characteristics at the micro and nano-scale including polymer crystalline structure and nanomaterial-polymer interactions [153].

As reported elsewhere [154], addition of CNT to PA12 resulted in more pronounced enhancement of the mechanical and thermal properties of PA12 compared to the corresponding property enhancement caused by addition of GNP to PA12. Both GNP/PA12 and CNT/PA12 composites were made by melt mixing followed by compression molding and surfactant was used to improve the distribution/dispersion of the nanofillers. A direct comparison of the GNP/PA12 composite films made by compression molding and the GNP/PA12 bulk specimens made by injection molding or SLS that are investigated in our study is not possible because the compounding method and the GNP size used in [154] and the present study are totally different. The smaller GNP used in our study (diameter of less than 1 micron) is expected to yield larger enhancement of the mechanical properties of PA12 compared to the larger GNP (diameter of ~5 microns) used in [154].

### 3.2 Melting and crystallization behavior of GNP/PA12 composites

The heat flow thermograms obtained by DSC during the melting transition of the GNP/PA12 composites made by SLS or IM are presented in Figure 3.4. The heat of fusion and the corresponding degree of crystallinity, calculated using equation (3.1), are shown in Table 3.1.

$$\chi\% = \frac{\Delta H}{\Delta H_m^\circ \left(1 - \frac{wt\%}{100}\right)} \times 100 \quad (3.1)$$

$\Delta H_m^\circ = 209.3$  J/g was used as the theoretical heat of melting for a 100% crystalline PA12 [155, 156].

The main observation is that when IM is used, both the neat PA12 and the composites exhibit a single melting point at ~ 178 °C, whereas in case of SLS processing the neat PA12 and the composites exhibit an additional melting transition at ~185 °C. These melting temperatures are also reported in Table 3.1. It is noted that the second

high-temperature melting peak gradually disappears with addition of GNP content. This complex melting transition is either the result of crystal polymorphism and/or recrystallization of unstable incomplete crystals during slow heating [134].

In the case of SLS, the second melting peak is associated with the presence of PA12 powder that has not melted during the sintering process and still exists in the composite parts as reported in our previous work [148]. This is confirmed by considering the melting behavior of as-received PA12 powder shown also in Figure 3.4. The pristine PA12 powder has higher melting point and significantly higher degree of crystallinity, as shown in Figure 3.4 and Table 3.1 respectively, than the PA12 processed by either SLS or IM. The double melting peak is characteristic either of alpha-phase or mix of alpha and gamma phase PA12 crystals as pure gamma phase crystals exhibit only one melting peak [157].

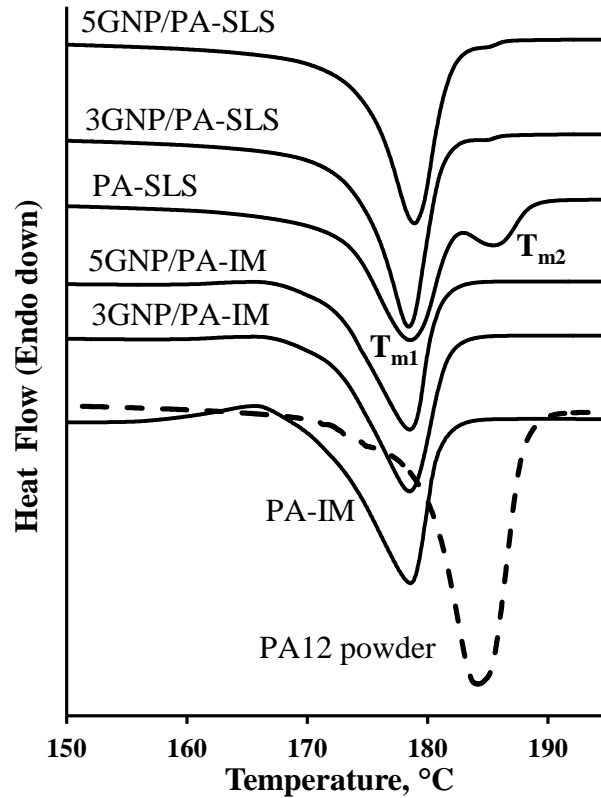


**Figure 3.4 Effect of manufacturing on the melting behavior of GNP/PA12 SLS ( $T_{m1}$  and  $T_{m2}$  main and secondary melting temperatures respectively)**

The degree of crystallinity of neat PA12 increases by 18% when SLS is used, which may explain the observed difference in mechanical properties of the SLS and IM neat PA12. However, upon addition of GNP the degree of crystallinity decreases regardless of the manufacturing method used. It is noted that the degree of crystallinity does not affect all the mechanical properties the same way. Tensile strength and modulus are expected to increase with crystallinity. This is not the case for the impact strength and ductility which tend to decrease with the degree of crystallinity and depend also on the size and type of crystallites. These results indicate the presence of a secondary mechanism, the reduction in the degree of crystallinity; which is acting against the main reinforcing mechanism responsible for the enhancement of tensile modulus which is the stiffening effect of GNP.

The crystallization characteristics of GNP/PA12 composites were further studied using XRD. As shown in Figure 3.5, the pristine PA12 powder exhibits two peaks very close to each other at  $2\theta$  equal to  $21^\circ$  and  $22^\circ$  respectively which are characteristics of the less common alpha phase crystals [158]. A hump on the right of the first peak at  $2\theta$  equal to  $21.3^\circ$ , characteristic of the gamma phase [158], can be also seen. The XRD pattern of the as-received pristine PA12 powder is in agreement with the melting behavior of the PA12 powder presented in Figure 3.4 confirming the presence of a mix of alpha and gamma crystalline forms. In the case of IM processed PA12 and GNP/PA12 composites, there is only one peak at about  $2\theta$  equal to  $21.3^\circ$  indicating the presence of gamma-phase crystal. The melting during the processing results in alpha-phase to gamma-phase transition as reported also elsewhere [157]. The SLS processed PA12 and GNP/PA12 composites also exhibit only one peak which, however, is at slightly higher  $2\theta$  values and is broader than the peak of the IM processed specimens indicating the presence of some residual alpha-phase crystals in the SLS processed specimens which is expected considering that the PA12 is not fully melted during SLS processing. The characteristic

graphite peak at  $2\theta=26.2^\circ$  is more evident on patterns of IM composites with high GNP content [159, 160].

**Table 3.1 Effect of manufacturing and GNP on melting temperature and crystallization characteristics of GNP/PA12 composites**

Sample	$T_{\text{melt}} (\text{°C})$	$\Delta H_f (\text{J/g})$	$\chi\%$
PA12 powder	184.2±0.1	104.2±3.3	49.8±1.6
PA-IM	178.6±0.1	61.2±0.2	29.3±0.1
PA-SLS	178.7±0.6	76.2±3.1	36.4±1.4
	185.9±0.3		
3GNP/PA-IM	178.7±0.5	49.6±0.4	24.4±0.2
3GNP/PA-SLS	178.4±0.1	56.6±0.7	27.9±0.4
	184.9±0.3		
5GNP/PA-IM	178.5±0.1	48.6±0.1	24.5±0.1
5GNP/PA-SLS	178.9±0.1	47.9±1.4	24.1±0.7
	185.1±0.1		

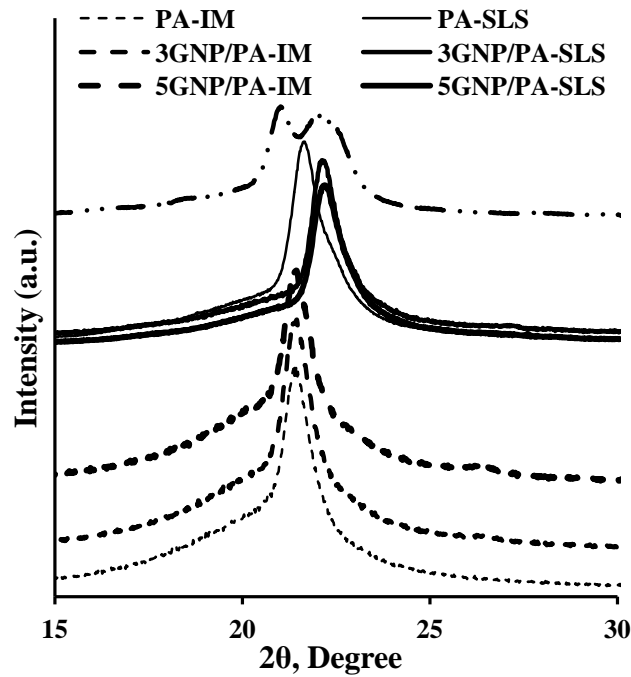


**Figure 3.5 Effect of manufacturing on the XRD patterns of GNP/PA12 composites (the curves are shifted vertically for clarity)**

The lamella thicknesses of the crystals were estimated using the Debye-Scherrer equation and the full width at half maximum (FWHM) of predominant reflections yielded by the XRD patterns:

$$L_t = \frac{K\lambda}{\beta \cos \theta} \quad (3.2)$$

where  $L_T$  is the lamella thickness,  $K$  is the crystal shape factor, which was taken as 0.9,  $\lambda$  is the wavelength of the x-ray radiation (0.154 nm),  $\beta$  is the full width at half maximum and  $\theta$  is the peak position of the XRD reflections [161]. It is noted that no deconvolution of the XRD peaks was performed and so, using equation 3.2, one can only obtain a rough estimate of the lamella thickness. In order to obtain more accurate quantitative values and exact information about the crystalline reflection peaks, it is essential to employ a deconvolution method and exclude the broad amorphous components [154, 162, 163]. It is observed that the lamella thickness remains invariant with respect to the GNP content and manufacturing process and it is in the range of ~ 10-12 nm. In particular, deconvoluting the observed original peaks is also of importance in evaluating presence of unmelted PA12  $\alpha$ -form crystals after sintering process as suggested earlier.

The effect of manufacturing on the crystallization of PA12 was further investigated by DSC. As shown in Figure 3.6, the crystallization onset temperature,  $T_{C/onset}$ , and the peak temperature,  $T_{C/peak}$ , of the GNP/PA12 composites increase monotonically upon addition of GNP in case of IM. When SLS is used addition of 3wt% GNP leads to an initial shift in  $T_{C/onset}$  and  $T_{C/peak}$  of neat PA12 with no further increase upon addition of more GNP. The increase in  $T_{C/onset}$  indicates that graphite acts as a nucleating agent for PA12, and this nucleating action is more dominant in case of IM-processed composites. It is noted that in SLS composites there are GNP agglomerates and thus a reduced number of effective nucleation sites at 5wt% GNP. Even the coating compounding method used cannot eliminate these agglomerates because there is not enough polymer to keep the platelets apart; however, the agglomerates may break by the

high shear forces present in the melting stage of IM. That is why there is a saturation effect on the nucleation action of GNP in SLS composites,  $T_{C/onset}$  does not increase for GNP content higher than 3 wt%. The neat effect of manufacturing on the initiation of crystallization (not accounting for the nucleating action of GNP) can be determined by comparing the  $T_{C/onset}$  and  $T_{C/peak}$  of the neat PA12 processed by the two methods. As shown in Figure 3.6, crystallization initiates earlier (at higher temperature) in the case of IM and takes less time to complete.

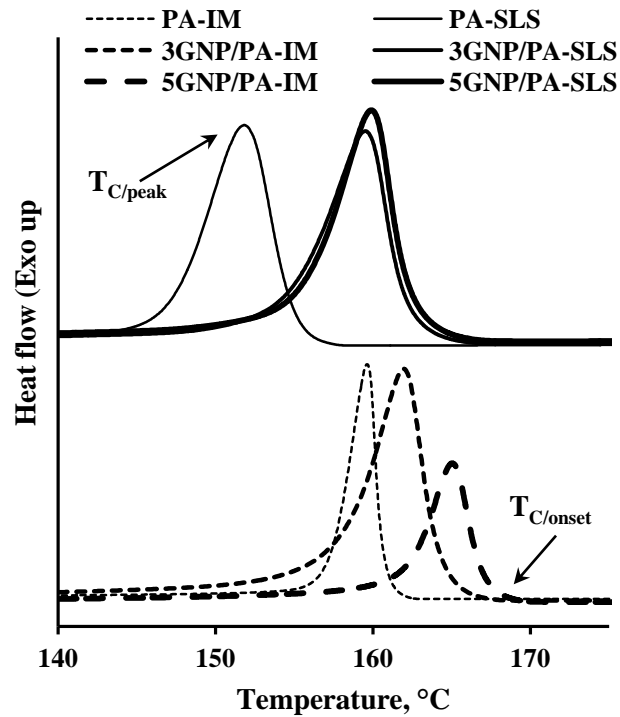


**Figure 3.6 Non-isothermal DSC cooling curves of SLS and IM GNP/PA12 composites v.s. temperature and GNP content**

### 3.3 GNP-PA12 Interfacial Interactions

Interfacial interactions dictate the load transfer mechanisms at the GNP-PA12 interface and thus the bulk properties of polymer composites and can lead to

immobilization of the polymer chain at the GNP surface. In case of SLS processing this pinning of the polymer segments may interfere with consolidation [164]. The interfacial interactions and their correlation to the bulk properties of the composites were assessed using DMA. The  $\tan\delta$  (the ratio of dissipated to stored energy) and the  $T_g$  of the GNP/PA12 composites made by either SLS or IM are shown in Figure 3.7 and Table 3.2 respectively. SLS processing results in both neat PA12 and GNP/PA12 composites with higher  $T_g$  than the corresponding counterparts made by IM (e.g. a difference of 10 and 5 % in case of neat and 5wt% GNP parts, respectively) . The increase in  $T_g$  of SLS processed PA12 indicates greater restriction against segmental motion of amorphous chains. The addition of GNP had no effect on the  $T_g$  of SLS-processed composites (~55.8 to 55.3 °C for neat and 3wt% GNP parts, respectively) whereas  $T_g$  was increased with GNP in the case of IM processing (~50.9 to 53.6 °C for neat and 3wt% GNP parts, respectively).

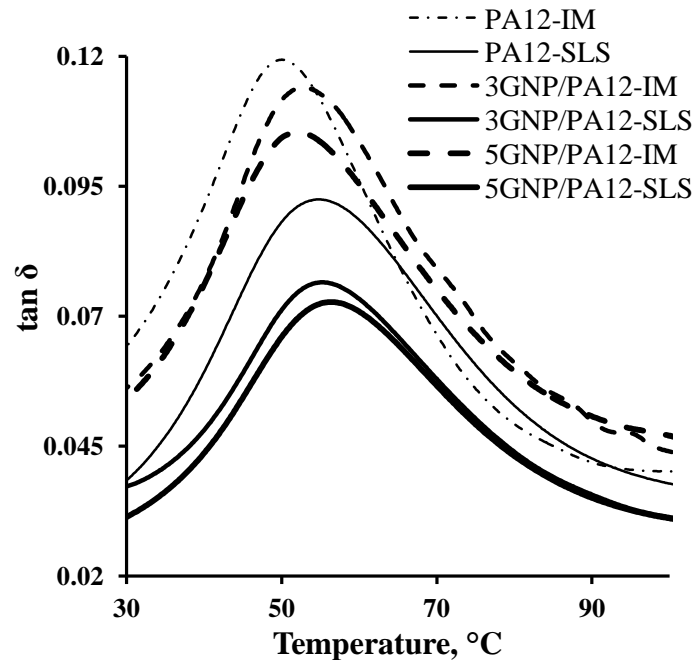


**Figure 3.7 Effect of manufacturing method on the  $\tan\delta$  (damping) of GNP/PA12 composites**

The observed changes in  $T_g$  are related to the competing effects of i) GNP and hard PA12 crystallites that enhance chain immobilization and thus  $T_g$ , ii) GNP agglomeration that increases the free volume among polymer chains, as compared to well dispersed GNP, and decreases available interface, decreasing  $T_g$ , and iii) porous structure and residues of unmelted PA12 powder, specific to the SLS process, that has negative effect on  $T_g$  [122, 165].

**Table 3.2  $T_g$ ,  $\tan\delta$  and storage modulus of GNP/PA12 composites processed by either SLS or IM (standard deviation is less than 10%)**

Sample	$T_g$ (°C)	$\tan\delta @ T_g$	Storage modulus above $T_g$ (MPa)	Storage modulus below $T_g$ (MPa)
PA-IM	50.9±0.8	0.119	391.2	1194.4
PA-SLS	55.8±0.5	0.114	431.7	1146.2
3GNP/PA-IM	53.6±0.7	0.105	465.3	1301.9
3GNP/PA-SLS	55.3±0.2	0.093	464.7	1184.1
5GNP/PA-IM	53.6±0.5	0.076	523.8	1096.5
5GNP/PA-SLS	56.3±0.3	0.072	623.3	1321.2

As shown in Figure 3.7,  $\tan\delta$  of both the neat PA12 and the GNP/PA12 composites significantly decreases across the temperature regime investigated when SLS is used and when GNP is added. The observed results indicate that the energy damping ability is compromised, which is in agreement with the observed decrease in impact strength, and the elastic behavior is enhanced. In addition to the compromise of the damping ability upon addition of GNP, the degree of crystallinity also decreases, significantly more in case of SLS-processed composites, although it still remains higher than the degree of crystallinity of their IM counterparts. Consequently, it is concluded that a rigid interface is formed that consists mainly of immobilized amorphous polymer chains.

The storage modulus of the GNP/PA12 composites as a function of the manufacturing method used and the GNP content at temperatures below and above  $T_g$  are also presented in Table 3.2. At temperatures below  $T_g$ , where the modulus is dictated by the stiffening effect of GNP there is no effect of the manufacturing method used. However, at temperatures above  $T_g$  neat PA12 and composites processed by SLS exhibit higher storage modulus than their corresponding counterparts made by IM. This indicates the presence of a secondary reinforcement mechanism that is more effective in SLS systems than IM ones, and is related to the immobilization of amorphous polymer chains at the GNP or PA12 crystal surface.

### 3.4 Electrical Behavior of GNP/PA12 Composites

The electrical conductivity of GNP/PA12 composites made by either SLS or IM is shown in Figure 3.8. The schematic in the insert of Figure 3.8 shows the direction along which the conductivity was measured. It is noted that sintering is occurring along the x-y plane, whereas injection molding along the x-direction. The 5wt% GNP/PA12 composites made by SLS exhibited the highest electrical conductivity, which is four orders of magnitude higher than the conductivity of the corresponding composite made by IM. The results demonstrate that the percolation threshold is lower than 5wt% GNP and that a GNP conductive network exists when composites are made using SLS. It is suggested that the shear forces during melt mixing/injection molding lead to breakage of the GNP conductive network that is formed as a result of the coating method used during compounding, resulting thus in an increase in the electrical percolation threshold. In addition, IM induces alignment of GNP along the injection molding direction and as reported in [22, 143, 166] the percolation threshold is higher in aligned than in randomly distributed filled systems. **It is noted that the more insulating samples (neat polymer and composites with graphite content lower than the percolation threshold) tend to be a lot**

noisier and therefore the error bars tend to be larger. It is possible that these samples are picking up some moisture that could potentially lower their resistance.

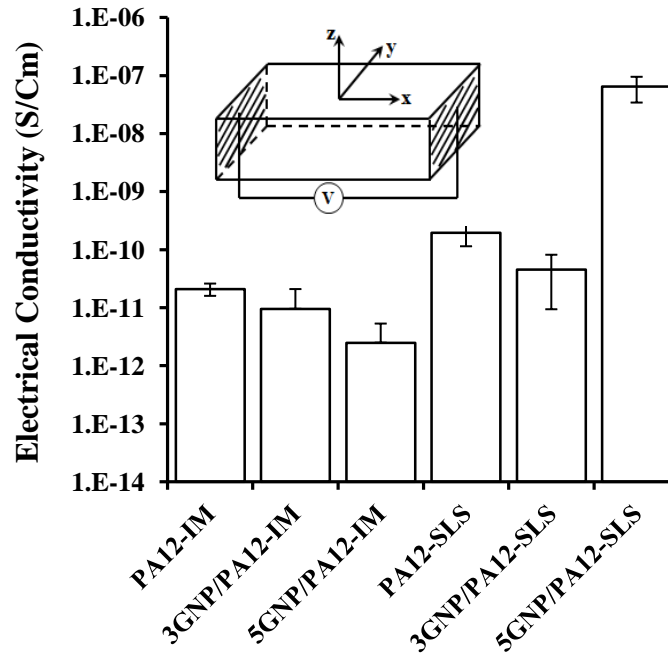


**Figure 3.8 Electrical conductivity of GNP/PA12 composites made by either SLS or IM**

### 3.5 Morphology of GNP/PA12 Composites

Representative SEM images of as received and coated with GNP PA12 powder are shown in Figures 3.9 a-d. At high GNP content, i.e., 5 wt%, there are so many platelets that there is not enough polymer to keep the platelets apart and thus agglomerates are forming no matter whether IM or SLS processing was used to make the composites. The agglomerates form during the coating/compounding process. The PA12 powder, shown in Figures 3.9a and 3.9b, is coated with GNP. The GNP coated PA12 powder is shown in Figures 3.9c and 3.9. According to theoretical calculations based on the PA12 particle/powder diameter (50-100 microns) and the dimensions of the GNP, a monolayer coverage of PA12 particle with GNP is achieved at 0.8-1.6 wt% of GNP.

Further addition of GNP forms multilayer coating of GNP and thus agglomerates. The high shear and elongation stresses during melt mixing and injection molding respectively and the flow of the PA12 viscous melt are able to break down some of these agglomerates when IM is used. However, in case of SLS processing where the PA12 particles are only locally melted and sintered the GNP agglomerates still exist.

A special feature on SLS-processed specimens is that the top surface is less dense, containing micro-size porosity and voids as shown in Figure 3.10a. This is because each layer beneath the top surface has been subjected to doses of thermal energy from the laser sintering of the layer above it. The energy dose for each layer is tuned to sinter that layer and to propagate through the thickness of that layer so as to remelt a shallow portion of the layer underneath to ensure good layer-to-layer bonding. The remelting seals off any residual surface porosity in the underlying layer. The last (top surface) layer does not experience such a dose and is thus left with a porous top surface. This micro-porosity is not present in the interior of the SLS-processed specimens as indicated in the fracture surface of 5GNP/PA12 SLS composite shown in Figure 3.10b. Finally, comparison of the fracture surface of SLS and IM composites at 5wt% GNP, shown in Figures 3.10b and c respectively, confirms the mechanical property results, especially those of impact strength. IM composites have a rougher surface, indicating more energy dissipation mechanisms. Finally, based on comparison of the fracture surfaces of SLS and IM composites at 5 wt% GNP, shown in Figures 3.10b and 3.10c respectively, it seems as there are more GNP in case of SLS. Considering that both composites contain the same amount of GNP, it can be concluded that the GNP is better dispersed in the case of IM composites so the agglomerates, if any, are smaller and cannot be seen at the magnification used. There are fewer GNP agglomerates in IM composites (Figure 3.10c) compared to those present in SLS composites (Figure 3.10b).

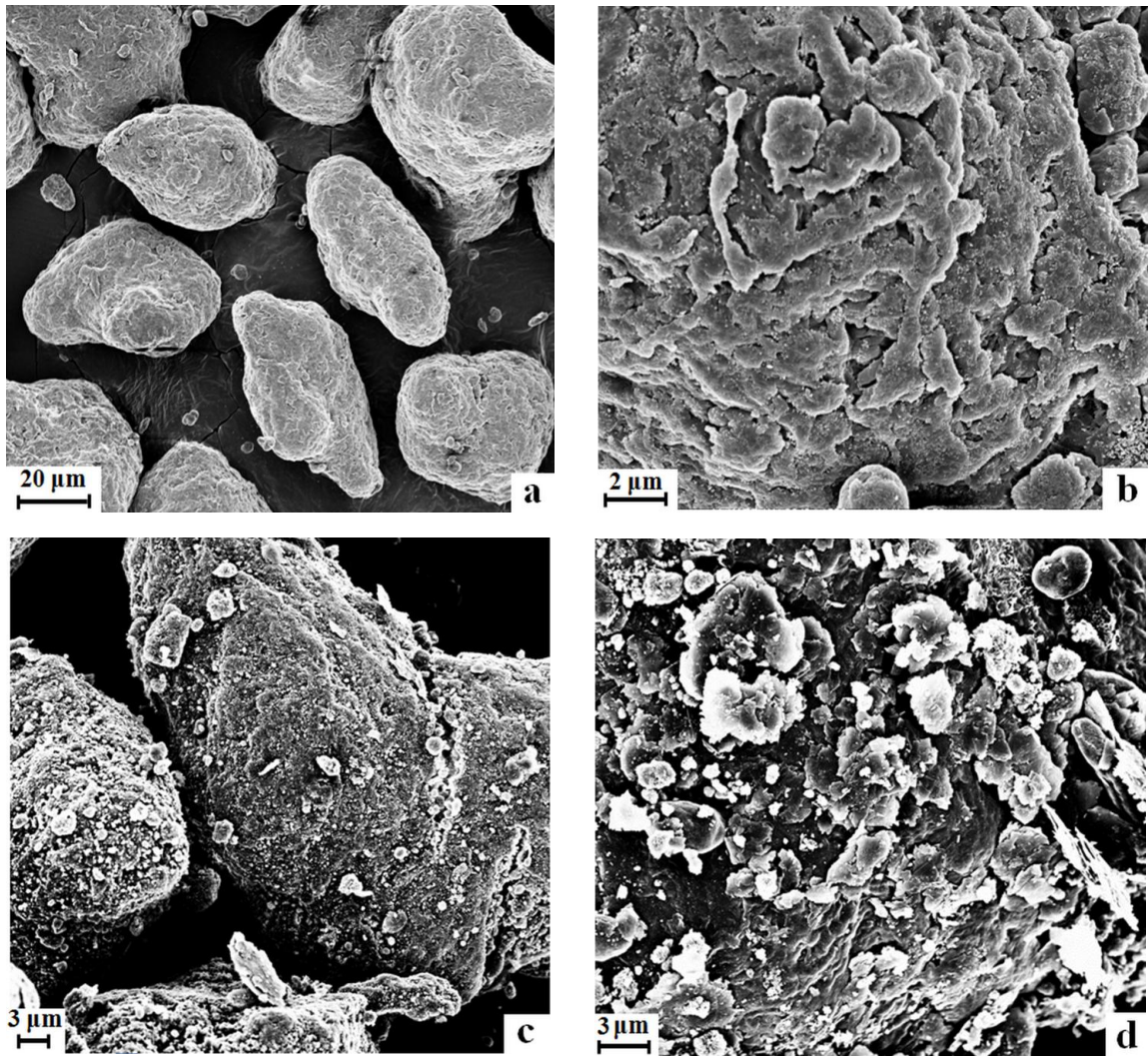


**Figure 3.9 SEM images of PA12 powder at a) low and b) high magnification and 3 wt% GNP-coated PA12 powder at c) low and d) high magnification**

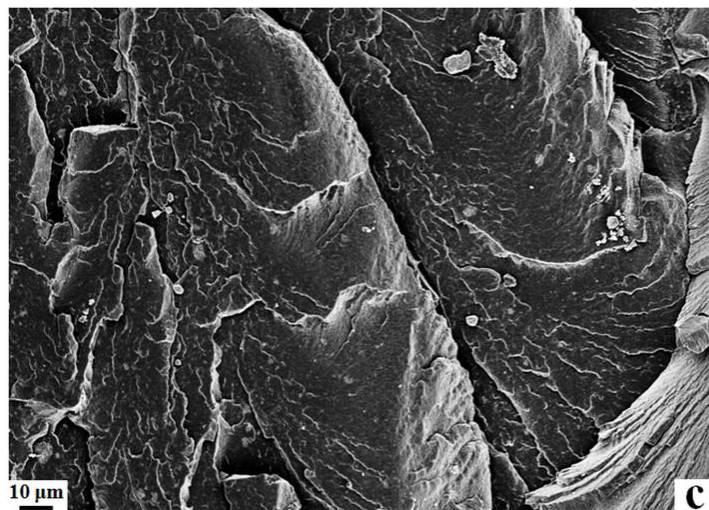
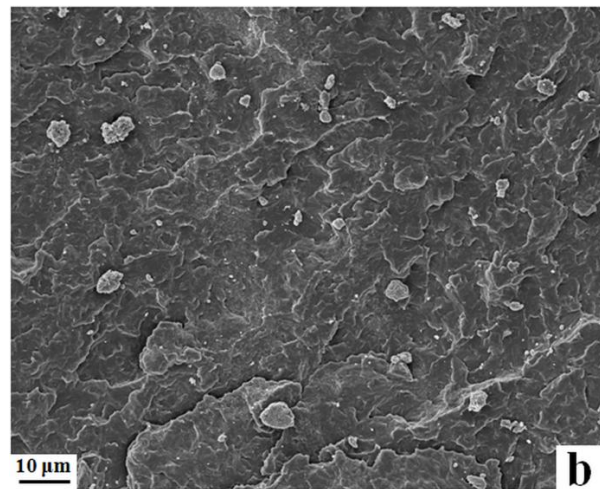
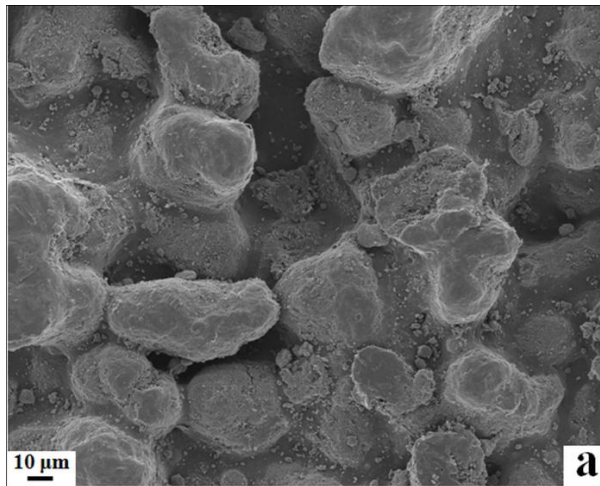


**Figure 3.10 SEM images of a) top surface of PA SLS b) fracture surface of 5GNP/PA12 SLS and c) fracture surface of 5 GNP/PA12 IM**

### 3.6 Conclusions

Multifunctional polymer composites were made and characterized in terms of their mechanical, thermomechanical and electrical properties. The study examined the processing-structure-property relationship in graphite reinforced polyamide 12 composites made by selective laser sintering or by injection molding. SLS led to comparable or higher tensile properties with respect to the IM process. In general it was demonstrated that SLS-made parts yielded comparable or better tensile and flexural performance, which was invariant or decreased upon addition of GNP, compared to IM-processed parts. In contrast to IM, SLS negatively affected the impact resistance of the composites that exhibited toughness decrease upon addition of GNP.

The effect of the sintering method on the physical properties and interfacial interactions of the specimens was evaluated and linked to the observed mechanical properties. It was observed that the degree of crystallinity of PA12 decreased with increasing GNP regardless of the technique used and that GNP acted as nucleating agent. SEM revealed the presence of a finer GNP dispersion in the IM composites. The decreased damping response and increased storage modulus of the specimens above  $T_g$  suggested the presence of a secondary reinforcing mechanism, a stiffening effect due maybe to the presence of smaller but numerous polymer crystallites, that is more effective in case of SLS. The latter effect, combined with improved crystallinity of sintered 0 and 3wt% parts compared with the corresponding IM ones, supported the observed variations in tensile behavior. 5wt% GNP composites processed by SLS exhibited the highest electrical conductivity in the longitudinal direction indicating that formation of conductive paths in IM composites may be destroyed by the high shear forces. SEM investigations confirmed a developed porous structure on the top surface of the SLS specimens and GNP aggregated phase that explained the suppressed impact and flexural performance exhibited by SLS parts with addition of GNP. The observations revealed how the manufacturing method influences the degree of crystallinity, level of

agglomeration and interfacial interactions and thus the macro-scale properties of the composites. This work provides an experimental methodology for understanding the role of nano- and micro structure and interfacial interactions in evaluating and engineering the macro-scale properties of semi-crystalline based composites.

In conclusion this study is the first to report on fabrication of multifunctional graphite nanoplatelets reinforced polymer composites made by selective laser sintering with properties equal to if not better than those of the corresponding composites made by more traditional methods such as injection molding, demonstrating thus the ability to create functionally graded multifunctional composites. The effect of the manufacturing methods used on the electrical properties of PNCs will be elaborated in chapter 6. Moreover, the ability of the SLS process to fabricate PNCs with anisotropic performance is demonstrated and compared with the melt mixing process.

## CHAPTER 4

### EFFECT OF INTERFACIAL INTERACTIONS ON MACRO-SCALE PROPERTIES OF GNP/PA12 NANOCOMPOSITES

Understanding how interfacial interactions at the nano-scale influence macro-scale properties is key in manufacturing of PNCs with properties engineered for specific applications. The high surface to volume ratio, small size and unique intrinsic properties of nanomaterials are expected to significantly enhance bulk performance of PNCs [1, 17, 167, 168]. However, the expected property improvement has not yet been achieved experimentally due mainly to poor nanomaterial-polymer interactions [124, 169, 170]. Although the interface effects can be ignored in the case of micro-sized reinforced polymer composites, they need to be accounted for in the case of PNCs because the interfacial interactions dictate the dispersion and agglomeration of the nanomaterials within the polymer. Moreover, the interfacial interactions significantly define the stress transfer mechanism and alter the physical properties of the polymer matrix dominating thus the macro-scale properties of PNCs in multiple ways [59, 169, 171-173]. The manufacturing process in particular dramatically defines the interfacial interactions and results in enhancing or limiting the overall properties at a given PNC system.

The goal of this chapter is to provide better understanding of how the presence of GNP alters the physical properties of PA12, including glass transition and crystallization behavior, and how a polymer constrained region at the GNP surface, which influences the bulk properties of the GNP/PA12 PNCs, can be assessed. To achieve these, a comprehensive methodology is introduced to determine the links between the interfacial interactions, physical properties of the polymer and macro-scale properties of the PNCs. The correlation between the tensile modulus and the glass transition temperature and the

amount of constrained phase, assessed through the mechanical, thermal, thermo-mechanical, crystallization behavior of the composites, is determined. The presence of a complex constrained phase, consisting of an immobilized amorphous region and a crystalline interphase region, of PA12 at the GNP surface is observed and correlated to a secondary reinforcing mechanism at the interface.

#### **4.1 Tensile Modulus and Glass Transition Temperature of the Nanocomposites**

The Young's modulus and the glass transition temperature, determined as the temperature value of the  $\tan\delta$  peak of GNP/PA12 composites as a function of the GNP content, are presented in Figure 4.1. Both properties follow exactly the same trend; they increase with GNP content up to 5wt%, reach a plateau value at intermediate GNP loadings in the range of 5-10 wt%, and finally continue to increase with GNP content. It is noted that changes in  $T_g$  are related to the primary relaxation of polymer chains and the extent of the immobilized chains [64, 112, 122, 123].

The non-monotonical increase of the modulus and  $T_g$  with GNP content indicates the presence of two competing effects: i) the reinforcing effect of the high modulus graphite ( $E=500-600$  GPa) [174] and ii) formation of GNP agglomerates due to poor GNP dispersion within the polymer [122, 133]. Other effects such as the effect of the polymer's crystallinity and the polymer chain mobility, which are altered upon addition of GNP, on the modulus of the composites, are also considered below. The results in Figure 4.1 indicate the presence of a secondary reinforcement mechanism which contributes to the enhancement of both the tensile modulus and  $T_g$  and is notably influenced by the GNP content and the microstructure of the composites. These observations motivated detailed investigations into the altered dynamics of polymer chains as a result of the extensive GNP-PA12 interfacial interactions.

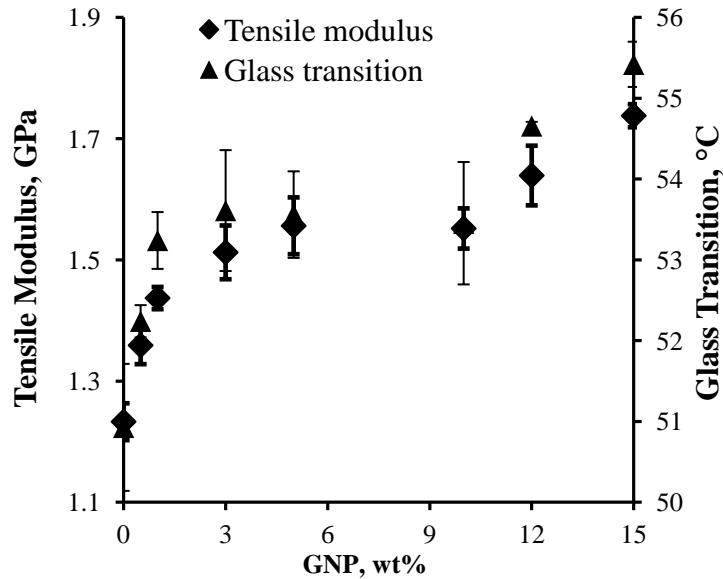


**Figure 4.1 Tensile modulus and  $T_g$  of GNP/PA12 PNCs as a function of the GNP content**

It has been demonstrated that mechanical and viscoelastic properties are slightly affected by the presence of moisture in PA12 polymer. This effect is more pronounced in other polymers in the family of polyamides such as polyamide 6. It has been, however, shown that water absorption influences molecular motions of PA12 chains and causes the glass transition to shift to lower temperatures compared to the  $T_g$  of dried PA12 [175, 176]. It is noted that in this study the moisture content in the fabricated specimens was not measured before experiments. However, the specimens once made were dried in a vacuum oven at 100 °C for 10 hrs and kept in sealed plastic bags until they were used in various tests to minimize hydrolysis.

## 4.2 Assessment of the Interfacial Interactions

### 4.2.1 Immobilized Amorphous Phase

The increase of  $T_g$  with GNP content indicates an increase of the immobilized polymer chains at the GNP surface. The question is what this immobilized phase consists of, amorphous or crystalline polymer segments? The fraction of polymer chains anchored

at the GNP surface, dictated by the interfacial interactions between the GNP and PA12, was assessed by determining the variations in the thermo-mechanical behavior of the GNP/PA12 composites as a function of GNP content and temperature. The theoretical model reported in [177] is employed here to estimate the fraction of the constrained region,  $C$ . The model [177] was used for neat semi-crystalline polymer, considering the constrained region as the crystalline phase and part of the amorphous phase that was immobilized at the crystal surface. The rest of the amorphous phase was considered as the mobile phase. In this study, the model is adopted in the case of polymer composites making the following modification. The amorphous phase can be immobilized not only on the crystal surface but also on the GNP surface. In other words, the constrained phase  $C$  consists of polymer crystalline phase and amorphous phase immobilized at the crystal and GNP surface. The mobile phase consists only of amorphous polymer chains. The constrained region does not contribute to loss or dissipated energy and can be expressed in terms of  $W_c$  and  $W_0$  the energy loss ratio of the composite and neat polymer at  $T_g$ , and  $C_0$  the degree of crystallinity for the pure PA12 as shown below:

$$C = 1 - \frac{W_c}{W_0} (1 - C_0) \quad (4.1)$$

where

$$W = \frac{\pi \tan \delta}{(\pi \tan \delta + 1)} \quad (4.2)$$

By rearranging equation 4.1, it can be seen that the ratio of energy loss  $W_c$  is directly proportional to the mobile amorphous phase  $(1-C)$ . So the fraction of amorphous immobilized phase can be found by subtracting the degree of crystallinity from the overall constrained region,  $C$ . The results are presented in Table 4.1. The  $\tan \delta$  and degree of crystallinity  $\chi$  used in equations 4.1 and 4.2 were determined using DMA and MDSC, respectively. The degree of crystallinity was calculated according to the following equation

$$\chi\% = \frac{\Delta H}{\Delta H_m^\circ (1 - \frac{wt\%}{100})} \times 100 \quad (4.3)$$

where  $\Delta H_m^\circ$  is the melting enthalpy of 100% crystalline PA12 equal to 209.3 J/g [155, 156].

**Table 4.1 Thermo-mechanical and crystallization parameters used for the estimation of the immobilized amorphous phase**

GNP wt%	$\chi\%$ based on MDSC	$\tan \delta @ T_g$ based on DMA	$W_c$ according to equation 4.2	C, % according to equation 4.1	immobilized amorphous % (C- $\chi$ )
0	32.9±0.8	0.119	0.271	32.6	0
0.5	27.6±0.3	0.110	0.257	35.7	8.1±0.3
1	28.7±0.9	0.107	0.250	37.3	8.6±0.9
3	26.2±0.5	0.114	0.263	35.0	8.7±0.3
5	26.2±0.5	0.105	0.248	39.0	12.8±0.5
10	24.9±0.8	0.099	0.237	41.0	16.1±0.8
12	24.1±0.2	0.098	0.235	41.4	17.3±0.2
15	22.6±0.7	0.095	0.228	43.0	20.3±0.7

The increase of immobilized amorphous phase with GNP content is expected and is in agreement with the observed increase in  $T_g$ . What needs to be explained is why GNP decreases the degree of crystallinity from ~32% for neat PA12 to ~22.5% for 15wt% of GNP and how that relates to the increase of the fraction of the amorphous immobilized phase. During cooling from melt, the highly mobile polymer chains move freely, in absence of GNP, in the polymer melt towards the homogeneous nucleation crystallization sites. When GNP is present, the polymer chains are either totally immobilized at the GNP surface (pinning effect) which results in increase of  $T_g$ , or they are slowed down, since GNP is an obstacle in their way, resulting in a decrease of degree of crystallinity.

The presence of this constrained amorphous phase is also confirmed by the viscoelastic behavior of the GNP/PA12 composites, which was determined as a function

of the GNP content and temperature at constant frequency of 1 Hz using DMA. The observed results in the linear viscoelastic behavior of PNCs are presented in Figure 4.2. As shown the  $\tan \delta$  peak value (value at  $T_g$ ) decreases and shifts to higher temperatures ( $T_g$  increases as also shown by DSC), indicating that the relaxation transition, which originates from the long segmental motions of the main polymer chain, requires more energy input, that is higher temperatures. This is because GNP decreases the viscous and enhances the elastic behavior of PA12 by pinning the polymer chains leading to formation of the immobilized constrained region [111, 126, 178]. This effect is more pronounced at low and intermediate GNP content. At higher loadings of GNP, unavoidable agglomeration compromises the GNP surface responsible for the pinning of the polymer chains [64, 174].

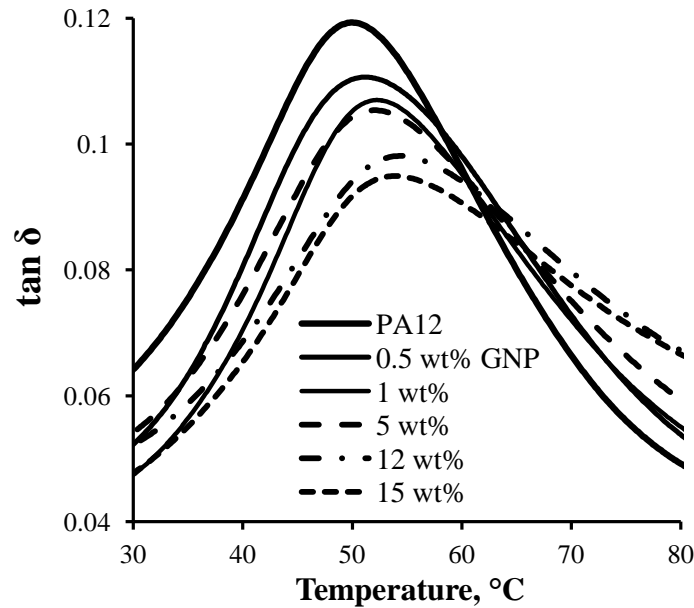


**Figure 4.2  $\tan \delta$  spectra of the PNCs as a function of temperature and GNP wt%**

The results are in agreement with those of other studies reporting that the free volume available to the polymer segments decreases upon addition of nanoreinforcements, restricting thus the polymer chains and resulting in a more compact

structure that requires more energy to activate the segmental motion of polymer chains [122, 128, 179]. It is noted that although the degree of crystallinity decreases with GNP content, as shown by DSC, the composites become more elastic because the increased amorphous phase is immobilized at the GNP surface, so it cannot contribute to viscous effects.

Changes in the thermo-mechanical properties of polymers upon addition of nanomaterials can be used to correlate the interfacial interactions at the nano-scale and macro-scale properties of PNCs. The storage modulus of the GNP/PA12 composites above and below  $T_g$ , normalized with respect to the corresponding modulus of neat PA12 as a function of the GNP content, is presented in Figure 4.3. As shown the normalized storage modulus at temperatures above  $T_g$  is higher for all GNP content values studied than the corresponding normalized storage at temperatures below  $T_g$ .

It is known that the storage modulus is related to the elastic (v.s. inelastic or viscose) response of the composites [128, 180, 181]. So as the amorphous phase increases with GNP content (degree of crystallinity decreases as shown in Table 4.1), it is expected that the storage modulus above  $T_g$ , where the viscous effects of the amorphous phase dominate, will not increase more than the storage modulus below  $T_g$ . Therefore, the observed not expected trend further supports the presence of immobilized amorphous phase. Specifically, the below  $T_g$  elastic behavior is predominantly a result of the stiffening effect of the hard GNP phase. The enhanced elastic behavior at temperatures above  $T_g$  indicates suppressed chains mobility due to extensive segmental immobilization of polymer chains as reported elsewhere [128, 181]. A final observation is that the normalized storage modulus above  $T_g$  increases dramatically upon addition of low GNP content, reaches a plateau and finally keeps increasing at higher GNP content, a trend very similar to the trend observed for the Young's modulus and  $T_g$  presented in Figure 4.1.

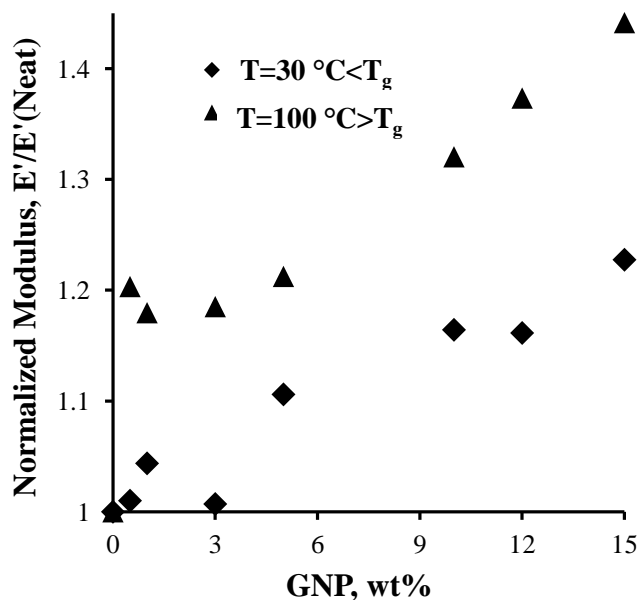


**Figure 4.3 Normalized storage at below and above glass transition temperatures as a function of GNP content**

The observed results are further confirmed by determining, using MDSC, the changes in the specific heat capacity of the GNP/PA12 composites near  $T_g$  as a function of GNP content, shown in Figure 4.4. The inset depicts the method utilized to measure the *relaxation strength*,  $\Delta C_p$ , at the midpoints of the corresponding glass-liquid transition on the heat capacity spectra. Table 4.2 gives the values of  $\Delta C_p$  for each composite system. It is clear that the  $\Delta C_p$  monotonously decreases with GNP content due to decreased entropy of the system induced by the enhanced immobilization of the polymer chains at and near the interface [123, 182-184]. As reported, the interfacial interactions limit mobilization of amorphous polymer chains, which is needed for liquid like behavior of polymer above  $T_g$ , and thus the entire cooperatively rearranging regions (CRR) near the interface [100, 111]. The result of this polymer chain immobilization is a reduction in liquid like motions of chains and thus the reduction in the increment of heat capacity at  $T_g$ . The immobilization then gradually reduces away from the surface of

nanoreinforcement to the bulk polymer where the bulk CRRs contribute to the liquid like behavior of the polymer.

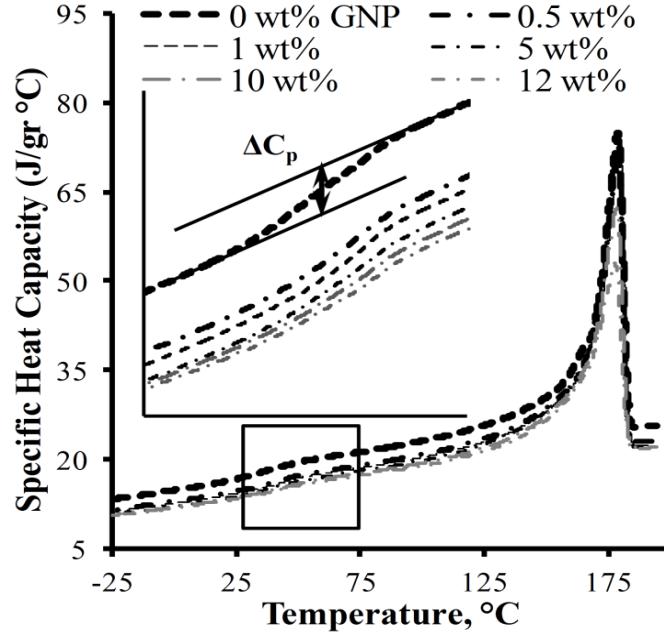


**Figure 4.4 MDSC specific heat capacity of GNP/PA12 nanocomposites as a function of GNP content obtained during heating scans. The inset is a zoomed-in plot of these traces near  $T_g$  demonstrating the decrease in the discontinuity of  $\Delta C_p$  with GNP**

**Table 4.2  $\Delta C_p$  of the GNP/PA12 nanocomposites as a function of GNP content at  $T_g$**

GNP wt%	$\Delta C_p$ (J/gr °C)
0	0.43±0.04
0.5	0.32±0.01
1	0.26±0.03
5	0.23±0.01
10	0.21±0.01
12	0.14±0.01

#### 4.2.2 Transcrystalline Phase

The crystallization of PA12 as a function of GNP content and temperature is shown in the non-isothermal cooling curves obtained by DSC presented in Figure 4.5. As shown the crystallization onset temperature ( $T_{C/onset}$ ) increases with GNP content, indicating that GNP is acting as a nucleating agent. The dramatic increase at low GNP content followed by a slight increase at GNP content higher than 0.5 wt% is due to the saturation effect reported also elsewhere [131, 133]. Specifically as the GNP surface available for nucleation increases dramatically at high GNP content, there is not enough polymer to nucleate at every available GNP surface or/and the mobility of the polymer chains becomes limited due to confinement effects of GNP. In addition, another competing factor, the presence of agglomerates at higher GNP content, contributes to the observed saturation effect [134, 185, 186].

The crystallization induction time,  $\Delta T_i$ , defined as the time from onset to endset of crystallization during non-isothermal crystallization of the GNP/PA12 composites as a function of GNP content calculated using the DSC curves of Figure 4.5, is presented in Figure 4.6. As the GNP content increases,  $\Delta T_i$  increases, that is, it takes longer for crystallization to complete. This indicates that the polymer chains have more time to rearrange and to organize, forming more perfect and/or thicker crystals [187]. This combined with the nucleating action of GNP leads to the conclusion that there is a transcrystalline phase formed at the GNP surface. The transcrystalline phase formed due to the nucleating ability of carbon nanomaterials has been confirmed in case of GNP in PP using in-situ hot stage optical microscopy [133] and in the case of carbon nanotubes (CNT) in PA12 using transmitted polarized optical microscopy [131]. Thus, the immobilized constrained phase, C, (shown in Table 4.1) consists of the

amorphous immobilized phase (also shown in Table 4.1) and the transcrystalline phase which is immobilized but crystalline.

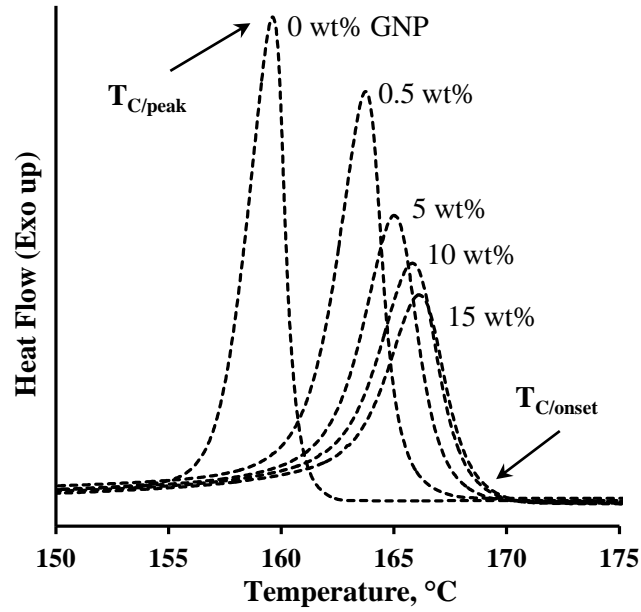
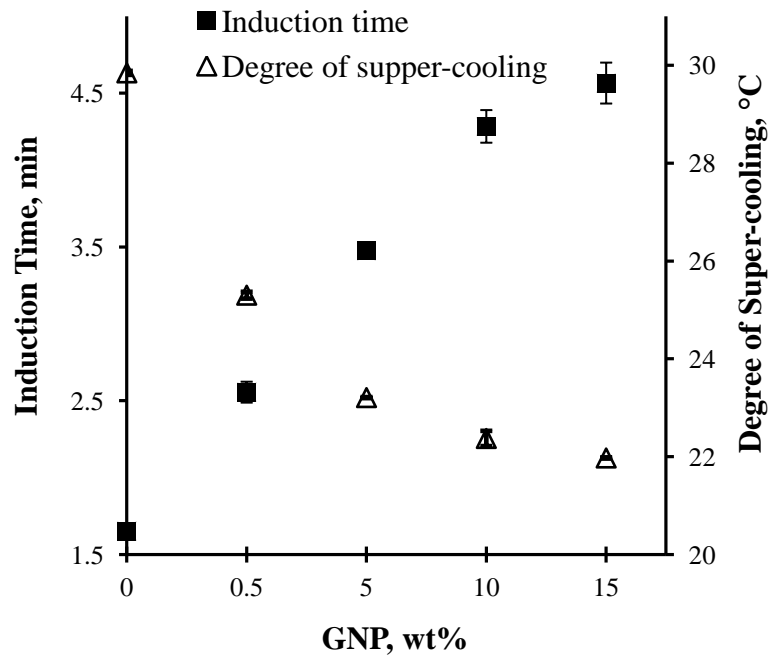


Figure 4.5 Non-isothermal DSC cooling curves of GNP/PA12 PNCs v.s. GNP content



**Figure 4.6 Crystallization induction time and degree of super-cooling with respect to the equilibrium melting temperature obtained from the non-isothermal DSC cooling curves of GNP/PA12 composites are a function of the GNP content**

### 4.2.3 Crystal Characteristics

The melting temperature of the crystalline regime is dictated by the lamellar thickness of crystals, based on the classical theory of polymer crystallization. The lamellar thickness is inversely proportional to the degree of super-cooling from the equilibrium melting temperature provided by

$$\Delta T = T_m^\infty - T_{C/onset} \quad (4.4)$$

where  $T_m^\infty$  is the equilibrium melting temperature and  $T_{C/onset}$  the onset crystallization temperature. The  $T_m^\infty$  was estimated based on the linear Hoffman-Weeks method [188] to be  $\sim 190$  °C. The  $T_m^\infty$  value estimated here is in agreement with values reported in literature for PA12 [189, 190]. As demonstrated in Figure 4.6, the degree of super-cooling ( $\Delta T$ ) decreases with GNP content. Therefore, according to equation 4.4 the lamella thickness increases with GNP.

The effect of GNP content on the lamella thickness and the PA12 polymorphism was investigated by XRD. As reported, PA12 is a semi-crystalline polymer that undergoes crystalline transitions showing four structural polymorphs:  $\alpha$ ,  $\alpha'$ ,  $\gamma$ , and  $\gamma'$  [191]. In our case however, there is only one strong predominant reflection that corresponds to the characteristic  $\gamma$ -crystal phase peak of PA12 with no indication of other crystalline forms [191-193] as shown in Figure 4.7. It is also shown that the characteristic graphite peak at  $2\theta=26.2^\circ$  becomes more dominant with GNP content [159, 160].

The lamella thicknesses of the crystals were estimated using the Debye-Scherrer equation and the full width at half maximum of predominant reflections yielded by the

XRD patterns. The patterns are presented in Figure 4.7 and the lamella thickness is calculated by equation

$$L_t = \frac{K\lambda}{\beta \cos \theta} \quad (4.5)$$

where  $L_t$  is the lamella thickness,  $K$  is the crystal shape factor which was taken as 0.9,  $\lambda$  is the wavelength of the x-ray radiation (0.154 nm),  $\beta$  is the full width at half maximum and  $\theta$  is the peak position of the XRD reflections [161]. It was estimated that the lamella thickness of crystals increases by addition of GNP and vary in the range of 10-12 nm. It is noted that no deconvolution of the XRD peaks was performed and so, using equation 3.2, one can only obtain a rough estimate of the lamella thickness. The results are in agreement with the increase of induction time with GNP content as shown in Figure 4.6. The observations also indicated possible recrystallization upon addition of GNP, a hypothesis that is investigated further in the following.

It is noted that one may estimate the thickness of GNP and variations in interplanar spacing of graphene sheets after processing the PNCs using the information corresponding to the characteristic reflection angle ( $\theta=26.2^\circ$ ) and peak intensity of graphite [159, 194]. However, it is expected that the distance between the graphene sheets remains invariant due to high viscosity of PA12 polymer, which impedes intercalation of polymer chains between the graphene galleries. The latter is further validated by the position of the observed reflection peaks corresponding to GNP on the XRD spectra of the nanocomposites. Figure 4.7 indicates that there is no change in position of the GNP reflection peaks in all systems with respect to the characteristic position of GNP. It can be understood, using Bragg's law ( $\lambda=2d_0 \sin\theta$ ) [194], that the d-spacing ( $d_0$ ) between two graphene sheets does not change during processing of the PNCs.

The melting behavior of the GNP/PA12 composites as a function of the GNP content was studied by MDSC. As shown in Figure 4.8a, where the reversing heat flow

signal is presented, there are two melting peaks, a major one at high temperatures ( $T_{m2}$ ) and a significantly smaller one at the left of the main peak ( $T_{m1}$ ). Both peaks correspond to the same PA12 crystal form since according to XRD patterns there is only one present. The small peak disappears because of recrystallization, which is suppressed with addition of GNP. Note that the reversing signal is one of the components of the total heat flow signal that excludes the recrystallization phenomena during the heating scans. In order to understand more about the recrystallization phenomenon the corresponding non-reversing heat flow signal, which along with the reversing signal make up the total heat flow signal, presented in Figure 4.8b, is used. The recrystallization effect is more pronounced for the neat PA12 and 0.5 wt% GNP composites. The results indicate that the exothermic peaks are progressively suppressed by increasing the GNP content. The recrystallization enthalpy was estimated according to Figure 4.8b as the area under the exothermic transition, and it was found that it decreases with GNP content which confirms the hypothesis that the PA12 crystals recrystallize resulting in more stable thickened lamella with only one melting peak, the major peak shown in Figure 4.8a [134, 195].

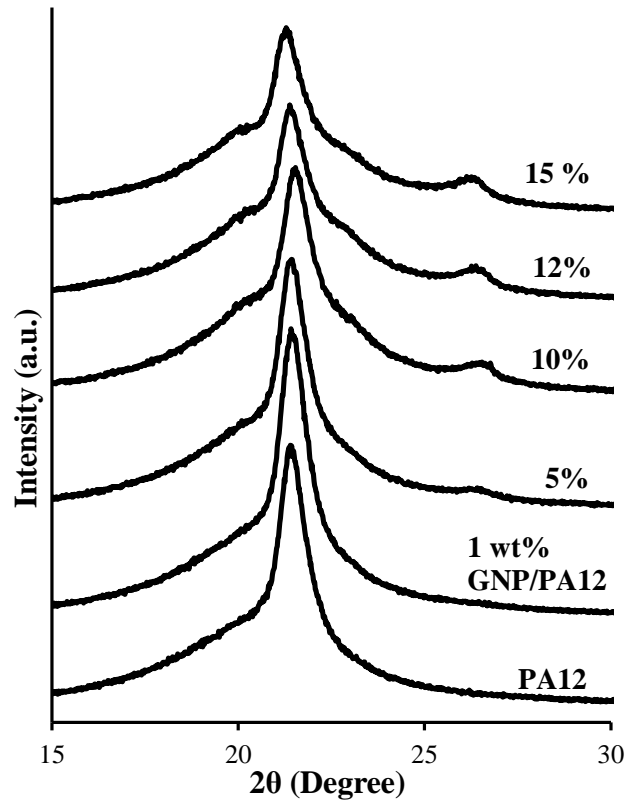
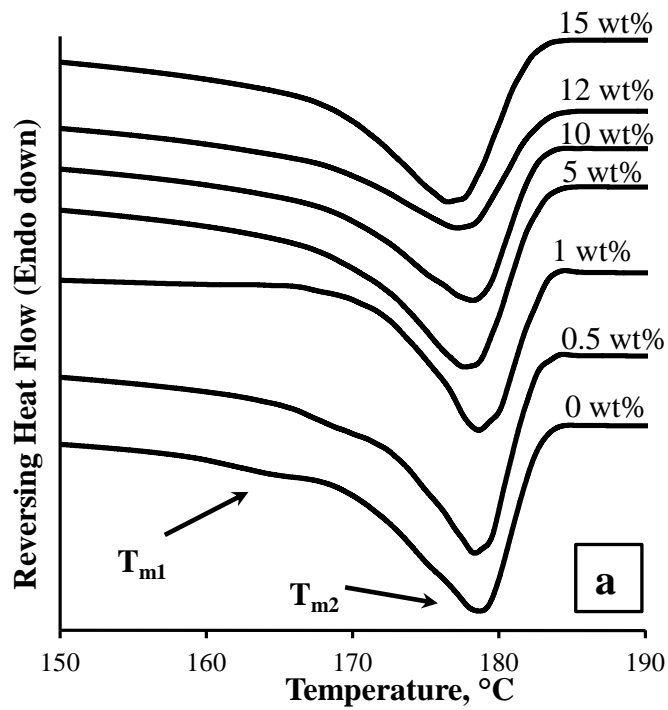
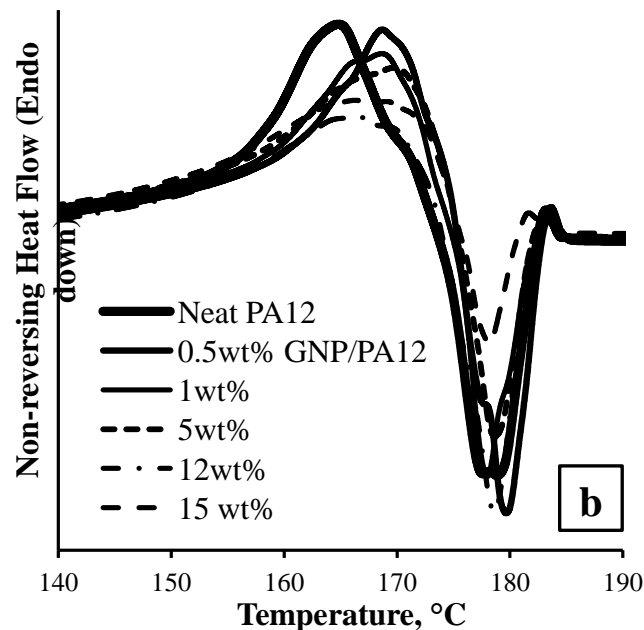


Figure 4.7 XRD patterns of GNP/PA12 PNCs (the curves are shifted vertically for clarity)





**Figure 4.8 a) MDSC reversing thermograms of the melting behavior of GNP/PA12 as a function of GNP content. The arrows indicate the first ( $T_{m1}$ ) and second ( $T_{m2}$ ) melting peaks, and b) MDSC non-reversing heat flow thermograms of the PA12 and nano-composites representing the recrystallization (exothermic) peaks over the melting transition**

In summary, addition of GNP leads to formation of a transcrystalline region, which, combined with the increase in the induction time and decrease in recrystallization, indicated the presence of more perfect/complete PA12 crystals upon addition of GNP. The hypothesis is that the imperfect/incomplete crystals that undergo recrystallization recrystallize at the transcrystalline region. No recrystallization of the transcrystalline region is supported by our results, which is in agreement with the fact that the presence of factors such as strong transcrystallinity/GNP interactions and geometry confinement does not facilitate recrystallization as reported in [134, 196]. The crystallization induction time based on DSC, the maximum temperature of the two melting peaks and the recrystallization enthalpy according to MSDC are presented in Table 4.3.

**Table 4.3 The effect of GNP content on transcrystalline region is indicated by variations in melting peaks, crystallization induction time, and recrystallization enthalpy of PA12 crystals**

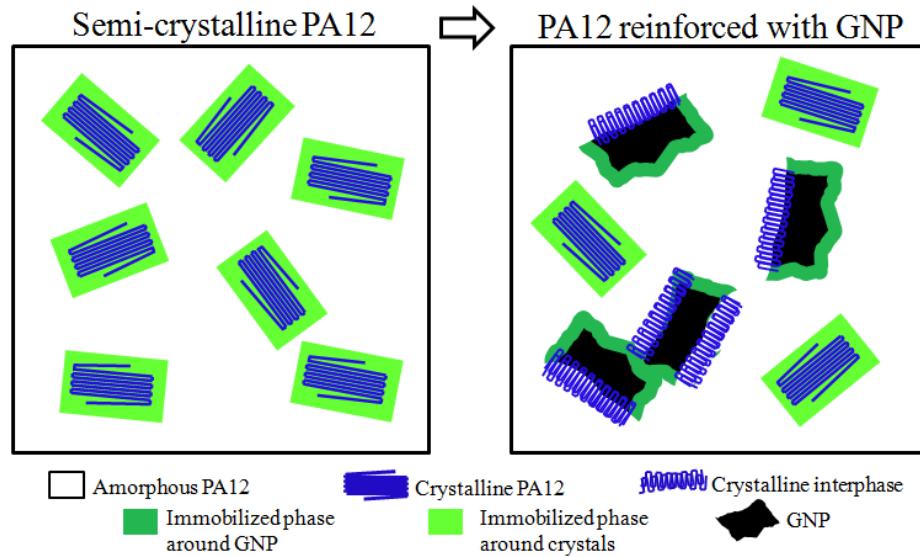
<b>GNP %</b>	<b>T<sub>melt/1</sub> (°C)</b>	<b>T<sub>melt/2</sub> (°C)</b>	<b>ΔT<sub>i</sub> (min)</b>	<b>recrystallization enthalpy heat (J/g)</b>
<b>0</b>	164.4	178.1	1.7±0.1	30.1±1.3
<b>0.5</b>	168.0	178.4	2.6±0.1	27.8±0.6
<b>1</b>		179.1		27.4±1.5
<b>3</b>		178.3		28.4±0.6
<b>5</b>		177.9	3.5±0.1	25.9±0.9
<b>10</b>		178.1	4.3±0.4	21.9±1.3
<b>12</b>		177.6		19.7±0.6
<b>15</b>		177.6	4.6±0.1	22.2±1.0

#### **4.2.4 Constrained Phase at the GNP Surface**

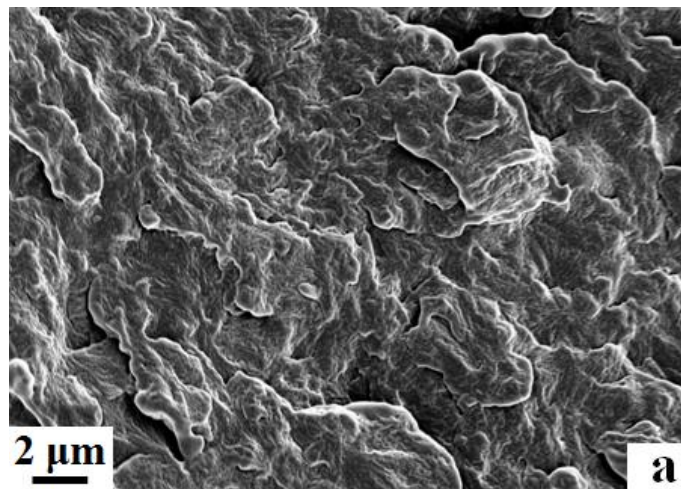
The results so far indicate the formation of a complex constrained phase at the GNP surface consisting of the amorphous immobilized phase, presented in Table 4.1, and the transcrystalline phase, presented in Table 4.3; both phases increase with GNP content. A simple schematic that summarizes the results and shows the formation of the constrained phase around the GNP is shown in Figure 4.9. Neat PA12 (depicted in the left square) consists of a bulk crystalline region (~32% according to MDSC) and an amorphous phase. Once GNP is added to PA12 (the right square depicts composites) the bulk crystalline region reduces significantly, and part of it shows up as a transcrystalline phase at the GNP surface (nucleating effect of GNP as indicated by DSC/MDSC). Also a significant portion of the amorphous phase becomes immobilized at the GNP surface.

As the constrained phase-both the transcrystalline and amorphous regions-increases with GNP, so do the elastic modulus and T<sub>g</sub> of the GNP/PA12 composites. When due to competing effects of GNP, increased surface area versus agglomeration, the amount of constrained phase reaches a plateau, the same exact trend is exhibited by the bulk properties including modulus and T<sub>g</sub>, revealing thus the presence of direct

correlation between phenomena at nano- or micro-scale and macro-scale properties of the composites. The formation of GNP agglomerates, which compromise the available GNP surface area at high GNP contents, has been confirmed by SEM and is presented in Figure 4.10.



**Figure 4.9 Proposed model representing formation of a complex constrained phase in PA12 upon addition of GNP**



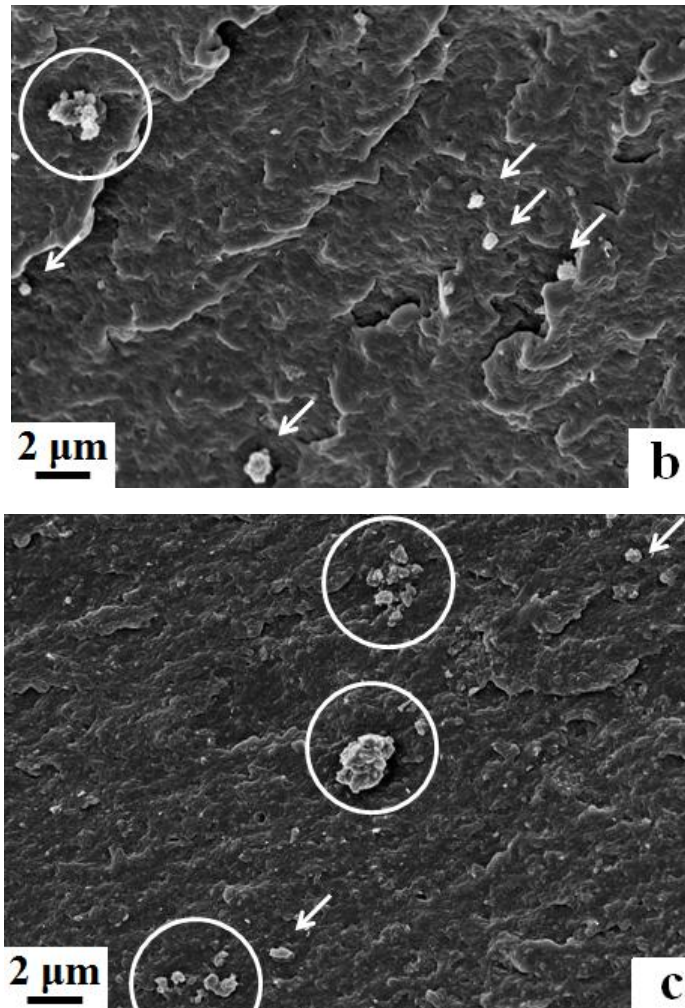


**Figure 4.10 Representative fracture surface of a) neat PA12 and GNP/PA12 composites containing b) 5wt% and c) 15wt% GNP, showing GNP agglomeration only at higher GNP contents**

The fracture surface of neat PA12 is shown in Figure 4.10a. Severe GNP agglomeration is not apparent in composites with GNP content ~ 5wt% (Figures 4.10b and c). The PNCs with high GNP wt%, however, contain GNP aggregation (circled and clearly seen in Figure 4.10c). The SEM images confirm that poorly dispersed GNP can compromise the constraining effect of nanomaterials by reducing the available interface between GNP and polymer and thus. The observations are in good agreement with the observed variations in the amount of the constrained region as well as bulk prosperities of the PNCs obtained over the range of the GNP content.

#### **4.2.5 Assessment of GNP-PA12 Interphase**

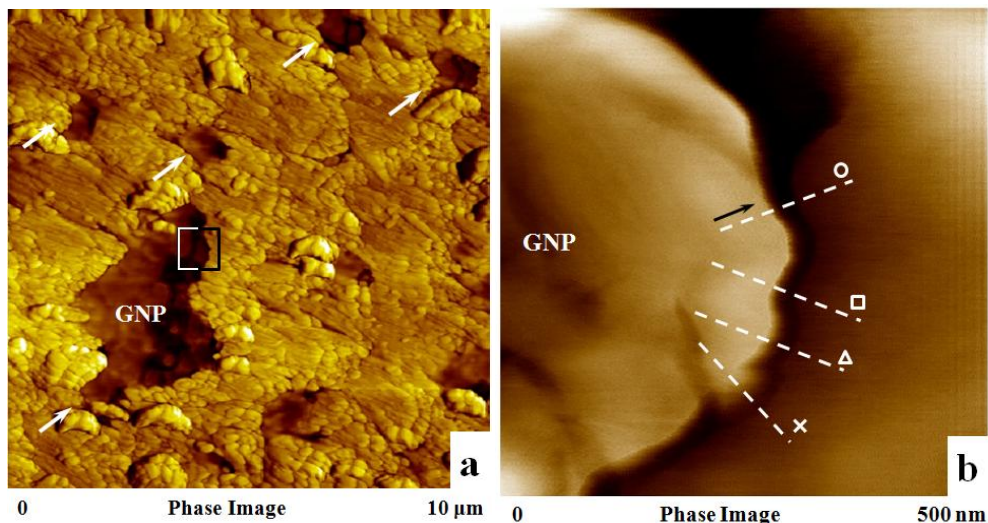
An important consideration in the design and fabrication of PNCs is the nanomaterial-matrix interface or interphase [60, 70, 171]. Although the interphase properties are distinct from those of the pure polymer matrix, this does not necessarily mean that the interphase is structurally homogenous all the way from the surface of nanomaterials to the polymer. The latter has been demonstrated in previous studies that illustrate the interphase as a transition region with varying properties [70]. Therefore, determination of the interphase characteristic has increasingly become a topic of interest in order to better understand detailed process-structure-property interplays. Moreover, the use of existing structure-property micromechanics models in the design of PNCs is no longer valid due to the presence of a remarkable amount of polymer chains with altered dynamics and thus the presence of secondary mechanisms that define macro-scale properties of PNCs [197].

The role of the interfacial constrained region in property enhancement and the methods to quantify its volume fraction within semi-crystalline PNCs were discussed in previous sections of this dissertation. Moreover, the results elucidated that the interfacial region contained polymer chains with an enhanced degree of immobilization and order due to the confinement and nucleation effect of GNP. According to the observations, the hypothesis is that this immobilized phase has an improved stiffness with respect to the rest of the PA12 polymer phase that is further away from the GNPs. The goal is to demonstrate other important aspects of the interphase to better explain the macro-scale behavior of PNCs in correlation with nano-scale interfacial interactions. This section serves to provide methodologies to determine interphase characteristics such as thickness and stiffness gradient within the nanomaterial-polymer transition zone for a given nanocomposite system. As the emphasis of the study is to understand the effect of the manufacturing technique on the macro-scale performance of PNCs, knowledge of the

interphase can also help enlighten the links between fabrication method and nano-structure of polymer within the interfacial zone too.

### Thickness Analysis of the GNP-PA12 Interphase

Information about the topography and qualitative properties of the surface of composites and the interfacial GNP-PA12 region was obtained by employing AFM (tapping mode) height and phase imaging. Phase imaging measures the phase lag information in the oscillation frequency when the AFM tip interacts with areas/materials of different mechanical properties under the tip [70]. Figure 4.11a is a representative phase image of the top surface of 0.1 wt% GNP/PA12 composite. Individual GNPs with an average diameter of 800 nm, which is within the diameter range provided by the supplier, as well as GNP aggregates are shown in Figure 4.11a. Figure 4.11b is a zoomed in phase image scanned over an arbitrary GNP-PA12 interfacial boundary shown in Figure 4.11a. It is clearly observed that there is a transition area, the interfacial region, between the PA12 matrix and the GNP.



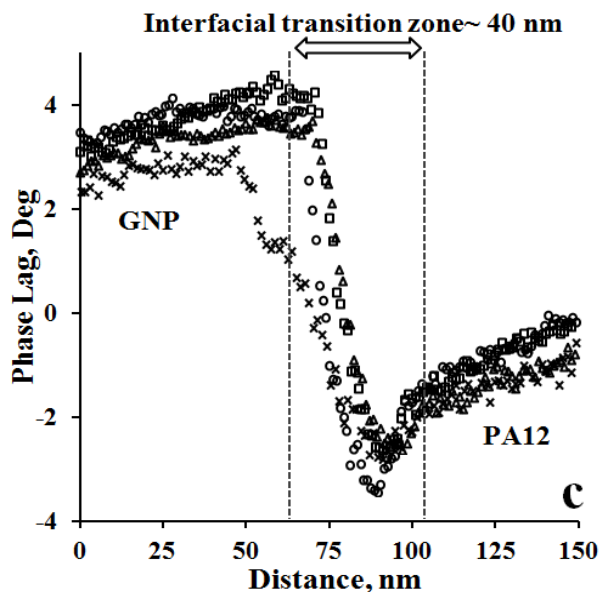
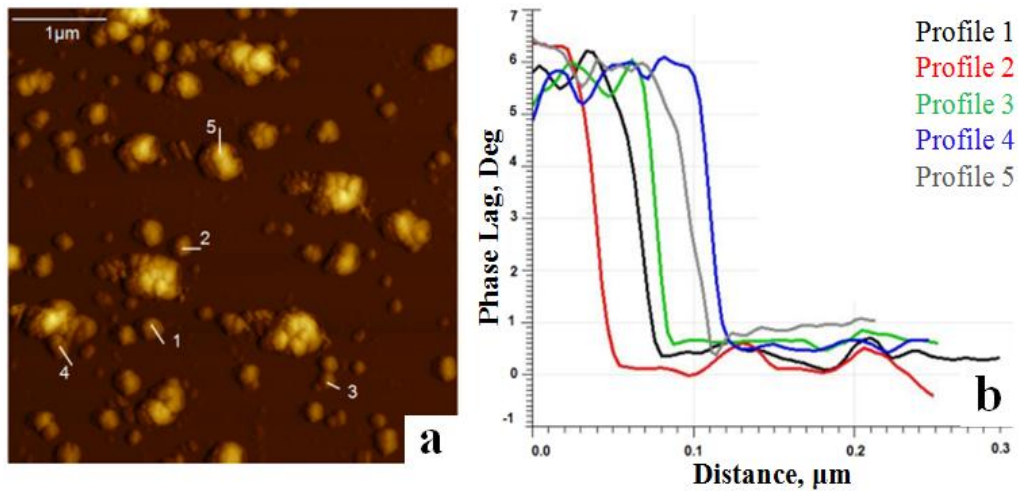


**Figure 4.11 Representative AFM phase image of 0.1 wt% GNP/PA12 PNCs: a) presence of GNP on the surface of PA12 matrix, b) a magnification of (a) showing the profile lines along the interfacial interaction zone, and c) phase lag v.s. distance for the profile lines shown in (b) indicating thickness of the interfacial region**

The thickness of this zone is determined using the AFM software by measuring the phase lag across lines (profiles) that are drawn over the interfacial boundary. Five such lines that are initiated from the polymer pass through the transition zone and terminate at the GNP are shown in Figure 4.11b. The phase lag variations across each line (profile) are shown in Figure 4.11c. Two distinct plateau values at  $\sim +4$  degrees and  $-2$  degrees that correspond to GNP (left) and PA12 (right) respectively are shown. Note that the phase lag data is linked with the stiffness of the compositions under the tip [198]. Therefore, it can be implied that the segment of the transition zone with phase lag values lower than that of pure PA12 indicates the existence of voids and weak GNP/PA12 interactions. It is noted that mechanical properties of the interphase reflect the type of nanomaterial-polymer interactions (attractive v.s. repulsive), nanomaterial-polymer adhesion and thus effectiveness of the load transfer. As shown in the current chapter,  $T_g$

and crystallization temperature increase with the GNP content, indicating the confinement effect of GNP on PA12 chains. This polymer immobilization supports the high average stiffness of the GNP/PA12 interphase presented in Figure 4.11c.

AFM phase image measurements were performed on the individual GNP onto a mica substrate to evaluate the occurrence of any instrumental artifact regarding the transition zone data in AFM tests of the PNCs. Figure 4.12a shows an AFM phase image of GNP onto a mica substrate. GNP was first sonicated into IPA, and a dilute solution was sprayed on the mica surface. As is clearly seen in Figure 4.12b, very sharp transition zones appear on the curves of phase lag data over the boundary of GNP- mica. It is noted that the same AFM scanning parameters were set as those adjusted for AFM imaging of the PNC surface.



4.12 a) representative AFM image of sonicated GNP onto a mica substrate (5x5 μm<sup>2</sup>), and b) phase lag v.s. distance for the profile lines shown in a revealing a sharp transition in phase lag data from the surface of GNP to the mica substrate

Topography information about the scanned area illustrated by the phase image is useful to ensure that the property gradient detected over the interphase region is induced by neither multiple superposed GNP layers nor stepped-height structure of an individual GNP. An uneven surface created by factors mentioned above may result in a difference in the overall stiffness of the composition under the tip. Figure 4.13a elucidates the AFM height image of the composite surface corresponding to the phase image represented in Figure 4.11a. To obtain detailed information about the variation in topography of the composite surface over the interphase zone and beyond, data analysis was performed by drawing lines over the boundary as shown in Figure 4.13b, which is a zoomed in image of Figure 4.13a.

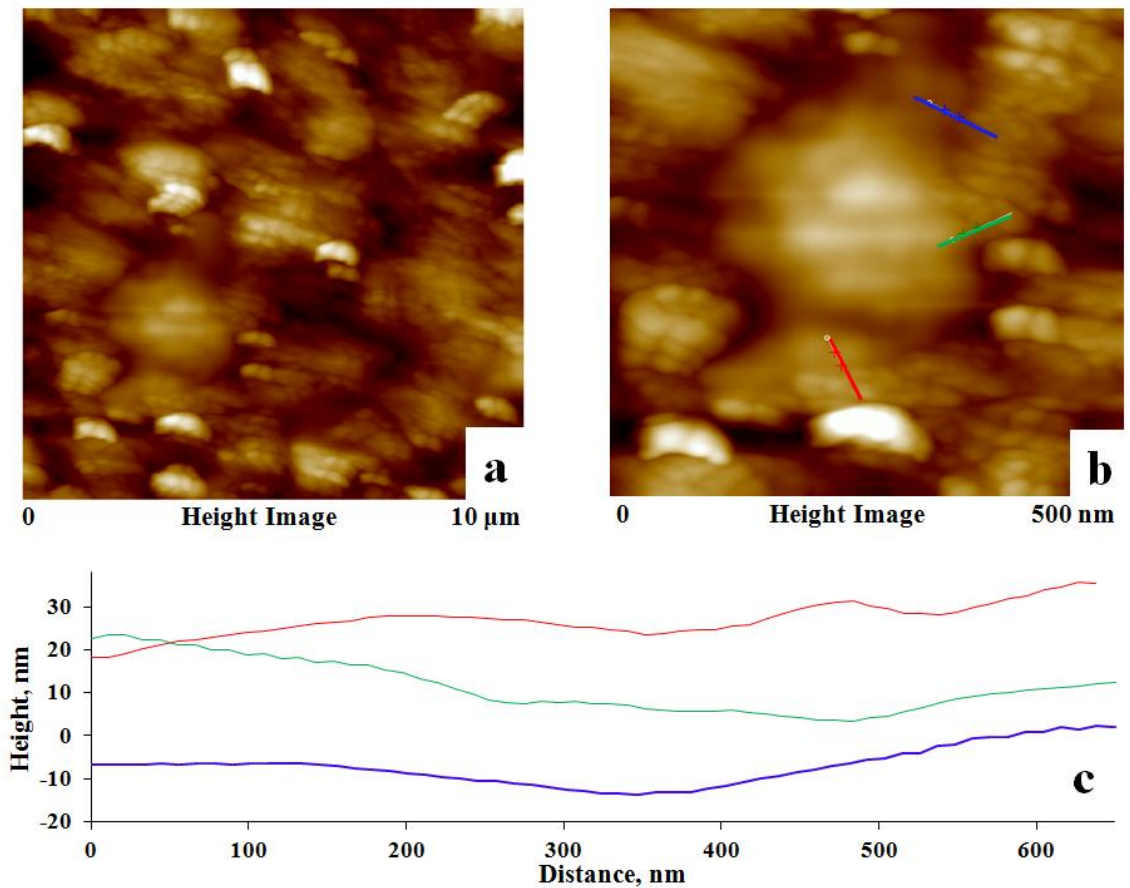


Figure 4.13 Representative AFM height image corresponding to the phase image illustrated in Figure 4.11a: a) topography of a  $10 \times 10 \mu\text{m}^2$  scan size, b) a

magnification of (a) showing the profile lines along the interfacial interaction zone between GNP and PA12, and c) height v.s. distance for the profile lines shown in (b)

As shown in Figure 4.13c, the curves represent a somewhat flat topography along the profile lines. It is clearly observed that the change in height data points is less than 10 nm over the length of each segment (~650 nm). In particular, it is shown that the slight slope of the blue curve (corresponding to one profile line used in phase analysis) gained on the GNP surface occurs over a distance of ~ 250 nm while the property gradient was displayed within 40 nm. It can be implied that the slight slope change is induced by the local topography change around the GNP-PA12 boarder.

Changes in the calorimetric heat capacity of reinforced polymers near  $T_g$  have been shown to provide information about the immobilized polymer chains at the interface. To evaluate the dependence of the interphase thickness on the GNP content, the calorimetric relaxation of immobilized polymer chains was linked to the CRR length. CRRs are the cooperative dynamics that reflect the length of the immobilized layer and are needed for liquid-like behavior of polymers above  $T_g$  as discussed earlier. A model first introduced by Donth et al. was utilized to determine the CRRs length using the variations in the heat capacity from solid to liquid behavior of PNCs around  $T_g$  of the PNCs [100]:

$$V_\alpha = \frac{\Delta(\frac{1}{C_v})}{\rho(\delta T)^2} K_B T^2 \quad (4.6)$$

$$\delta = \sqrt[3]{V_\alpha} \quad (4.7)$$

where  $V_\alpha$  is the volume of the cooperative region,  $C_v$  is the specific heat capacity,  $\rho$  is density of the specimen,  $K_B$  is the Boltzman constant,  $\delta_T$  is temperature fluctuation, and  $\delta$  is the characteristic length of the glass transition. In this study, the heat capacity of the PNCs was determined using the MDSC heat capacity signal as is shown in Figure. 4.4. Table 4.4 summarizes the observed results as a function of the GNP content. It can be

clearly understood that the theoretical characteristic length, which is a measure of the immobilized polymer chains, somewhat is independent of GNP content and that the average of this length is about 5 nm. In addition, it is shown that the theoretical length is one order of magnitude less than that of the experimentally detected interphase in this study using AFM. The thicker interphase found means a larger interaction area which although it is not favored thermodynamically, it is the result of forces present due to processing [10]. The 5 nm interphase thickness is expected considering the surface energies of GNP and PA12 [199]. Although PA12 has a lower moisture absorbance than many of the other commercially available polyamides, PA12 is sensitive to hydrolysis and has been considered partially hydrophilic. The contact angle of nylons has been shown much less than 90° (i.e. ~40°-60°) [200]. On the other hand, the contact angle of water with the graphite surface as reported in literature is in the range of 80°-107° indicating that graphite is hydrophobic [201, 202]. Thus, it is concluded that there repulsive forces between GNP and PA12 leading to spontaneous dewetting at the interface of GNP and PA12. However, the poor wettability of GNP by PA12 is overcome by the forces present during processing as mentioned above and GNP and polymer are eventually brought in contact with thermodynamic stability [10].

**Table 4.4 Characteristic length of the glass transition estimating the thickness of the immobilized amorphous chains**

GNP, wt%	CRR length scale (nm)
0	4.5±0.4
0.5	4.8±0.2
1	5.4±0.2
5	5.5±0.2
10	5.9±0.4
12	5.8±0.1
15	5.5±0.3

### 4.3 Conclusions

This chapter focused on evaluating the formation of a complex constrained region of PA12 at the GNP surface that consists of immobilized amorphous and crystalline regions and strongly affects the physical properties of the polymer including glass transition, the viscoelastic properties and the tensile modulus. The results indicated a strong correlation among Young's modulus and  $T_g$  of the GNP/PA12 composites and the amount of the complex constrained phase which follow the same exact trend upon addition of GNP. The more pronounced effect of GNP on both the physical properties of the polymer and the macro-scale properties of PNCs at low GNP content is related to better dispersion. The results suggested that the complex constrained phase at the GNP surface enables a secondary reinforcing mechanism, which, in addition to the primary stiffening effect of the high modulus GNP, dramatically contributes to the macro-scale properties of semi-crystalline PNCs. Moreover, this chapter provided a methodology to qualitatively assess properties of the GNP-PA12 interphase region such as thickness and stiffness gradient to enable better understanding of the links between nanomaterial-polymer interfacial interactions and macro-scale properties of PNCs. The interphase with an average thickness of several tens of nanometers and a gradual stiffness gradient was visualized according to the AFM phase imaging.

The main findings of this study are applicable to thermoplastic polymer PNCs that contain a degree of crystallinity. The methodology presented in the study can be utilized to understand the detailed picture of interfacial interactions and representative elements of polymers in order to develop three-phase structure-property models that incorporate presence and properties of the immobilized interfacial zone surrounding nanomaterials.

## **CHAPTER 5**

### **EFFECT OF MANUFACTURING METHOD ON ELECTRICAL BEHAVIOR OF PNCS**

#### **5.1 Introduction**

Fabrication of PNCS that demonstrate simultaneous enhancement in multiple properties has been widely favored for development of structural and non-structural materials for various applications. Conductive nanomaterials such as carbon black [203], carbon nanotubes [204] and graphite [27, 205] are able to convert non-conductive polymers into semi-conductive or conductive composites with multi-functional performance [206, 207]. A gradual increase in the electrical conductivity of insulating polymers has been observed when a conductive network of nanomaterials forms and creates suitable paths for an applied electrical current. The processing of PNCS with conductive properties, however, remains a major challenge since desired improvement in electrical properties of PNCS highly depends upon factors such as the level of nanomaterial dispersion and alignment in the matrix and the compromise of mechanical

properties at high nanomaterial content required to induce electrical conductivity. Two key characteristics identify the electrical performance of PNCs: i) electrical conductivity, which is mainly dictated by the loading of conductive fillers and ii) the percolation threshold, which is referred to as the minimum required loading of fillers necessary to form a conductive interconnected network that results in a sharp increase in electrical conductivity [208]. Extremely low percolation thresholds have been reported and correlated to remarkably huge aspect ratio and homogenous spatial dispersion of highly conductive fillers [203].

As reported in literature, research in electrically conductive PNCs reinforced with carbon nanomaterials is dominated by CNT. However, as discussed in chapter 2, GNP has a remarkably large electrical conductivity with significant surface-to-volume ratio, is less expensive than CNT and can be readily prepared from natural graphite. These characteristics have currently made GNP a favored carbon based filler, since the interplay among processability, properties and cost criteria is key in large-scale manufacturing of PNCs. Therefore, fabrication of graphite-based conductive PNCs of relatively low percolation threshold with enhanced mechanical performance motivated this part of the research. Furthermore, it was of interest to this research to investigate how the manufacturing methods used affect electrical performance of PNCs with directionally preferred behavior.

The hypothesis is that manufacturing techniques can lead to PNCs with directionally dependent properties or anisotropic performance. The goal of this chapter is to provide a deeper knowledge that can lead to introduction of new engineered functionalities to polymer composites designed for targeted applications. Electrical property measurements have been shown to be amongst the most reliable methods, due to producibility and the level of certainty of the measurements. Therefore, in this study the electrical properties of PNCs were used as indicators of anisotropic behavior. Dependence of electrical conductivity of PNCs on the manufacturing methods is

highlighted, and underlying interplays between micro-structure and electrical conductivity of PNCs are illustrated. The hypothesis is that advanced manufacturing methods such as SLS have technical advantages and can be used to fabricate PNCs that exhibit multifunctional performance by providing better control of the nanomaterial dispersion and alignment within the polymer.

## **5.2 Factors Affecting Electrical Performance of PNCs- A Literature Review**

A range of independent factors defines the electrical conductivity and percolation threshold of PNCs. Understanding the effect of each of these factors is essential to identify the mechanisms that contribute to the electrical characteristics of PNCs. In summary these factors are [209-211]:

- electrical conductivity of PNC components and loading of conductive fillers
- geometric characteristics of the fillers such as aspect ratio, shape and morphology
- dispersion, distribution and alignment of fillers
- manufacturing method
- nanomaterial-polymer interactions (formation of thin dielectric insulating polymer around conductive fillers [212] or hopping between neighboring nanomaterials that are geometrically separate [213]), and
- crystallization characteristics such as degree of crystallization and size of crystals [213, 214].

Percolation values reported in the case of PNCs are lower than those for micro-size reinforced composites as reported in the case of CNT [210, 213, 215] and GNP [205]. A percolation threshold as low as 0.1vol% for graphene based PNCs [203] and 0.0025wt% for CNT-based PNCs has been reported [206]. In particular, the electrical behavior of PNCs is largely influenced by the manufacturing technique used [213, 216]. During the processes, conductive paths of nanomaterials may be constructed or destroyed to different extents depending on the technique and the conditions used. For example,

excessive shear forces produced in regular conventional techniques such as in melt mixing and injection molding can break the conductive network [31], reduce the aspect ratio of nanomaterials [217] or induce unintentional alignment of nanomaterials, which negatively affect electrical conductivity of end-use products [215].

Understanding the effect of interfacial interactions on the percolation threshold has been a topic of interest in recent studies. For instance, the concurrent property enhancement for electrically conductive PNCs has been linked to the quality of the interfacial interactions and proper mechanical integrity of nanomaterials with polymer [218, 219]. In particular, fabrication techniques that incorporate surface modification strategies generally have been useful to improve interfacial interactions between nanomaterial/polymer, and thus dispersion state, leading to decrease in the percolation threshold [8, 220]. However, in some studies it has been demonstrated that these techniques might be beneficial to mechanical and thermomechanical properties but may negatively influence the electrical behavior of PNCs [8, 221, 222]. Moreover, it has been revealed that factors such as heterogeneous spatial distribution of nanomaterials and degree of alignment of conductive nanomaterials are defined by manufacturing techniques and are key requirements for the formation of nanomaterial junctions and complete conductive paths [223]. Table 5.1 summarizes prior results on electrical properties of graphite based PNCs made by various methods. It is immediately apparent that the electrical behavior of PNCs is remarkably reflected by the fabrication technique and composite system.

A key consideration in the development of multifunctional light PNCs with designed macro-scale performance is understanding the interrelationship between the electrical conductivity threshold and the sharp transition in other macro-scale properties [224]. Previous studies have extensively demonstrated correlations among the enhanced electrical conductivity and the mechanical and thermomechanical behavior of PNCs reinforced with mostly CNT [208] and to a limited extent with graphite [225]. It has been

shown that the improvement in the stiffening effect of expanded graphite in PMMA is linked to the creation of networks of conductive nanomaterials and the percolation for transition in electrical conductivity [205]. In recent studies, SLS has been used to fabricate conductive PNCs of carbon black/PA12 with lower percolation while exhibiting better enhancement in mechanical performance with respect to the melt-mixed and injection molded counterpart specimens due to advantages offered by SLS [35].

**Table 5.1 Dependence of percolation threshold and electrical conductivity of graphite based PNCs on the fabrication method and PNC system**

Composite system	Manufacturing method	Percolation threshold	Electrical conductivity (S/cm)	
PMMA/GNP	Melt-mixing extruded	2.5 vol%	$10^{-5}$	[226]
Epoxy/EG	Polymer solution	5 wt%	$10^{-3}$	[143]
PMMA/EG	In-situ polymerization	3 wt%	$10^{-2}$	[143]
Nylon 6/GNP	In-situ polymerization	1.2 wt%	$10^{-5}$	[143]
HDPE/GNP	Melt-mixing Injection molding	2 wt%	$10^{-4}$ at 8 wt%	[219]
PLA/GNP	Melt-mixing and quenching	3-5 wt%	$10^{-7}$ at 7 wt%	[227]
PP/GNP	Coating-compression molding	0.1 vol%	$10^{-4}$ at 3 vol%	[25]
Epoxy/GNP	Ultrasonication mixing	<0.5 vol%	$10^{-4}$ at 4 vol%	[25]
Nylon6/EG	In-situ polymerization	1 vol%	$10^{-2}$ at 3vol%	[223]
poly (phenylene sulfide)/EG	EG ultrasonication melt-blending and hot press	1 wt%	$10^{-3}$ at 1.5 wt%	[218]
poly(vinylidene fluoride)/xGnP	Solution-cast and hot-press	0.76 vol%	$10^{-3}$ at 1.5 vol%	[212]
PMMA/EG	Solution-mixing and hot press	1 wt%	$10^{-5}$ at 2 wt%	[205]
polystyrene (PS)/EG	Solution-mixing and hot pressing	1.5 vol%	$\sim 10^{-8}$ at 2.5 vol%	[228]

(HDPE: high density polyethylene)

The effect of interfacial interactions between nanomaterial/polymer, and thus the quality of adhesion on the electrical behavior of PNCs, has been emphasized in previous research too. For example, a difference in the electrical and rheological percolation thresholds for single wall carbon nanotubes (SWNT)/PPMA has been found and ascribed to the difference in the distance required to form a conductive network and that required to effectively constrain mobility of polymer chains. It has been shown that a denser nanomaterial network is required for electrical conductivity than for improved rheological behavior and for effective elastic load transfer in PNCs [210]. In another work, concurrent improvement in thermal, mechanical, and electrical properties of PNCs with increase in expanded graphite content has been confirmed and attributed to the enhanced mechanical interlocking between the fillers and the polystyrene matrix used [228].

In several studies, the dependence of the electrical conductivity of PNCs on the aspect ratio (diameter-to-thickness) and exfoliation degree of graphite nanofillers has been highlighted, and it has been shown that high aspect ratio fillers result in a low percolation threshold [229, 230]. However, maintaining a proper dispersion state remains a main challenge in fabrication of conductive reinforced polymers. This limitation originates from large interactions among nanomaterials (0.5 eV per nanometer in the case of CNT) that results in a notable reduction in the number of discrete conductive sites and thus an increase of the percolation threshold [206]. Anisotropic electrical response of CNT-based PNCs induced by intentional alignment of nanomaterials has been vastly reported in literature. It has been illustrated that irrespective of the manufacturing technique used, preferential alignment of CNTs can lead to lower percolation threshold and can cause anisotropic electrical properties compared to PNCs filled with randomly oriented nanotubes [215, 231].

Lately, studies have been conducted for understanding correlations among crystallization characteristics, nanomaterial dispersion and occurrence of conductive

networks in semi-crystalline PNCs reinforced with conductive nanomaterials. It has been shown that in some systems a highly crystalline matrix more effectively promotes formation of the conductive networks than a less crystalline polymer, since the amorphous phase enhances homogeneous distribution of fillers [232]. In another work [133], destructive effect of crystals on the formation of the percolated network of GNP in PP matrix has been reported and linked to the population and size distribution of PP spherulites dictated by the nucleating effect of GNP. It has been also revealed that weakly-crystallized low density polyethylene (LDPE) causes more homogenous dispersion of carbon nanofibers (CNFs) than strongly crystallized high density polyethylene (HDPE), while amorphous polystyrene (PS) represents the best dispersion and thus lowest percolation threshold [214]. Other studies have correlated the network construction and reconstruction of conductive fillers to the type of nanomaterials and level of agglomerates during melt, crystallization and annealing using in-situ thermal observations [216].

In summary, this review emphasizes that understanding of process-structure-property relationships is key in describing the macro-scale properties of PNCs and is an important consideration in order to fabricate electrically conductive PNCs with multifunctional performance. In particular, apart from its dependence on structure and composite constituents, the electrical behavior of PNCs has been shown notably sensitive to alignment, distribution and dispersion of nanomaterials, which can remarkably define the degree of anisotropy exhibited by a given PNC system.

### **5.3 Characterization of Electrical Properties of PNCs**

SLS and IM-processed specimens were cut into small strips (20-25 mm long, 12-13 mm wide and 2-3 mm thick) across the cross sections normal to the sintering plane (x-y) and injection flow direction (x axis). No annealing for removal of thermal history was used in order to compare the neat effect of manufacturing method on the properties of

interest and to avoid likely reconstruction or/and destruction of the existing GNP network [216]. Electrical conductivity measurements were made with a Solartron 1260 coupled with a 1296 Dielectric Interface using 0.1 Vac for frequencies ranging from 10 MHz down to  $10^{-2}$  Hz at room temperature.

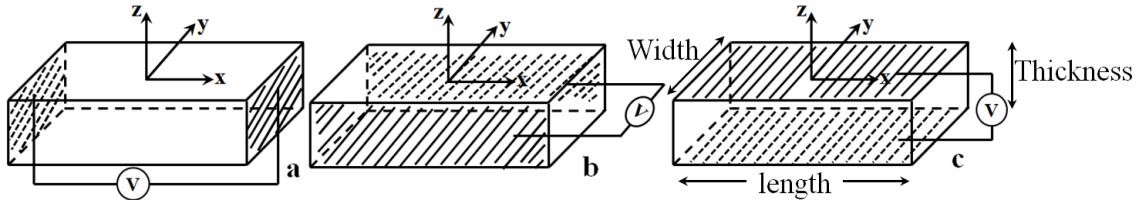


**Figure 5.1 Measurement directions used to determine electrical resistance of the SLS and IM-processed specimens through (a) longitudinal (in-plane) and transverse direction through (b) the width and (c) thickness of specimens**

The measurements were performed through cross-sectional planes normal to the sintering plane and injection flow direction (in-plane) for “longitudinal” measurements (distance between contacts is 20-25 mm) along the direction schematically shown in Figure 5.1a. The ‘transverse’ resistance of the samples was separately characterized through the width (distance between contacts is 12-13 mm), and thickness (distance between contacts is 2-3 mm) which are mutually orthogonal to the longitudinal directions. Figure 5.1b and c represent the schematic configuration of the transverse measurements through the width and thickness of the specimens. In order to reduce the contact resistance and increase the contact surface between metal probes and samples, each pair of parallel cross sections corresponding to measurements through the desired direction was silver painted and air dried for at least 24 hours before measurements. The conductive paint on the sides of the samples was perfectly removed before performing measurements through other directions. To obtain the true value of the conductivity of the

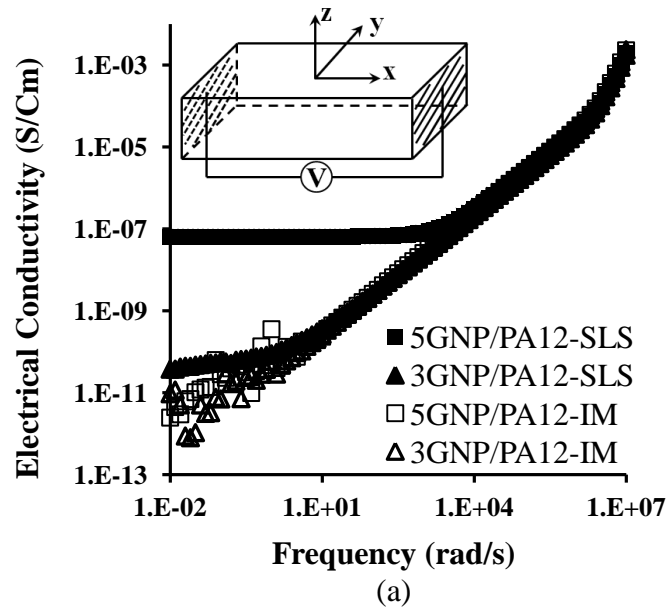
PNCs, the measurements were performed on three samples and the average values were considered.

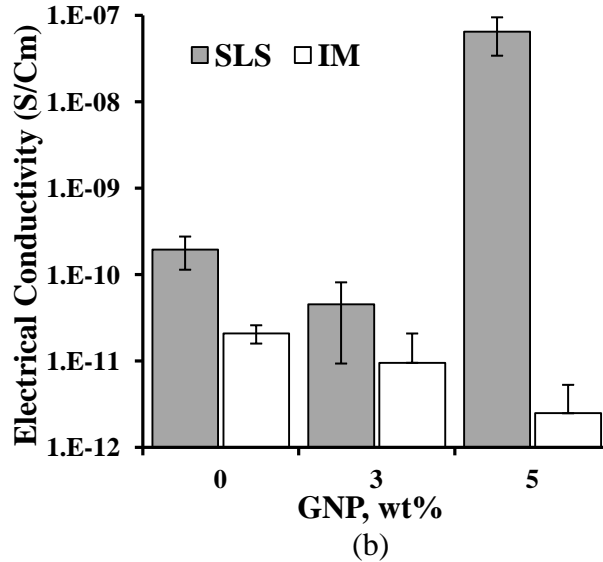
#### **5.4 Electrical Properties of GNP/PA12 PNCs: SLS v.s. IM**

Figure 5.2 represents the electrical conductivity through the length (x direction as schematically shown in Figure 5.1a) of parts fabricated by SLS and IM as a function of frequency of the AC voltage and GNP content. Figure 5.2a displays that the electrical conductivity of the sintered composites reinforced with 5wt% GNP is invariant over the range of low and intermediate frequencies beyond which the conductivity increases with increasing frequencies. Electrical conductivity of 3wt% SLS parts becomes somewhat invariant only within the low frequency range. In contrast, the electrical conductivity of IM-processed parts shows a monotonous increase over the range of frequencies investigated. It is noted that electrical conductivity spectra corresponding to the sintered and injection molded neat PA12 are identical to those of IM-made PNCs and are not presented for the sake of clarity. Figure 5.2b compares the electrical conductivity of SLS and IM parts as a function of the GNP content at the low frequency of 0.01 rad/S. It is shown that the sintered composites filled with 5wt% GNP yield the greatest electrical conductivity, which is about 5 orders of magnitude higher than their IM counterpart systems. It is also clear that 5wt% SLS parts give the electrical conductivity 3 orders of magnitudes greater than 3wt% SLS parts. However, IM-made systems remain non-conductive with addition of GNP up to 5wt%.

As described earlier, the onset of the percolation threshold is enough to convert the matrix to a semiconductor. Therefore, the observations indicate that 5wt% GNP is above the onset of percolation threshold when SLS is used, whereas it is apparent that this loading is less than the percolation onset in case of IM process. The observed difference between the electrical conductivity behavior of SLS and IM-made composites was correlated to the morphology and crystallization characteristics that are altered by the

manufacturing techniques. The results suggest formation of complete conductive paths formed by GNP in case of 5wt% SLS PNCs. However these paths are incomplete in case of IM due to the high level of GNP agglomeration as discussed in chapter 3 and/or are destroyed due to high shear forces present during IM process and thus unintentional alignment of GNP along the injection flow. Other factors that may affect the enhancement in electrical conductivity of PNCs are degree of crystallization and the size of the crystallites [232]. As shown in chapter 3, melt and crystallization behavior of the fabricated PNCs are influenced by the manufacturing method used.





**Figure 5.2 a) dependence of longitudinal electrical conductivity on the frequency of the AC voltage, process and GNP concentration of SLS and IM-made specimens and b) electrical conductivity values at AC frequency of 0.01 rad/s of the parts measured**

Figures 5.3 and 5.4 elucidate the transverse electrical behavior of the PNCs through the width and thickness (y and z directions as schematically shown in Figure 5.1b and 5.1c, respectively) with respect to the manufacturing method and GNP loading. The observations clearly show that manufacturing methods used resulted in similar trends for electrical conductivity against the range of A.C. frequencies regardless of the measurement directions investigated. Moreover, as was observed in the case of longitudinal measurements (through the length of specimens), 5wt% GNP PNCs made by SLS display greater low frequency electrical conductivity that is ~ three orders of magnitude greater than that of their IM counterparts. On the other hand, SLS does not provide better enhancement in electrical conductivity of 3wt% GNP PNCs with respect to the corresponding IM PNCs. By comparing the measurements made through the length, width and thickness of the PNCs, one may conclude that SLS was more effective in

introduction of electrical conductivity through the length of the parts than other directions (Figure 5.2 v.s. Figures 5.3 and 5.4).

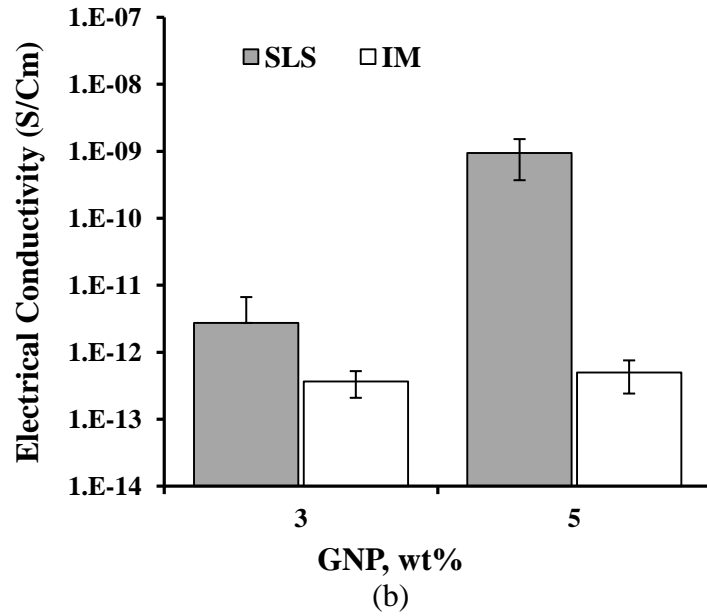
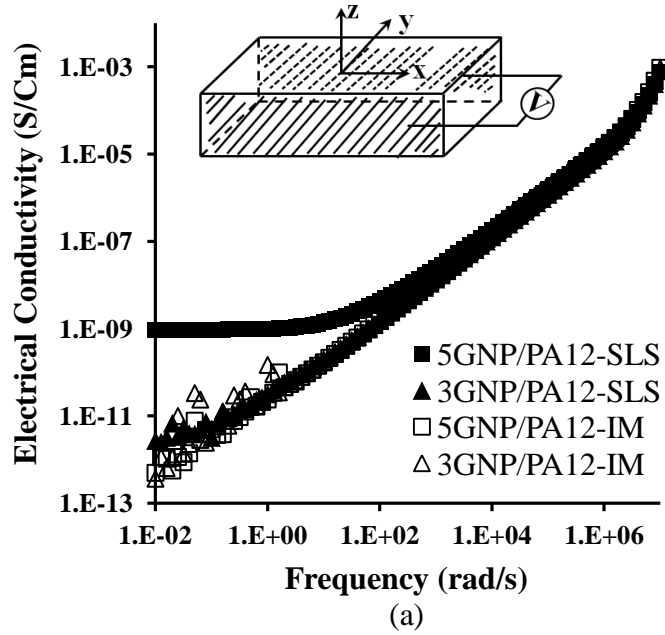
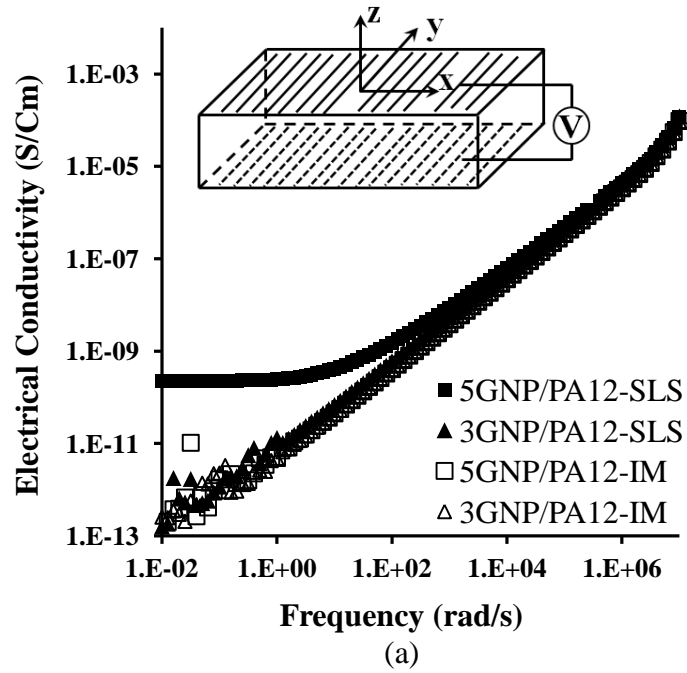
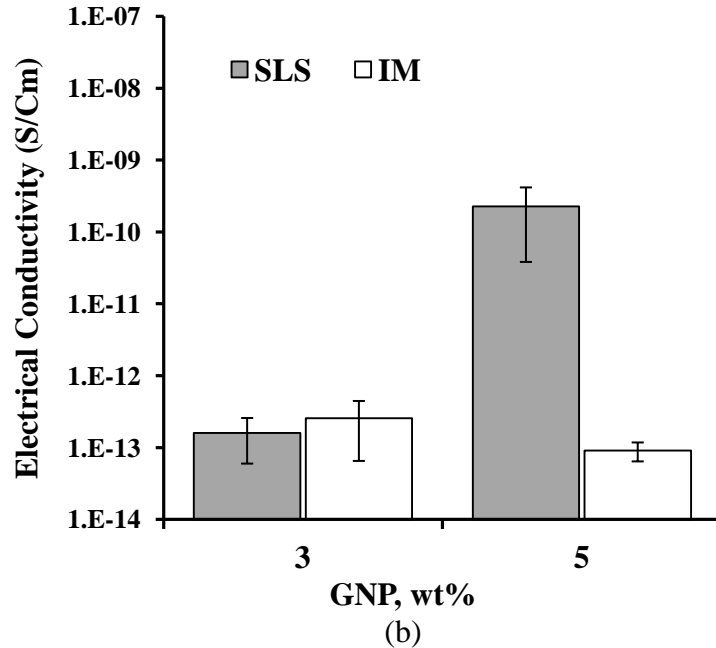


Figure 5.3 a) dependence of electrical conductivity on the frequency of the AC voltage, process and GNP concentration of SLS and IM specimens and b) electrical conductivity values at AC frequency of 0.01 rad/s of the parts measured through the width (y axis)





**Figure 5.4 a) dependence of electrical conductivity on the frequency of the AC voltage, process and GNP concentration of SLS and IM-made specimens and b) electrical conductivity values measured through the thickness (z axis) of the parts at AC frequency of 0.01 rad/s**

In this study, GNP is coated onto the surface of PA12 powder before processing of PNCs as described in chapter 2. Figure 5.5 represents SEM images of neat PA12 powder and GNP-coated PA12 used in SLS and IM processes. According to the quality of GNP dispersion/distribution as observed in figure 5.5b the presence of conductive paths formed in between neighboring polymer grains is suggested. Figure 5.6 schematically shows possible configurations for distribution, dispersion and alignment of GNP before and after SLS and IM processing of GNP-coated PA12. When the GNP/PA12 melt undergoes the IM process, it is expected that GNP is aligned along the flow direction. In addition, as explained earlier, the high shear forces induced during melt-mixing and injection processes may break the existing conductive network formed during the coating process and thus result in non-conductive behavior in the case of IM-made PNCs.

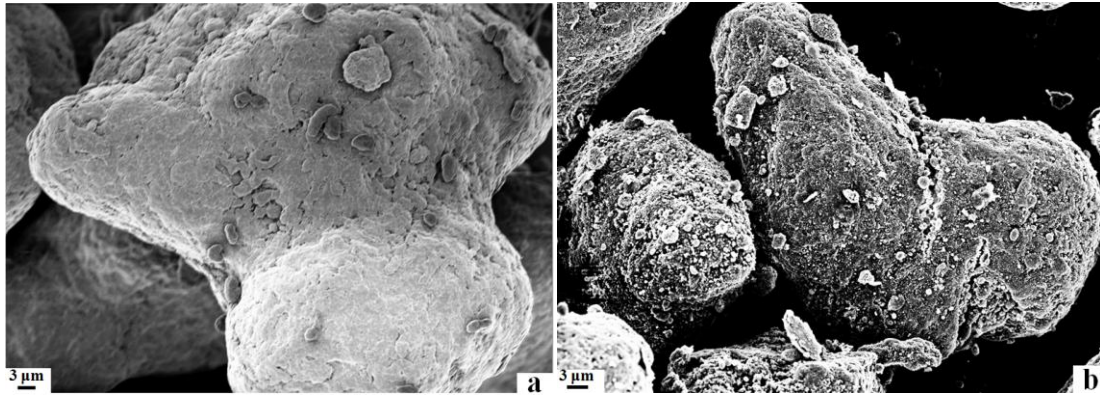
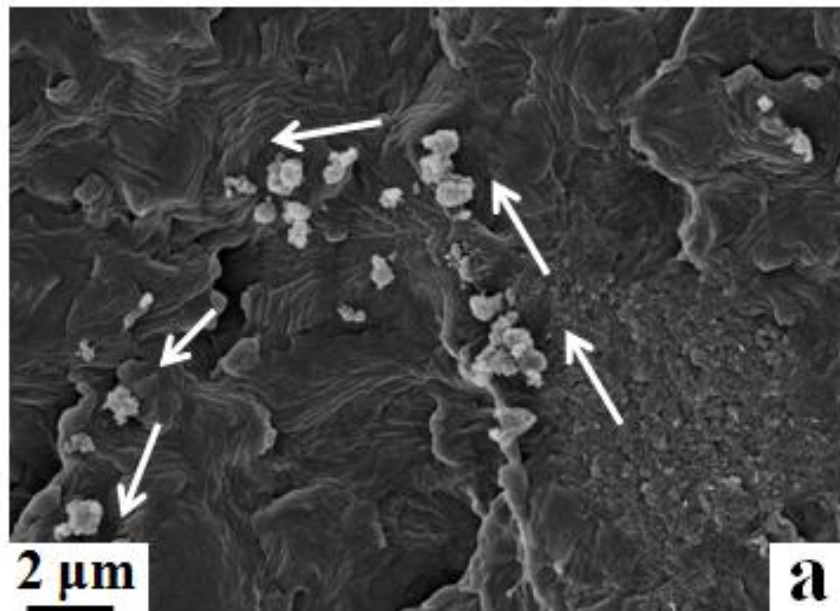


**Figure 5.5 SEM images of a) neat PA12 powder and b) 5wt% GNP coated PA12 powder representing the dispersion and distribution of GNP before processing**

A directionally preferred alignment of conductive nanomaterials is beneficial to electrical conductivity of the parts along the direction of the aligned fillers [231]. However, PNCs made by IM in this study do not exhibit enhanced electrical conductivity with respect to pure PA12 specimens, since 5wt% GNP is still below the electrical percolation threshold of IM-made parts.

The SEM micrographs of the fracture surface of 5wt% PNCs processed by SLS and IM are shown in Figure 5.6a and 5.6b, respectively. It is seen that SLS resulted in GNP aggregates that seem to promote the formation of the conductive paths of nanomaterials. However, such networks are absent in case of IM-processed composites, which confirms the non-conductive behavior of the IM-made PNCs. The bottom left model in Figure 5.7a schematically illustrates the presence of incomplete conductive

networks in the composites after IM processing of the starting GNP-coated powder schematically shown in Figure 5.7. On the other hand, the powder is sintered with no shear or extensional forces present in SLS. This effect causes the SLS step either to maintain the original conductive networks with spatial random orientation of GNP present before sintering with no or minimum discontinuity, or to reconstruct new networks with slight changes in their spatial direction when PA12 powder particles are sintered as schematically shown in Figure 5.7b. This process-induced difference is the main reason for the lower percolation threshold of SLS-made PNCs than that of their corresponding IM specimens.



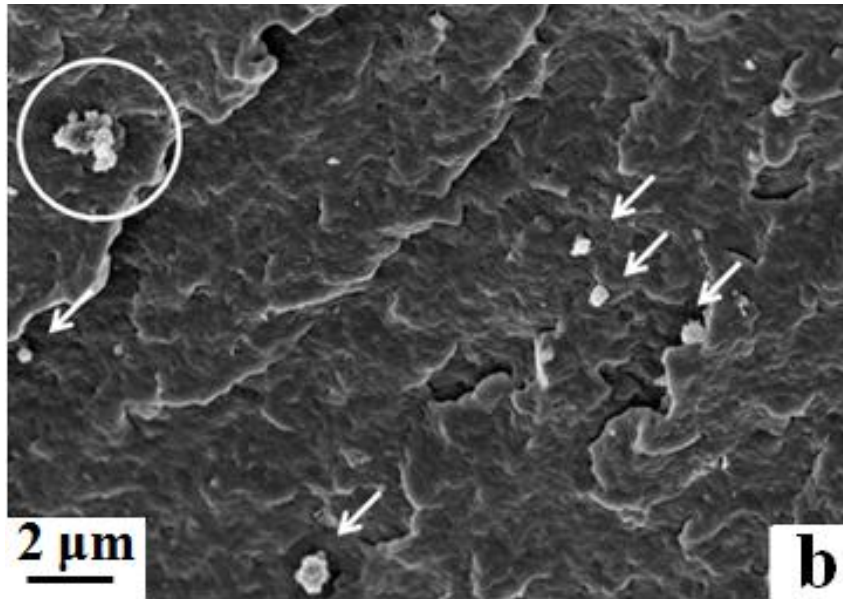


**Figure 5.6 Fracture surface of 5wt% GNP/PA12 composites made by a) SLS and b) IM indicating presence of GNP aggregates promoting formation of conductive networks in SLS-made PNCs and absence of these paths in IM-made PNCs due to GNP agglomeration and increase of the interparticle distance**

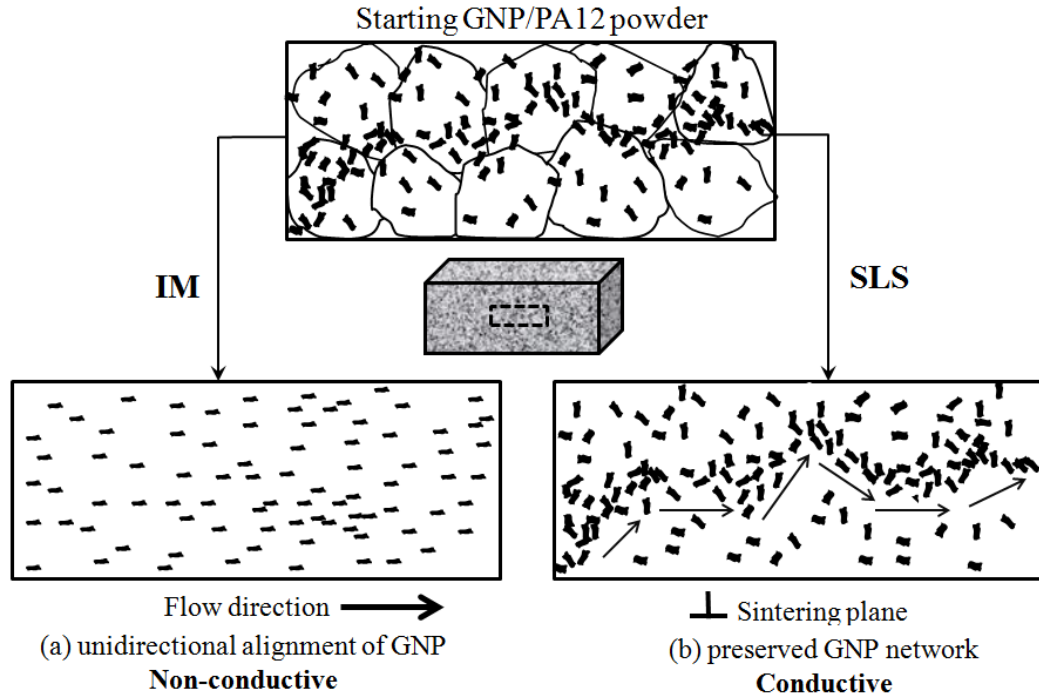


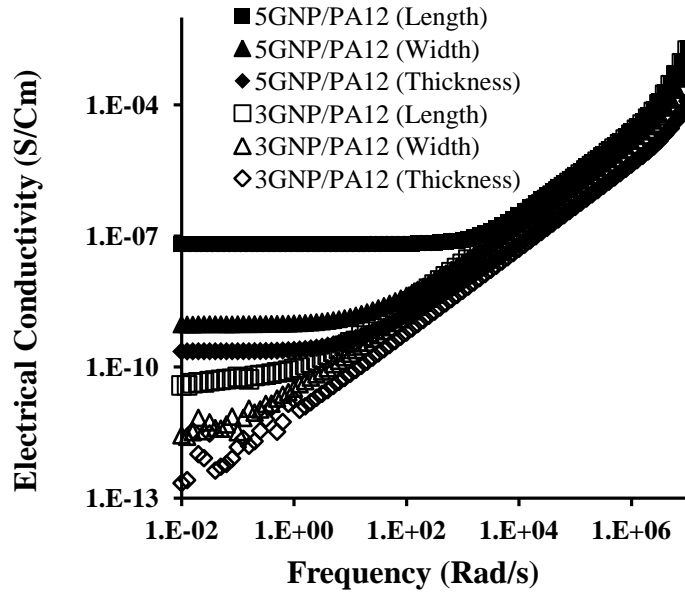
**Figure 5.7 Schematic configurations representing dispersion/distribution and alignment of GNP in PA12 before processing steps (top), and in processed parts after IM (bottom left) and SLS (bottom right). Cross sections display planes normal to the injection flow direction and sintering plane in IM and SLS, respectively: incomplete v.s. complete conductive network of GNP**

#### Directional Dependence of Electrical Behavior of PNCs

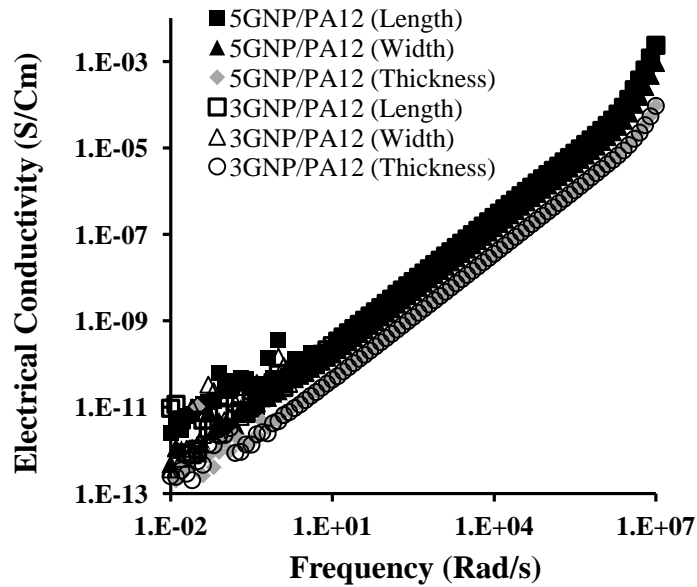
As discussed in chapter 1, the manufacturing method is one key factor that remarkably affects the dispersion state and the alignment of nanomaterials within polymers. The latter in particular may define the anisotropic functions of PNCs for a range of properties [215, 233]. Depending on applications of the end-use parts, anisotropic performance may be of a desired target when tailoring macro-scale properties of PNCs. Considering the platelet (2-D) shape of GNP [140], the orientation of the fillers is a prime variable and can lead to PNCs that are transversely isotropic by directionally preferred alignment of GNP or to PNCs with isotropic properties induced by random

orientation of GNP. This section compares the directional dependence of electrical behavior to better understand effect of manufacturing on GNP dispersion and morphology of the PNCs fabricated by SLS and IM.

Figures 5.8a and 5.8b demonstrate the electrical conductivity of the PNCs with respect to measurement directions, the frequency of the AC voltage and the GNP concentration for the SLS and IM process respectively. Figure 5.8a shows that the conductivity of the 5wt% SLS PNCs remains invariant within a greater range of AC frequencies than that observed from measurements through the width and thickness. However, 3wt% SLS-made PNCs represent fairly identical trends irrespective of the directions investigated. As is seen in Figure 5.8b, IM-processed PNCs, however, exhibit perfectly similar trends with respect to the frequency range regardless of the GNP loading and measurement direction. It is clear that IM-made PNCs do not exhibit enhanced electrical performance through the width and thickness. This observation was expected, since the IM PNCs do not even exhibit improved longitudinal conductivity with the possibility of favorable alignment of GNP along the injection flow.



(a)



(b)

**Figure 5.8 Electrical conductivity of the PNCs with respect to measurement direction for a) SLS and b) IM process as a function of the frequency of the AC voltage and GNP concentration**

Figure 5.9 summarizes the low frequency electrical conductivity of 3 and 5wr% PNCs fabricated by SLS. These values are not reported for the IM-made PNCs, as they

exhibited very low or no conductivity at low frequencies. Two important observations can be made in accordance with the results represented in Figure 5.9: i) PNCs made by SLS show greater conductivity through the length than other directions, and ii) 5wt% SLS-processed PNCs demonstrate an electrical conductivity that is three orders of magnitude greater than that of the 3wt% PNCs through a given direction. The results so far cannot be however sufficient to conclude that IM-processed PNCs demonstrate isotropic performance.

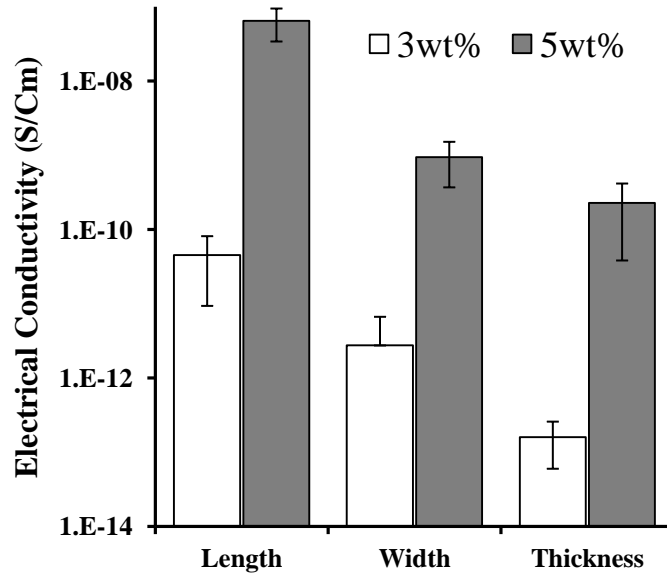


**Figure 5.9 Comparison of electrical conductivity values in x,y and z direction of the SLS parts at AC frequency of 0.01 rad/s**

To understand effect of manufacturing processes used on the structural uniformity of the fabricated parts, SLS samples were chosen from two different zones of the powder bed (identified by letters “L” and “S” in the experiments) and examined. The results represent average values obtained by measurement of three samples corresponding to each powder zone. Figure 5.10 elucidates the electrical conductivity of sintered and

injection molded 5wt% PNCs with respect to the AC frequencies. The results demonstrate a non-uniform behavior in electrical conductivity of PNCs. It is clearly understood that the electrical behavior of the SLS PNCs measured at a given direction is sensitive to the location of the sintered specimens on the powder bed as shown in figure 5.10a. Figure 5.10b illustrates that the electrical behavior of the IM-made PNCs follows identical trends with slight variations in low frequency electrical conductivity at a given direction. The results show that SLS-made specimens may have altered morphology and structure that are dictated by the local sintering conditions and GNP dispersion/distribution.

In the IM process, all processing conditions such as the melt temperature, mold temperature and molding time remain invariant in the fabrication of the PNCs. In contrast, the process mechanics that influences the sintering of polymer powder is complex. Sintered PNCs in SLS might undergo different local pertinent phenomena, such as the spatial heat transfer behavior in the powder bed, doses of thermal energy delivered to the powder, cooling rate, and number of effective exposures [234, 235]. In particular, the latter factors may affect the physical properties of the fabricated parts such as density and crystallization characteristics. The response of the SLS process to the parameters mentioned above might be an explanation for the observed inhomogeneity of the SLS parts with respect to their IM-made counterparts.

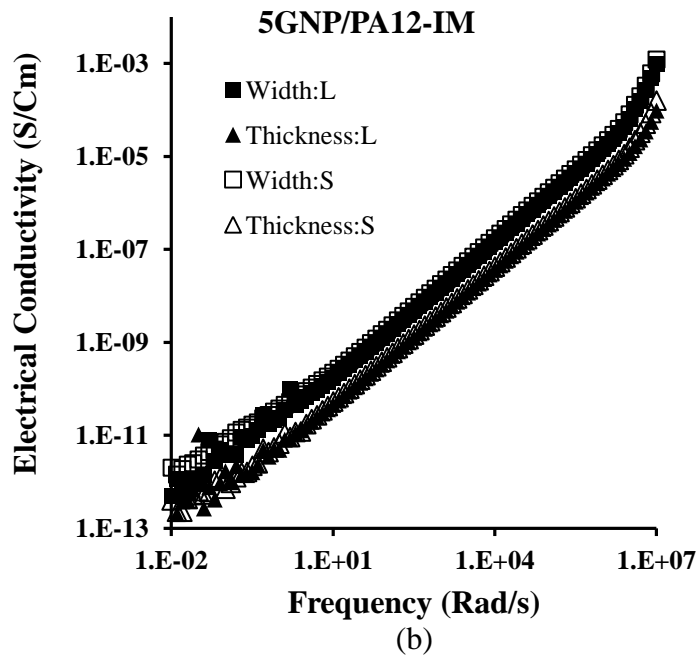
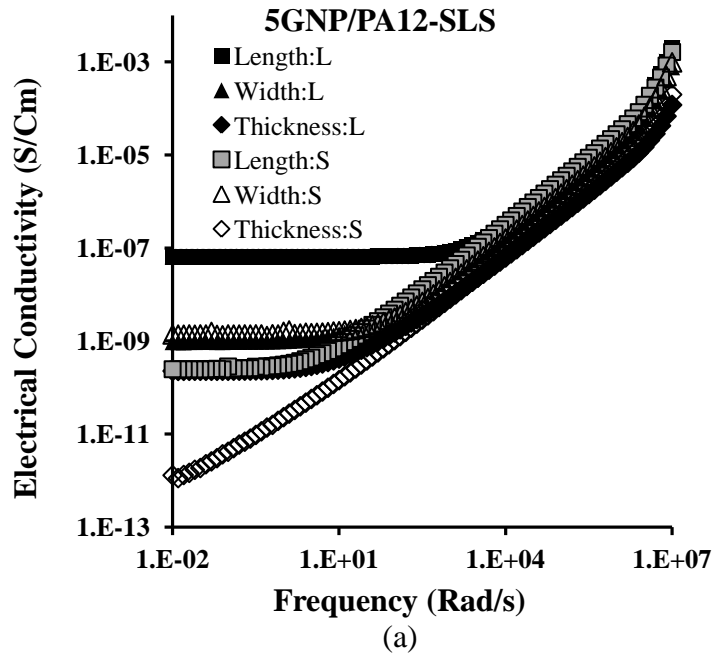


**Figure 5.10 a) inhomogeneity of SLS v.s. b) homogeneity of IM parts observed by electrical conductivity of the 5wt% GNP/PA12 PNCs measured through the length, width and thickness**

## 5.5 Conclusions

The effect of the manufacturing method on the electrical behavior of PNCs fabricated by SLS and IM processes was examined and compared. The electrical behavior of the fabricated PNCs was of interest due to the high sensitivity of electrical properties to the microstructure and morphology of the PNCs. The study highlighted the interrelationships among process, structure and electrical behavior of PNCs by: i) evaluating the dependence of the electrical properties on manufacturing method, ii) determining effect of manufacturing technique on the anisotropic performance of PNCs, and iii) investigating morphological and structural uniformity of parts induced by SLS and IM.

The results convincingly indicate that the manufacturing techniques used influenced the electrical behavior of fabricated PNCs, which was correlated to the GNP dispersion state and orientation and forces present during processing. It was demonstrated that 5wt% SLS-made parts exhibited an electrical conductivity five orders of magnitude greater than their counterpart IM-processed PNCs. Moreover, the observations showed that the sintering process led to PNCs with lower percolation threshold than that obtained with the IM process. The results revealed that SLS-made PNCs had directionally dependent electrical properties while IM-made specimens exhibited isotropic performance in terms of electrical conductivity. In general, longitudinal electrical conductivity of the 5wt% SLS PNCs was found greater than that corresponding to the transverse directions at low frequencies. The observed effect was correlated to the numerous original GNP conductive paths maintained even after the sintering process. The study also examined the effect of manufacturing technique on structural and morphological uniformity of PNCs chosen from different zones on the powder bed. The observations indicated that SLS may result in inhomogeneous bulk PNCs in terms of structure and morphology. The variations in electrical conductivity of the samples were attributed to phenomena specific to the SLS process, such as non-uniform thermal

gradient and inconsistent cooling rates and thus local variations on physical properties of sintered zones. The results support the view that SLS has the potential to become a key industrial processing tool for fabrication of conductive multifunctional GNP/PA12 PNCs. However, further understanding about physics of sintering is essential for large-scale fabrication of electrical conductive PNCs with unvarying structure.

## **CHAPTER 6**

### **SUMMARY, CONCLUSIONS AND RECOMMENDATIONS**

A summary of the dissertation including the main findings of the research is provided in section 6.1. Section 6.2 and 6.3 outline the conclusions and scientific/technical contributions of the study, respectively. Finally section 6.4 provides potential avenues of future research and recommendations for related research and expansion of this study.

#### **6.1 Summary of the Dissertation**

One main challenge to the expected rapid growth in technology and commercial advancement of PNCs made for desired applications is a lack of sufficient technical and scientific understanding of the links between the manufacturing method and macro-scale properties of this class of materials. In this research, the manufacturing method was suggested as a key independent variable that dramatically defines micro/nanostructure, morphology and thus macro-scale properties of PNCs. It was shown that knowledge of nanomaterial-polymer interfacial interactions is critical to correlate the manufacturing method and bulk behavior leading to multifunctional PNCs with engineered properties. In this study, exfoliated graphite nanoplatelets as a reinforcement with superior electrical and mechanical properties were used to introduce concurrent property enhancement in PA12 matrix. SLS, an additive manufacturing technique, was considered in order to introduce multifunctional performance to the PNCs while exhibiting superior electrical and mechanical properties over conventional polymer processing methods such as IM. The main objectives of the dissertation were pursued utilizing systematic methods of fabrication and experimental procedures as follows.

Chapter 3 revealed the underlying correlations between manufacturing method and macro-scale properties of SLS and IM-made PNCs. A systematic experimental methodology was utilized to characterize a range of mechanical properties as well as thermal, thermomechanical and electrical behavior of the fabricated PNCs. The results indicated that SLS enabled fabrication of multifunctional PNCs with equal or better tensile and flexural performance than those fabricated by the IM process. It was found that SLS led to more pronounced GNP-PA12 interactions and thus greater reinforcing efficiency of GNP in PA12. Moreover, the observations revealed that the 5wt% GNP/PA12 PNCs processed by SLS had a longitudinal electrical conductivity several orders of magnitude greater than that of IM composites.

Chapter 4 focused on providing a methodology to understand correlations among nano-scale interfacial interactions, physical and structural properties of the polymer at the interface and macro-scale behavior of PNCs. The study demonstrated formation of a complex constrained region of PA12 at the GNP surface that consists of immobilized amorphous and transcrystalline regions. Strong correlations among the amount of the constrained region, Young's modulus and  $T_g$  of GNP/PA12 parts were demonstrated. The results indicated that the interfacial interactions enable a secondary reinforcing mechanism, which in addition to the primary stiffening effect of the high modulus GNP, remarkably contributes to the elastic response and the  $T_g$  of semi-crystalline PNCs. The investigations further revealed the presence of a transition zone generated between GNP and PA12 with a thickness of several tens of nanometers. The results indicated that the interphase region was stiffer than the PA12 matrix, which confirmed the presence of polymer chains with enhanced degrees of immobilization near the interface.

Chapter 5 investigated the effect of manufacturing method on electrical behavior in order to better understand the links among the manufacturing method, structure and morphology of PNCs. It was also of interest to evaluate how the manufacturing method can lead to anisotropic characteristics of PNCs by altering factors such as dispersion and

alignment of nanomaterials. The study revealed 5wt% PNCs made with SLS exhibited the greatest electrical conductivity compared to IM-processed PNCs regardless of the measurement direction. The results indicated that SLS-processed parts exhibited anisotropic behavior with enhanced electrical properties while IM PNCs remained non-conductive irrespective of the measurement directions and the GNP content. Moreover, it was found that SLS led to greater electrical conductivity through the length of the specimens than the transverse directions.

## **6.2 Conclusions**

The main conclusions of this dissertation are represented as follows:

- The research demonstrated that processing can be tuned to improve electrical properties of semi-crystalline PNCs without compromising the tensile and flexural performance, leading to fabrication of electrically conductive multifunctional PNCs.
- Macro-scale mechanical and viscoelastic properties of GNP/PA12 PNCs demonstrated the same trends indicating the presence of a secondary reinforcing mechanism that concurrently favors the observed enhancement in mechanical and thermomechanical behavior of the fabricated PNCs.
- GNP created a complex constrained region, consisting of both an amorphous and a crystalline region, whose amount is highly defined by the GNP content and dispersion and crystallization characteristic.
- In PNCs, the enhancement in elastic response is due to not only the reinforcement offered by the stiffening effect of high modulus nanomaterials but also to changes in physical property and structure of polymers at the vicinity of interfaces.

## **6.3 Research Contributions**

The research further enlightened the scientific and technical aspects of PNCs for fabrication of multifunctional high performance materials with directionally tailorable

properties for desired application. The main contributions of the dissertation are described as follows.

### **6.3.1 Scientific Contributions**

The study provides an understanding about interrelationships among process, nano-scale interfacial interactions and macro-scale properties of semi-crystalline PNCs that can lead to design and fabrication of reinforced polymers with multifunctional performance. The research gives a detailed insight into effect of nanomaterial-polymer interfacial interactions on formation and properties of the interfacial zone to better understand the links between governing reinforcing mechanisms and mechanical response of PNCs. More particularly, the methodologies and results provided in the study can be employed to determine representative constituents including the interphase, which is considered significant at the nano-size, in order to develop accurate structure-property models for semi-crystalline PNCs. The research also provides detailed process-structure-property relationships for a new class of multifunctional graphite based PNCs made by SLS.

### **6.3.2 Technical Contributions**

The dissertation allows for implementation of a comprehensive set of methodologies including experimental characterization and analysis from nano-size to a macro-scale level that enables advancements in large-scale manufacturing of nano-structured polymer materials. Moreover, the knowledge of interface/interphase is becoming an emerging focus that finds applications in a broad and interdisciplinary set of technical subjects. The methodologies introduced in the research can be utilized for evaluation of phenomena at polymer-solid interfaces induced by interfacial interactions. In addition, the findings of the study can be used as provisions for analytical/computational tools to minimize excessive and costly trial-and-error experiments that are currently employed to characterize PNCs. In particular, the study illustrated the potential capability of SLS as a key industrial processing tool for

development of electrically conductive PNCs with enhanced control of overall performance and with minimized limitations associated with conventional processing of PNCs.

#### **6.4 Future Research and Recommendations**

Potential paths for future research can be made by incorporation of the methodologies, concepts and outcomes of the research represented in this dissertation. First, the research points to a potential study that examines the effects of nanomaterial surface functionalization on the nonmaterial-nanomaterial and nanomaterial-polymer interfacial interactions and thus macro-scale properties of PNCs processed by traditional or advanced techniques. Additional research may also benefit from the concurrent use of different types of conductive nanomaterials such as CNT and GNP to evaluate effect of synergistic phenomena offered by multiple-reinforcement on bulk properties and in particular electrical conductivity. A framework of future research in micromechanics might also consider development of multi-phase structural models by implementation of the findings of this research that can thus lead to more accurate design tools for PNCs. The observations in the study suggest that SLS may result in inhomogeneous PNCs due to factors such as inconsistent local sintering and cooling phenomena. The observed challenge necessitates a thorough understanding of the SLS processing of polymer based composites and proper operational optimizations that favor sintering of parts with uniform morphology.

## REFERENCES

- [1] Hussain F, Hojjati M, Okamoto M, Gorga RE. Review article: polymer-matrix nanocomposites, processing, manufacturing, and application: an overview. *Journal of composite materials* 2006;40(17):1511-75.
- [2] Thostenson ET, Li C, Chou T-W. Nanocomposites in context. *Composites Science and Technology* 2005;65(3):491-516.
- [3] Jordan J, Jacob KI, Tannenbaum R, Sharaf MA, Jasiuk I. Experimental trends in polymer nanocomposites—a review. *Materials Science and Engineering: A* 2005;393(1):1-11.
- [4] Tjong S. Structural and mechanical properties of polymer nanocomposites. *Materials Science and Engineering: R: Reports* 2006;53(3):73-197.
- [5] Zhu H, Xu C, Wu D, Wei B, Vajtai R, Ajayan P. Direct synthesis of long single-walled carbon nanotube strands. *Science* 2002;296(5569):884-6.
- [6] Fiedler B, Gojny FH, Wichmann MH, Nolte M, Schulte K. Fundamental aspects of nano-reinforced composites. *Composites Science and Technology* 2006;66(16):3115-25.
- [7] Krishnamoorti R, Vaia RA. Polymer nanocomposites. *Journal of Polymer Science Part B: Polymer Physics* 2007;45(24):3252-6.
- [8] Ma P-C, Siddiqui NA, Marom G, Kim J-K. Dispersion and functionalization of carbon nanotubes for polymer-based nanocomposites: A review. *Composites Part A: Applied Science and Manufacturing* 2010;41(10):1345-67.
- [9] Shi H, Lan T, Pinnavaia TJ. Interfacial effects on the reinforcement properties of polymer-organoclay nanocomposites. *Chemistry of materials* 1996;8(8):1584-7.
- [10] Moczo J, Pukanszky B. Polymer micro and nanocomposites: structure, interactions, properties. *Journal of Industrial and Engineering Chemistry* 2008;14(5):535-63.

- [11] Vaia RA, Wagner HD. Framework for nanocomposites. *Materials Today* 2004;7(11):32-7.
- [12] Pogodina NV, Cerclé C, Avérous L, Thomann R, Bouquey M, Muller R. Processing and characterization of biodegradable polymer nanocomposites: detection of dispersion state. *Rheologica Acta* 2008;47(5-6):543-53.
- [13] Thostenson ET, Chou T-W. On the elastic properties of carbon nanotube-based composites: modelling and characterization. *Journal of Physics D: Applied Physics* 2003;36(5):573.
- [14] Jancar J, Douglas J, Starr FW, Kumar S, Cassagnau P, Lesser A, et al. Current issues in research on structure–property relationships in polymer nanocomposites. *Polymer* 2010;51(15):3321-43.
- [15] Hamming LM, Qiao R, Messersmith PB, Catherine Brinson L. Effects of dispersion and interfacial modification on the macroscale properties of TiO<sub>2</sub> polymer–matrix nanocomposites. *Composites Science and Technology* 2009;69(11):1880-6.
- [16] Thostenson ET, Ren Z, Chou T-W. Advances in the science and technology of carbon nanotubes and their composites: a review. *Composites Science and Technology* 2001;61(13):1899-912.
- [17] Fischer H. Polymer nanocomposites: from fundamental research to specific applications. *Materials Science and Engineering: C* 2003;23(6):763-72.
- [18] Ji XL, Jing JK, Jiang W, Jiang BZ. Tensile modulus of polymer nanocomposites. *Polymer Engineering & Science* 2002;42(5):983-93.
- [19] Fan Z, Advani SG. Characterization of orientation state of carbon nanotubes in shear flow. *Polymer* 2005;46(14):5232-40.
- [20] Desai A, Haque M. Mechanics of the interface for carbon nanotube–polymer composites. *Thin-walled structures* 2005;43(11):1787-803.
- [21] Sinha Ray S, Okamoto M. Polymer/layered silicate nanocomposites: a review from preparation to processing. *Progress in polymer science* 2003;28(11):1539-641.

- [22] Moniruzzaman M, Winey KI. Polymer nanocomposites containing carbon nanotubes. *Macromolecules* 2006;39(16):5194-205.
- [23] Njuguna J, Pielichowski K. Polymer nanocomposites for aerospace applications: properties. *Advanced Engineering Materials* 2003;5(11):769-78.
- [24] Brandrup J, Immergut E, Grulke E, Bloch D. *Polymer Handbook*. 4th. A wiley-interscience publication 1999.
- [25] Li B, Zhong W-H. Review on polymer/graphite nanoplatelet nanocomposites. *Journal of materials science* 2011;46(17):5595-614.
- [26] Dennis H, Hunter D, Chang D, Kim S, White J, Cho J, et al. Effect of melt processing conditions on the extent of exfoliation in organoclay-based nanocomposites. *Polymer* 2001;42(23):9513-22.
- [27] Kalaitzidou K, Fukushima H, Drzal LT. A new compounding method for exfoliated graphite-polypropylene nanocomposites with enhanced flexural properties and lower percolation threshold. *Composites Science and Technology* 2007;67(10):2045-51.
- [28] Zhao X, Lv L, Pan B, Zhang W, Zhang S, Zhang Q. Polymer-supported nanocomposites for environmental application: A review. *Chemical Engineering Journal* 2011;170(2):381-94.
- [29] Athreya SR, Kalaitzidou K, Das S. Microstructure, thermomechanical properties, and electrical conductivity of carbon black-filled nylon-12 nanocomposites prepared by selective laser sintering. *Polymer Engineering & Science* 2011;52(1):12-20.
- [30] Banerjee P, Mandal BM. Conducting Polyaniline Nanoparticle Blends with Extremely Low Percolation Thresholds. *Macromolecules* 1995;28(11):3940-3.
- [31] Chen GH, Wu DJ, Weng WG, Yan WL. Preparation of polymer/graphite conducting nanocomposite by intercalation polymerization. *Journal of Applied Polymer Science* 2001;82(10):2506-13.
- [32] Ajayan PM, Schadler LS, Giannaris C, Rubio A. Single-walled carbon nanotube-polymer composites: strength and weakness. *Advanced Materials* 2000;12(10):750-3.

- [33] Moniruzzaman M, Du F, Romero N, Winey KI. Increased flexural modulus and strength in SWNT/epoxy composites by a new fabrication method. *Polymer* 2006;47(1):293-8.
- [34] Schadler L, Giannaris S, Ajayan P. Load transfer in carbon nanotube epoxy composites. *Applied Physics Letters* 1998;73:3842.
- [35] Athreya SR, Kalaitzidou K, Das S. Processing and characterization of a carbon black-filled electrically conductive Nylon-12 nanocomposite produced by selective laser sintering. *Materials Science and Engineering: A* 2010;527(10):2637-42.
- [36] Goodridge R, Shofner M, Hague R, McClelland M, Schlea M, Johnson R, et al. Processing of a Polyamide-12/carbon nanofibre composite by laser sintering. *Polymer Testing* 2011;30(1):94-100.
- [37] Kim HC, Hahn HT, Yang YS. Synthesis of PA12/functionalized GNP nanocomposite powders for the selective laser sintering process. *Journal of composite materials* 2013;47(4):501-9.
- [38] Chung H, Das S. Functionally graded Nylon-11/silica nanocomposites produced by selective laser sintering. *Materials Science and Engineering: A* 2008;487(1):251-7.
- [39] Chunze Y, Yusheng S, Jinsong Y, Jinhui L. A nanosilica/nylon-12 composite powder for selective laser sintering. *Journal of Reinforced Plastics and Composites* 2009;28(23):2889-902.
- [40] Yan C, Shi Y, Yang J, Liu J. An organically modified montmorillonite/nylon-12 composite powder for selective laser sintering. *Rapid Prototyping Journal* 2011;17(1):28-36.
- [41] Wahab M, Dalgarno K, Cochrane R, Hassan S. Development of Polymer Nanocomposites for Rapid Prototyping Process. *Proceedings of the World Congress on Engineering WCE*.
- [42] Gibson I, Shi D. Material properties and fabrication parameters in selective laser sintering process. *Rapid Prototyping Journal* 1997;3(4):129-36.
- [43] Kruth J-P, Levy G, Schindel R, Craeghs T, Yasa E. Consolidation of polymer powders by selective laser sintering. Ghent, Belgium: PMI 2008.

- [44] Goodridge R, Tuck C, Hague R. Laser sintering of polyamides and other polymers. *Progress in Materials Science* 2012;57(2):229-67.
- [45] Kim HC, Hahn HT, Yang YS. Synthesis of PA12/functionalized GNP nanocomposite powders for the selective laser sintering process. *Journal of composite materials* 2012.
- [46] Petrović ZS, Javni I, Waddon A, Bánhegyi G. Structure and properties of polyurethane–silica nanocomposites. *Journal of Applied Polymer Science* 2000;76(2):133-51.
- [47] Adams M, Mullier M, Seville J. Agglomerate strength measurement using a uniaxial confined compression test. *Powder Technology* 1994;78(1):5-13.
- [48] Pukánszky B, Fekete E, Tüdós F. Surface tension and mechanical properties in polyolefin composites. *Makromolekulare Chemie Macromolecular Symposia: Wiley Online Library*; p. 165-86.
- [49] Szleifer I, Yerushalmi-Rozen R. Polymers and carbon nanotubes—dimensionality, interactions and nanotechnology. *Polymer* 2005;46(19):7803-18.
- [50] Bhattacharyya AR, Sreekumar T, Liu T, Kumar S, Ericson LM, Hauge RH, et al. Crystallization and orientation studies in polypropylene/single wall carbon nanotube composite. *Polymer* 2003;44(8):2373-7.
- [51] Davis VA, Ericson LM, Parra-Vasquez ANG, Fan H, Wang Y, Prieto V, et al. Phase behavior and rheology of SWNTs in superacids. *Macromolecules* 2004;37(1):154-60.
- [52] MASUDA J, Torkelson JM. Dispersion and major property enhancements in polymer/multiwall carbon nanotube nanocomposites via solid-state shear pulverization followed by melt mixing. *Macromolecules* 2008;41(16):5974-7.
- [53] Wagner HD, Vaia RA. Nanocomposites: issues at the interface. *Materials Today* 2004;7(11):38-42.
- [54] Ash B, Schadler L, Siegel R. Glass transition behavior of alumina/polymethylmethacrylate nanocomposites. *Materials Letters* 2002;55(1):83-7.

[55] Derjaguin B. Some results from 50 years' research on surface forces: Springer; 1987.

[56] Bansal A, Yang H, Li C, Cho K, Benicewicz BC, Kumar SK, et al. Quantitative equivalence between polymer nanocomposites and thin polymer films. *Nature materials* 2005;4(9):693-8.

[57] Manias E, Kупpa V, Yang D-K, Zax D. Relaxation of polymers in 2 nm slit-pores: confinement induced segmental dynamics and suppression of the glass transition. *Colloids and Surfaces A: Physicochemical and Engineering Aspects* 2001;187:509-21.

[58] Hodzic A, Kim JK, Stachurski Z. Nano-indentation and nano-scratch of polymer/glass interfaces. II: model of interphases in water aged composite materials. *Polymer* 2001;42(13):5701-10.

[59] Jancar J. Review of the role of the interphase in the control of composite performance on micro-and nano-length scales. *Journal of materials science* 2008;43(20):6747-57.

[60] Kim J-K, Hodzic A. Nanoscale characterisation of thickness and properties of interphase in polymer matrix composites. *The Journal of Adhesion* 2003;79(4):383-414.

[61] Metin D, Tihminlioğlu F, Balköse D, Ülkü S. The effect of interfacial interactions on the mechanical properties of polypropylene/natural zeolite composites. *Composites Part A: Applied Science and Manufacturing* 2004;35(1):23-32.

[62] Fu SY, Feng XQ, Lauke B, Mai YW. Effects of particle size, particle/matrix interface adhesion and particle loading on mechanical properties of particulate-polymer composites. *Composites Part B: Engineering* 2008;39(6):933-61.

[63] Karevan M, Pucha RV, Kalaitzidou K, Bhuiyan MA. Effect of interphase Modulus and nanofiller Agglomeration on the Tensile Modulus of Graphite Nanoplatelets and Carbon Nanotube

Reinforced Polypropylene Nanocomposites. *Carbon letters* 2011;11(4).

[64] Qiao R, Deng H, Putz KW, Brinson LC. Effect of particle agglomeration and interphase on the glass transition temperature of polymer nanocomposites. *Journal of Polymer Science Part B: Polymer Physics* 2011;49(10):740-8.

- [65] Bower C, Rosen R, Jin L, Han J, Zhou O. Deformation of carbon nanotubes in nanotube–polymer composites. *Applied Physics Letters* 1999;74:3317.
- [66] Hodzic A, Stachurski Z, Kim J. Nano-indentation of polymer–glass interfaces Part I. Experimental and mechanical analysis. *Polymer* 2000;41(18):6895-905.
- [67] Putz K, Krishnamoorti R, Green PF. The role of interfacial interactions in the dynamic mechanical response of functionalized SWNT–PS nanocomposites. *Polymer* 2007;48(12):3540-5.
- [68] Ramanathan T, Liu H, Brinson L. Functionalized SWNT/polymer nanocomposites for dramatic property improvement. *Journal of Polymer Science Part B: Polymer Physics* 2005;43(17):2269-79.
- [69] Pukánszky B. Interfaces and interphases in multicomponent materials: past, present, future. *European Polymer Journal* 2005;41(4):645-62.
- [70] Downing T, Kumar R, Cross W, Kjerengtroen L, Kellar J. Determining the interphase thickness and properties in polymer matrix composites using phase imaging atomic force microscopy and nanoindentation. *Journal of adhesion science and technology* 2000;14(14):1801-12.
- [71] Mäder E, Gao S. Prospect of nanoscale interphase evaluation to predict composite properties. *Journal of adhesion science and technology* 2001;15(9):1015-37.
- [72] Ma PC, Mo SY, Tang BZ, Kim JK. Dispersion, interfacial interaction and re-agglomeration of functionalized carbon nanotubes in epoxy composites. *Carbon* 2010;48(6):1824-34.
- [73] Zhang Q, Fang F, Zhao X, Li Y, Zhu M, Chen D. Use of dynamic rheological behavior to estimate the dispersion of carbon nanotubes in carbon nanotube/polymer composites. *The Journal of Physical Chemistry B* 2008;112(40):12606-11.
- [74] Yang F, Nelson GL. Polymer/silica nanocomposites prepared via extrusion. *Polymers for advanced technologies* 2006;17(4):320-6.
- [75] Tjong S, Bao S, Liang G. Polypropylene/montmorillonite nanocomposites toughened with SEBS-g-MA: Structure–property relationship. *Journal of Polymer Science Part B: Polymer Physics* 2005;43(21):3112-26.

- [76] Zuiderduin W, Westzaan C, Huetink J, Gaymans R. Toughening of polypropylene with calcium carbonate particles. *Polymer* 2003;44(1):261-75.
- [77] Albert K, Pfleiderer B, Bayer E, Schnabel R. Characterization of chemically modified glass surfaces by <sup>13</sup>C and <sup>29</sup>Si CP/MAS NMR spectroscopy. *Journal of colloid and interface science* 1991;142(1):35-40.
- [78] Ishida H, Wellinghoff ST, Baer E, Koenig JL. Spectroscopic Studies of Poly [N, N'-bis (phenoxyphenyl) pyromellitimide]. 1. Structures of the Polyimide and Three Model Compounds. *Macromolecules* 1980;13(4):826-34.
- [79] Preto M, Tavares MIB, Silva EPd. Low-field NMR study of Nylon 6/silica composites. *Polymer Testing* 2007;26(4):501-4.
- [80] Liu X, Thomason JL, Jones FR. XPS and AFM study of interaction of organosilane and sizing with E-glass fibre surface. *The Journal of Adhesion* 2008;84(4):322-38.
- [81] Thomason J, Dwight D. The use of XPS for characterisation of glass fibre coatings. *Composites Part A: Applied Science and Manufacturing* 1999;30(12):1401-13.
- [82] Barber AH, Cohen SR, Wagner HD. Measurement of carbon nanotube-polymer interfacial strength. *Applied Physics Letters* 2003;82(23):4140-2.
- [83] Yu M-F, Lourie O, Dyer MJ, Moloni K, Kelly TF, Ruoff RS. Strength and breaking mechanism of multiwalled carbon nanotubes under tensile load. *Science* 2000;287(5453):637-40.
- [84] Hu Y, Shen L, Yang H, Wang M, Liu T, Liang T, et al. Nanoindentation studies on Nylon 11/clay nanocomposites. *Polymer Testing* 2006;25(4):492-7.
- [85] Tanaka T, Montanari G, Mulhaupt R. Polymer nanocomposites as dielectrics and electrical insulation-perspectives for processing technologies, material characterization and future applications. *Dielectrics and Electrical Insulation, IEEE Transactions on* 2004;11(5):763-84.
- [86] Williams J, Donnellan M, James M, Morris W. Properties of the interphase in organic matrix composites. *Materials Science and Engineering: A* 1990;126(1):305-12.

- [87] Lee S-H, Wang S, Pharr GM, Xu H. Evaluation of interphase properties in a cellulose fiber-reinforced polypropylene composite by nanoindentation and finite element analysis. *Composites Part A: Applied Science and Manufacturing* 2007;38(6):1517-24.
- [88] Tsukruk VV. Scanning probe microscopy of polymer surfaces. *Rubber chemistry and technology* 1997;70(3):430-67.
- [89] Kim J-K, Mai Y-W. *Engineered interfaces in fiber reinforced composites: Elsevier science; 1998.*
- [90] Mai K, Mäder E, Mühle M. Interphase characterization in composites with new non-destructive methods. *Composites Part A: Applied Science and Manufacturing* 1998;29(9):1111-9.
- [91] Munz M, Sturm H, Schulz E, Hinrichsen G. The scanning force microscope as a tool for the detection of local mechanical properties within the interphase of fibre reinforced polymers. *Composites Part A: Applied Science and Manufacturing* 1998;29(9-10):1251-9.
- [92] Winter R, Houston J. Interphase mechanical properties in an epoxy-glass fiber composites as measured by interfacial microscopy. *PROCEEDINGS OF THE SEM SPRING CONFERENCE ON EXPERIMENTAL MECHANICS: SEM SOCIETY FOR EXPERIMENTAL MECHANICS INC; p. 355-8.*
- [93] Shen L, Phang IY, Chen L, Liu T, Zeng K. Nanoindentation and morphological studies on nylon 66 nanocomposites. I. Effect of clay loading. *Polymer* 2004;45(10):3341-9.
- [94] Watcharotone S, Wood CD, Friedrich R, Chen X, Qiao R, Putz K, et al. Interfacial and substrate effects on local elastic properties of polymers using coupled experiments and modeling of nanoindentation. *Advanced Engineering Materials* 2011;13(5):400-4.
- [95] Karevan M, Kalaitzidou K. Understanding the property enhancement mechanism in exfoliated graphite nanoplatelets reinforced polymer nanocomposites. *Composite Interfaces* 2013.
- [96] Magonov SN, Reneker DH. Characterization of polymer surfaces with atomic force microscopy. *Annual Review of Materials Science* 1997;27(1):175-222.

- [97] Pakzad A, Simonsen J, Yassar RS. Gradient of nanomechanical properties in the interphase of cellulose nanocrystal composites. *Composites Science and Technology* 2012;72(2):314-9.
- [98] Bogetti T, Wang T, VanLandingham M, Gillespie Jr J. Characterization of nanoscale property variations in polymer composite systems: 2. Numerical modeling. *Composites Part A: applied science and manufacturing* 1999;30(1):85-94.
- [99] VanLandingham M, Dagastine R, Eduljee R, McCullough R, Gillespie J. Characterization of nanoscale property variations in polymer composite systems: 1. Experimental results. *Composites Part A: applied science and manufacturing* 1999;30(1):75-83.
- [100] Donth E. Characteristic length of the glass transition. *Journal of Polymer Science Part B: Polymer Physics* 1996;34(17):2881-92.
- [101] Strong AB. *Fundamentals of composites manufacturing: materials, methods and applications*: Sme; 2008.
- [102] Adame D, Beall GW. Direct measurement of the constrained polymer region in polyamide/clay nanocomposites and the implications for gas diffusion. *Applied Clay Science* 2009;42(3):545-52.
- [103] Chen Y, Balani K, Agarwal A. Analytical model to evaluate interface characteristics of carbon nanotube reinforced aluminum oxide nanocomposites. *Applied Physics Letters* 2008;92(1):011916--3.
- [104] Angell CA. Formation of glasses from liquids and biopolymers. *Science* 1995;267(5206):1924-35.
- [105] Jackson CL, McKenna GB. The melting behavior of organic materials confined in porous solids. *The Journal of Chemical Physics* 1990;93:9002.
- [106] Lu H, Nutt S. Restricted relaxation in polymer nanocomposites near the glass transition. *Macromolecules* 2003;36(11):4010-6.
- [107] Ceccorulli G, Zini E, Scandola M. Study of Organic Phase Mobility in Nanocomposite Organic-Inorganic Coatings. *Macromolecular Chemistry and Physics* 2006;207(10):864-9.

- [108] Rao Y, Pochan JM. Mechanics of polymer-clay nanocomposites. *Macromolecules* 2007;40(2):290-6.
- [109] Tsagaropoulos G, Eisenburg A. Direct observation of two glass transitions in silica-filled polymers. Implications to the morphology of random ionomers. *Macromolecules* 1995;28(1):396-8.
- [110] Liu H, Brinson LC. Reinforcing efficiency of nanoparticles: A simple comparison for polymer nanocomposites. *Composites Science and Technology* 2008;68(6):1502-12.
- [111] Sargsyan A, Tonoyan A, Davtyan S, Schick C. The amount of immobilized polymer in PMMA SiO<sub>2</sub> nanocomposites determined from calorimetric data. *European polymer journal* 2007;43(8):3113-27.
- [112] Prado Lda, Kwiatkowska M, Funari S, Roslaniec Z, Broza G, Schulte K. Studies on morphology and interphase of poly (butylene terephthalate)/carbon nanotubes nanocomposites. *Polymer Engineering & Science* 2010;50(8):1571-6.
- [113] Bershtein VA, Egorova LM, Yakushev PN, Pissis P, Sysel P, Brozova L. Molecular dynamics in nanostructured polyimide-silica hybrid materials and their thermal stability. *Journal of Polymer Science Part B: Polymer Physics* 2002;40(10):1056-69.
- [114] Kalogeras I, Neagu E. Interplay of surface and confinement effects on the molecular relaxation dynamics of nanoconfined poly (methyl methacrylate) chains. *The European Physical Journal E* 2004;14(2):193-204.
- [115] Lipatov YS, Privalko V. Glass transition in filled polymer systems. *Polymer Science USSR* 1972;14(7):1843-8.
- [116] Arrighi V, McEwen I, Qian H, Serrano Prieto M. The glass transition and interfacial layer in styrene-butadiene rubber containing silica nanofiller. *Polymer* 2003;44(20):6259-66.
- [117] Mijovic J, Lee H, Kenny J, Mays J. Dynamics in polymer-silicate nanocomposites as studied by dielectric relaxation spectroscopy and dynamic mechanical spectroscopy. *Macromolecules* 2006;39(6):2172-82.

- [118] González-Irún Rodríguez J, Carreira P, García-Diez A, Hui D, Artiaga R, Liz-Marzán L. Nanofiller effect on the glass transition of a polyurethane. *Journal of Thermal Analysis and Calorimetry* 2007;87(1):45-7.
- [119] Karaman VM, Privalko VP, Privalko EG, Lehmann B, Friedrich K. Structure/Property Relationships for Polyamide 6/Organoclay Nanocomposites in the Melt and in the Solid State. *Macromolecular Symposia: Wiley Online Library*; p. 85-94.
- [120] Suzuki H, Grebowicz J, Wunderlich B. Glass transition of poly (oxymethylene). *British polymer journal* 1985;17(1):1-3.
- [121] Wunderlich B. Reversible crystallization and the rigid–amorphous phase in semicrystalline macromolecules. *Progress in polymer science* 2003;28(3):383-450.
- [122] Zhang X, Loo LS. Study of glass transition and reinforcement mechanism in polymer/layered silicate nanocomposites. *Macromolecules* 2009;42(14):5196-207.
- [123] Putz KW, Palmeri MJ, Cohn RB, Andrews R, Brinson LC. Effect of cross-link density on interphase creation in polymer nanocomposites. *Macromolecules* 2008;41(18):6752-6.
- [124] Rong M, Zhang M, Ruan W. Surface modification of nanoscale fillers for improving properties of polymer nanocomposites: a review. *Materials science and technology* 2006;22(7):787-96.
- [125] Qian D, Dickey EC, Andrews R, Rantell T. Load transfer and deformation mechanisms in carbon nanotube-polystyrene composites. *Applied Physics Letters* 2000;76:2868.
- [126] Rittigstein P, Torkelson JM. Polymer–nanoparticle interfacial interactions in polymer nanocomposites: confinement effects on glass transition temperature and suppression of physical aging. *Journal of Polymer Science Part B: Polymer Physics* 2006;44(20):2935-43.
- [127] Gacitua W, Ballerini A, Zhang J. Polymer nanocomposites: synthetic and natural fillers. A review. *Maderas Cien Tecnol* 2005;7(3):159-78.
- [128] Kalfus J, Jancar J. Immobilization of polyvinylacetate macromolecules on hydroxyapatite nanoparticles. *Polymer* 2007;48(14):3935-7.

[129] Rong MZ, Zhang MQ, Pan SL, Lehmann B, Friedrich K. Analysis of the interfacial interactions in polypropylene/silica nanocomposites. *Polymer International* 2004;53(2):176-83.

[130] Klein N, Marom G, Pegoretti A, Migliaresi C. Determining the role of interfacial transcrystallinity in composite materials by dynamic mechanical thermal analysis. *Composites* 1995;26(10):707-12.

[131] Zhang S, Minus ML, Zhu L, Wong C-P, Kumar S. Polymer transcrystallinity induced by carbon nanotubes. *Polymer* 2008;49(5):1356-64.

[132] Fujiyama M, Wakino T, Kawasaki Y. Structure of skin layer in injection-molded polypropylene. *Journal of Applied Polymer Science* 1988;35(1):29-49.

[133] Kalaitzidou K, Fukushima H, Askeland P, Drzal LT. The nucleating effect of exfoliated graphite nanoplatelets and their influence on the crystal structure and electrical conductivity of polypropylene nanocomposites. *Journal of materials science* 2008;43(8):2895-907.

[134] Miltner HE, Grossiord N, Lu K, Loos J, Koning CE, Van Mele B. Isotactic polypropylene/carbon nanotube composites prepared by latex technology. Thermal analysis of carbon nanotube-induced nucleation. *Macromolecules* 2008;41(15):5753-62.

[135] Benetti EM, Causin V, Marega C, Marigo A, Ferrara G, Ferraro A, et al. Morphological and structural characterization of polypropylene based nanocomposites. *Polymer* 2005;46(19):8275-85.

[136] Evonik Industries, Polyamide 12 Coating Powders, 2008, <http://www.vestosint.com>.

[137] Fukushima H, Drzal L. Graphite nanoplatelets as reinforcements for polymers: structural and electrical properties. 17th Annual American Society for Composites Technical Conference.

[138] Kumar S, Sun L, Caceres S, Li B, Wood W, Perugini A, et al. Dynamic synergy of graphitic nanoplatelets and multi-walled carbon nanotubes in polyetherimide nanocomposites. *Nanotechnology* 2010;21(10):105702.

[139] Stankovich S, Dikin DA, Piner RD, Kohlhaas KA, Kleinhammes A, Jia Y, et al. Synthesis of graphene-based nanosheets via chemical reduction of exfoliated graphite oxide. *Carbon* 2007;45(7):1558-65.

[140] XG Sciences Inc. xGnPTM Brand Graphene Nanoplatelets Product Information, 5020 Northwind Drive, Suite 212, East Lansing, MI 48823. 2013.

[141] Kalaitzidou K, Fukushima H, Drzal LT. Multifunctional polypropylene composites produced by incorporation of exfoliated graphite nanoplatelets. *Carbon* 2007;45(7):1446-52.

[142] Kalaitzidou K, Fukushima H, Miyagawa H, Drzal LT. Flexural and tensile moduli of polypropylene nanocomposites and comparison of experimental data to Halpin-Tsai and Tandon-Weng models. *Polymer Engineering & Science* 2007;47(11):1796-803.

[143] Ramanathan T, Stankovich S, Dikin D, Liu H, Shen H, Nguyen S, et al. Graphitic nanofillers in PMMA nanocomposites—an investigation of particle size and dispersion and their influence on nanocomposite properties. *Journal of Polymer Science Part B: Polymer Physics* 2007;45(15):2097-112.

[144] Partoens B, Peeters F. From graphene to graphite: Electronic structure around the K point. *Physical Review B* 2006;74(7):075404.

[145] Durmus A, Kasgoz A, Macosko CW. Linear low density polyethylene (LLDPE)/clay nanocomposites. Part I: Structural characterization and quantifying clay dispersion by melt rheology. *Polymer* 2007;48(15):4492-502.

[146] Zhao J, Morgan AB, Harris JD. Rheological characterization of polystyrene–clay nanocomposites to compare the degree of exfoliation and dispersion. *Polymer* 2005;46(20):8641-60.

[147] Corcione CE, Cavallo A, Pesce E, Greco A, Maffezzoli A. Evaluation of the degree of dispersion of nanofillers by mechanical, rheological, and permeability analysis. *Polymer Engineering & Science* 2011;51(7):1280-5.

[148] Athreya SR, Kalaitzidou K, Das S. Mechanical and microstructural properties of Nylon-12/carbon black composites: Selective laser sintering versus melt compounding and injection molding. *Composites Science and Technology* 2011;71(4):506-10.

[149] Partee B, Hollister SJ, Das S. Selective laser sintering process optimization for layered manufacturing of CAPA® 6501 polycaprolactone bone tissue engineering scaffolds. *Journal of manufacturing science and engineering* 2006;128(2):531-40.

[150] Yu L. Amorphous pharmaceutical solids: preparation, characterization and stabilization. *Advanced Drug Delivery Reviews* 2001;48(1):27-42.

[151] Phang IY, Liu T, Mohamed A, Pramoda KP, Chen L, Shen L, et al. Morphology, thermal and mechanical properties of nylon 12/organoclay nanocomposites prepared by melt compounding. *Polymer international* 2004;54(2):456-64.

[152] Cho J, Paul D. Nylon 6 nanocomposites by melt compounding. *Polymer* 2001;42(3):1083-94.

[153] Fu S-Y, Feng X-Q, Lauke B, Mai Y-W. Effects of particle size, particle/matrix interface adhesion and particle loading on mechanical properties of particulate-polymer composites. *Composites Part B: Engineering* 2008;39(6):933-61.

[154] Chatterjee S, Nüesch F, Chu BT. Comparing carbon nanotubes and graphene nanoplatelets as reinforcements in polyamide 12 composites. *Nanotechnology* 2011;22(27):275714.

[155] Gogolewski S, Czerntawska K, Gastorek M. Effect of annealing on thermal properties and crystalline structure of polyamides. Nylon 12 (polylauro lactam). *Colloid & Polymer Science* 1980;258(10):1130-6.

[156] Zhao F, Bao X, McLauchlin AR, Gu J, Wan C, Kandasubramanian B. Effect of POSS on morphology and mechanical properties of polyamide 12/montmorillonite nanocomposites. *Applied Clay Science* 2010;47(3):249-56.

[157] Ishikawa T, Nagai S, Kasai N. Thermal behavior of  $\alpha$  nylon-12. *Journal of polymer Science: Polymer Physics Edition* 1980;18(6):1413-9.

[158] Salmoria G, Leite J, Paggi R. The microstructural characterization of PA6/PA12 blend specimens fabricated by selective laser sintering. *Polymer Testing* 2009;28(7):746-51.

[159] Gopakumar T, Pagé D. Polypropylene/graphite nanocomposites by thermo-kinetic mixing. *Polymer Engineering & Science* 2004;44(6):1162-9.

- [160] Yasmin A, Luo J-J, Daniel IM. Processing of expanded graphite reinforced polymer nanocomposites. *Composites Science and Technology* 2006;66(9):1182-9.
- [161] Bhattacharya SN, Kamal MR, Gupta RK. *Polymeric nanocomposites: theory and practice*: Hanser Gardner Publications; 2008.
- [162] Fong H, Liu W, Wang C-S, Vaia RA. Generation of electrospun fibers of nylon 6 and nylon 6-montmorillonite nanocomposite. *Polymer* 2002;43(3):775-80.
- [163] Zheng J, Siegel RW, Toney CG. Polymer crystalline structure and morphology changes in nylon-6/ZnO nanocomposites. *Journal of Polymer Science Part B: Polymer Physics* 2003;41(10):1033-50.
- [164] Kim J, Creasy T. Selective laser sintering characteristics of nylon 6/clay-reinforced nanocomposite. *Polymer Testing* 2004;23(6):629-36.
- [165] Goertzen WK, Kessler M. Dynamic mechanical analysis of fumed silica/cyanate ester nanocomposites. *Composites Part A: Applied Science and Manufacturing* 2008;39(5):761-8.
- [166] Kim S, Drzal LT. Comparison of exfoliated graphite nanoplatelets (xGnP) and CNTs for reinforcement of EVA nanocomposites fabricated by solution compounding method and three screw rotating systems. *Journal of Adhesion Science and Technology* 2009;23(12):1623-38.
- [167] Seal S, Kuiry S, Georgieva P, Agarwal A. Manufacturing nanocomposite parts: present status and future challenges. *MRS bulletin* 2004;29(1):16-21.
- [168] Thostenson ET, Li C, Chou TW. Nanocomposites in context. *Composites Science and Technology* 2005;65(3):491-516.
- [169] Deng F, Van Vliet KJ. Prediction of elastic properties for polymer-particle nanocomposites exhibiting an interphase. *Nanotechnology* 2011;22(16):165703.
- [170] Song YS, Youn JR. Influence of dispersion states of carbon nanotubes on physical properties of epoxy nanocomposites. *Carbon* 2005;43(7):1378-85.

- [171] Ciprari D, Jacob K, Tannenbaum R. Characterization of polymer nanocomposite interphase and its impact on mechanical properties. *Macromolecules* 2006;39(19):6565-73.
- [172] Odegard G, Clancy T, Gates T. Modeling of the mechanical properties of nanoparticle/polymer composites. *Polymer* 2005;46(2):553-62.
- [173] Jasiuk I, Kouider M. The effect of an inhomogeneous interphase on the elastic constants of transversely isotropic composites. *Mechanics of Materials* 1993;15(1):53-63.
- [174] Winey KI, Vaia RA. Polymer nanocomposites. *MRS bulletin* 2007;32(04):314-22.
- [175] Baschek G, Hartwig G, Zahradnik F. Effect of water absorption in polymers at low and high temperatures. *Polymer* 1999;40(12):3433-41.
- [176] Griehl W, Ruestem D. Nylon-12-Preparation, Properties, and Applications. *Industrial & Engineering Chemistry* 1970;62(3):16-22.
- [177] Kojima Y, Usuki A, Kawasumi M, Okada A, Fukushima Y, Kurauchi T, et al. Mechanical properties of nylon 6-clay hybrid. *Journal of Materials Research(USA)* 1993;8(5):1185-9.
- [178] Rittigstein P, Priestley RD, Broadbelt LJ, Torkelson JM. Model polymer nanocomposites provide an understanding of confinement effects in real nanocomposites. *Nature materials* 2007;6(4):278-82.
- [179] Dixit M, Gupta S, Mathur V, Rathore K, Sharma K, Saxena N. Study of glass transition temperature of PMMA and CdS-PMMA composite. *Chalcogenide Letters* 2009;6(3):131-6.
- [180] Dealy JM, Wissbrun KF. *Melt rheology and its role in plastics processing: theory and applications*: Springer; 1999.
- [181] Eitan A, Fisher F, Andrews R, Brinson L, Schadler L. Reinforcement mechanisms in MWCNT-filled polycarbonate. *Composites Science and Technology* 2006;66(9):1162-73.

- [182] Greco A, Gennaro R, Rizzo M. Glass transition and cooperative rearranging regions in amorphous thermoplastic nanocomposites. *Polymer International* 2012;61(8):1326-33.
- [183] Greco A, Rizzo M, Maffezzoli A. Effect of the addition of organically modified nanofiller on the relaxation behavior of a thermoplastic amorphous matrix. *Thermochimica Acta* 2012;543:226-31.
- [184] Sargsyan A, Tonoyan A, Davtyan S, Schick C. The amount of immobilized polymer in PMMA SiO<sub>2</sub> nanocomposites determined from calorimetric data. *European Polymer Journal* 2007;43(8):3113-27.
- [185] Sandler J, Pegel S, Cadek M, Gojny F, Van Es M, Lohmar J, et al. A comparative study of melt spun polyamide-12 fibres reinforced with carbon nanotubes and nanofibres. *Polymer* 2004;45(6):2001-15.
- [186] Wakabayashi K, Pierre C, Dikin DA, Ruoff RS, Ramanathan T, Brinson LC, et al. Polymer-graphite nanocomposites: Effective dispersion and major property enhancement via solid-state shear pulverization. *Macromolecules* 2008;41(6):1905-8.
- [187] Pham D, Dotchev K, Yusoff W. Deterioration of polyamide powder properties in the laser sintering process. *Proceedings of the Institution of Mechanical Engineers, Part C: Journal of Mechanical Engineering Science* 2008;222(11):2163-76.
- [188] Hoffman JD, Weeks JJ. Melting process and the equilibrium melting temperature of polychlorotrifluoroethylene. *J Res Natl Bur Stand A* 1962;66:13-28.
- [189] Jakisch L, Komber H, Wursche R, Böhme F. Multifunctional coupling agents. II. Chain extension and terminal group modification of polyamides. *Journal of applied polymer science* 2004;94(5):2170-7.
- [190] Plummer C, Zanetto J-E, Bourban P-E, Månson J-A. The crystallization kinetics of polyamide-12. *Colloid & Polymer Science* 2001;279(4):312-22.
- [191] Li L, Koch MH, de Jeu WH. Crystalline structure and morphology in nylon-12: A small-and wide-angle X-ray scattering study. *Macromolecules* 2003;36(5):1626-32.
- [192] McNally T, Raymond Murphy W, Lew CY, Turner RJ, Brennan GP. Polyamide-12 layered silicate nanocomposites by melt blending. *Polymer* 2003;44(9):2761-72.

- [193] Ha H, Kim SC, Ha K. Morphology and properties of polyamide/multi-walled carbon nanotube composites. *Macromolecular Research* 2010;18(7):660-7.
- [194] Uhl FM, Wilkie CA. Polystyrene/graphite nanocomposites: effect on thermal stability. *Polymer degradation and stability* 2002;76(1):111-22.
- [195] Strobl G, Hagedorn W. Raman spectroscopic method for determining the crystallinity of polyethylene. *Journal of Polymer Science: Polymer Physics Edition* 2003;16(7):1181-93.
- [196] Pompe G, Mäder E. Experimental detection of a transcrystalline interphase in glass-fibre/polypropylene composites. *Composites Science and Technology* 2000;60(11):2159-67.
- [197] Hu H, Onyebueke L, Abatan A. Characterizing and modeling mechanical properties of nanocomposites-review and evaluation. *Journal of Minerals & Materials Characterization & Engineering* 2010;9(4):275-319.
- [198] Magonov S, Elings V, Whangbo M-H. Phase imaging and stiffness in tapping-mode atomic force microscopy. *Surface Science* 1997;375(2):L385-L91.
- [199] Jung YC, Bhushan B. Contact angle, adhesion and friction properties of micro- and nanopatterned polymers for superhydrophobicity. *Nanotechnology* 2006;17(19):4970.
- [200] Carroll B. The accurate measurement of contact angle, phase contact areas, drop volume, and Laplace excess pressure in drop-on-fiber systems. *Journal of colloid and interface science* 1976;57(3):488-95.
- [201] Fowkes FM. Dispersion force contributions to surface and interfacial tensions, contact angles, and heats of immersion. *Adv Chem Ser* 1964;43(1):99-111.
- [202] Werder T, Walther JH, Jaffe R, Halicioglu T, Koumoutsakos P. On the water-carbon interaction for use in molecular dynamics simulations of graphite and carbon nanotubes. *The Journal of Physical Chemistry B* 2003;107(6):1345-52.
- [203] Stankovich S, Dikin DA, Dommett GH, Kohlhaas KM, Zimney EJ, Stach EA, et al. Graphene-based composite materials. *Nature* 2006;442(7100):282-6.

- [204] Kumar S, Doshi H, Srinivasarao M, Park JO, Schiraldi DA. Fibers from polypropylene/nano carbon fiber composites. *Polymer* 2002;43(5):1701-3.
- [205] Zheng W, Wong S-C. Electrical conductivity and dielectric properties of PMMA/expanded graphite composites. *Composites Science and Technology* 2003;63(2):225-35.
- [206] Winey KI, Kashiwagi T, Mu M. Improving electrical conductivity and thermal properties of polymers by the addition of carbon nanotubes as fillers. *MRS bulletin* 2007;32(04):348-53.
- [207] Gangopadhyay R, De A. Conducting polymer nanocomposites: a brief overview. *Chemistry of materials* 2000;12(3):608-22.
- [208] Hu N, Masuda Z, Yan C, Yamamoto G, Fukunaga H, Hashida T. The electrical properties of polymer nanocomposites with carbon nanotube fillers. *Nanotechnology* 2008;19(21):215701.
- [209] Ramasubramaniam R, Chen J, Liu H. Homogeneous carbon nanotube/polymer composites for electrical applications. *Applied Physics Letters* 2003;83:2928.
- [210] Du F, Scogna RC, Zhou W, Brand S, Fischer JE, Winey KI. Nanotube networks in polymer nanocomposites: rheology and electrical conductivity. *Macromolecules* 2004;37(24):9048-55.
- [211] Jing X, Zhao W, Lan L. The effect of particle size on electric conducting percolation threshold in polymer/conducting particle composites. *Journal of materials science letters* 2000;19(5):377-9.
- [212] He F, Lau S, Chan HL, Fan J. High dielectric permittivity and low percolation threshold in nanocomposites based on poly (vinylidene fluoride) and exfoliated graphite nanoplates. *Advanced Materials* 2009;21(6):710-5.
- [213] Jeon K, Lumata L, Tokumoto T, Steven E, Brooks J, Alamo RG. Low electrical conductivity threshold and crystalline morphology of single-walled carbon nanotubes–high density polyethylene nanocomposites characterized by SEM, Raman spectroscopy and AFM. *Polymer* 2007;48(16):4751-64.

- [214] Tjong S, Liang G, Bao S. Effects of crystallization on dispersion of carbon nanofibers and electrical properties of polymer nanocomposites. *Polymer Engineering & Science* 2008;48(1):177-83.
- [215] Wang Q, Dai J, Li W, Wei Z, Jiang J. The effects of CNT alignment on electrical conductivity and mechanical properties of SWNT/epoxy nanocomposites. *Composites Science and Technology* 2008;68(7):1644-8.
- [216] Deng H, Skipa T, Zhang R, Lellinger D, Bilotti E, Alig I, et al. Effect of melting and crystallization on the conductive network in conductive polymer composites. *Polymer* 2009;50(15):3747-54.
- [217] Clingerman ML, Weber EH, King JA, Schulz KH. Development of an additive equation for predicting the electrical conductivity of carbon-filled composites. *Journal of Applied Polymer Science* 2003;88(9):2280-99.
- [218] Zhao Y, Xiao M, Wang S, Ge X, Meng Y. Preparation and properties of electrically conductive PPS/expanded graphite nanocomposites. *Composites Science and Technology* 2007;67(11):2528-34.
- [219] Zheng W, Lu X, Wong SC. Electrical and mechanical properties of expanded graphite-reinforced high-density polyethylene. *Journal of Applied Polymer Science* 2004;91(5):2781-8.
- [220] Spitalsky Z, Tasis D, Papagelis K, Galiotis C. Carbon nanotube-polymer composites: chemistry, processing, mechanical and electrical properties. *Progress in polymer science* 2010;35(3):357-401.
- [221] Geng Y, Liu MY, Li J, Shi XM, Kim JK. Effects of surfactant treatment on mechanical and electrical properties of CNT/epoxy nanocomposites. *Composites Part A: Applied Science and Manufacturing* 2008;39(12):1876-83.
- [222] Sahoo NG, Rana S, Cho JW, Li L, Chan SH. Polymer nanocomposites based on functionalized carbon nanotubes. *Progress in polymer science* 2010;35(7):837-67.
- [223] Zou JF, Yu ZZ, Pan YX, Fang XP, Ou YC. Conductive mechanism of polymer/graphite conducting composites with low percolation threshold. *Journal of Polymer Science Part B: Polymer Physics* 2002;40(10):954-63.

- [224] Kota AK, Cipriano BH, Duesterberg MK, Gershon AL, Powell D, Raghavan SR, et al. Electrical and rheological percolation in polystyrene/MWCNT nanocomposites. *Macromolecules* 2007;40(20):7400-6.
- [225] Sengupta R, Bhattacharya M, Bandyopadhyay S, Bhowmick AK. A review on the mechanical and electrical properties of graphite and modified graphite reinforced polymer composites. *Progress in polymer science* 2011;36(5):638-70.
- [226] Wang L, Hong J, Chen G. Comparison study of graphite nanosheets and carbon black as fillers for high density polyethylene. *Polymer Engineering & Science* 2010;50(11):2176-81.
- [227] Kim IH, Jeong YG. Polylactide/exfoliated graphite nanocomposites with enhanced thermal stability, mechanical modulus, and electrical conductivity. *Journal of Polymer Science Part B: Polymer Physics* 2010;48(8):850-8.
- [228] Goyal R, Jagdale P, Mulik U. Thermal, mechanical, and dielectric properties of polystyrene/expanded graphite nanocomposites. *Journal of Applied Polymer Science* 2009;111(4):2071-7.
- [229] Debelak B, Lafdi K. Use of exfoliated graphite filler to enhance polymer physical properties. *Carbon* 2007;45(9):1727-34.
- [230] Pan YX, Yu ZZ, Ou YC, Hu GH. A new process of fabricating electrically conducting nylon 6/graphite nanocomposites via intercalation polymerization. *Journal of Polymer Science Part B: Polymer Physics* 2000;38(12):1626-33.
- [231] Lanticse LJ, Tanabe Y, Matsui K, Kaburagi Y, Suda K, Hoteida M, et al. Shear-induced preferential alignment of carbon nanotubes resulted in anisotropic electrical conductivity of polymer composites. *Carbon* 2006;44(14):3078-86.
- [232] Chodak I, Krupa I. "Percolation effect" and mechanical behavior of carbon black filled polyethylene. *Journal of materials science letters* 1999;18(18):1457-9.
- [233] Cooper CA, Ravich D, Lips D, Mayer J, Wagner HD. Distribution and alignment of carbon nanotubes and nanofibrils in a polymer matrix. *Composites Science and Technology* 2002;62(7):1105-12.

[234] Yadroitsev I, Bertrand P, Smurov I. Parametric analysis of the selective laser melting process. *Applied surface science* 2007;253(19):8064-9.

[235] Williams JD, Deckard CR. Advances in modeling the effects of selected parameters on the SLS process. *Rapid Prototyping Journal* 1998;4(2):90-100.